WL-TR-95-4032

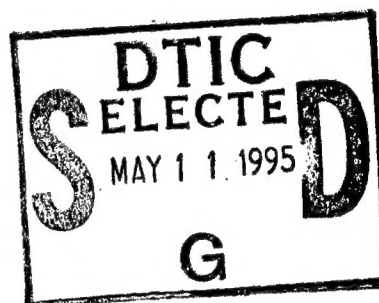# LEADING EDGE MATERIAL THERMAL AND ABLATION TEST EVALUATIONS FOR EXTENDED RANGE REENTRY MISSIONS

Henry L. Moody
Craig M. Graves
Daniel S. Moody
James L. Deleget

Nichols Research Corporation
2201 Buena Vista SE, Suite 203
Albuquerque NM   87106-4265

January 1995

Final Report for Period May 1994 to January 1995

MATERIALS DIRECTORATE
WRIGHT LABORATORY
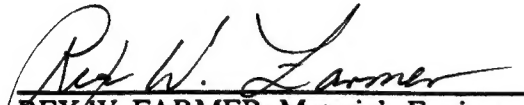AIR FORCE MATERIEL COMMAND
WRIGHT-PATTERSON AIR FORCE BASE OHIO   45433-7734
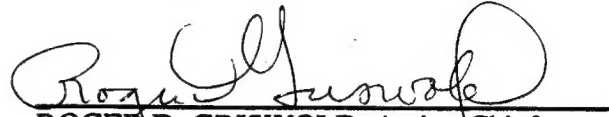
19950509 038

NOTICE

When government drawings, specifications, or other data are used for any purpose other than in connection with a definitely related government procurement operation, the United States Government thereby incurs no responsibility nor any obligation whatsoever; and the fact that the government may have formulated, furnished, or in any way supplied the said drawings, specifications, or other data, is not to be regarded by implication or otherwise as in any manner licensing the holder or any other person or corporation, or conveying any rights or permission to manufacture, use, or sell any patented invention that may in any way be related thereto.
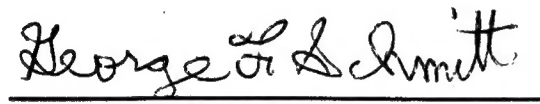
This technical report has been reviewed and is approved for publication.

REX W. FARMER, Materials Engineer
Thermal Protective Materials Section
Structural Materials Branch

ROGER D. GRISWOLD, Acting Chief
Structural Materials Branch
Nonmetallic Materials Division

GEORGE F. SCHMITT, Assistant Chief
Nonmetallic Materials Division
Materials Directorate

If your address has changed, if you wish to be removed from our mailing list, or if the addressee is no longer employed by your organization, please notify WL/MLBC, Bldg 654, 2941 P Street, Suite 1, Wright-Patterson AFB OH 45433-7750 to help maintain a current mailing list.

Copies of this report should not be returned unless return is required by security considerations, contractual obligations, or notice on a specific document.

DISCLAIMER NOTICE
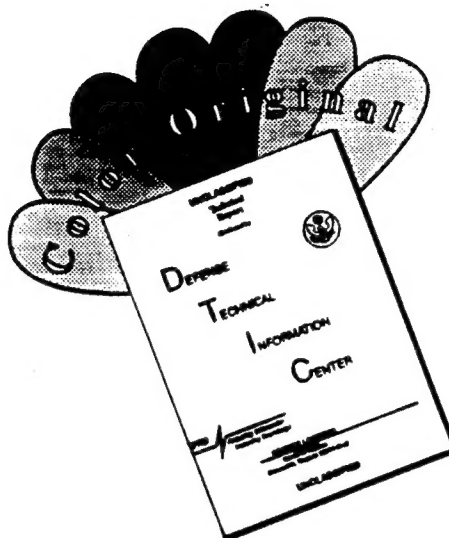
THIS DOCUMENT IS BEST QUALITY AVAILABLE. THE COPY FURNISHED TO DTIC CONTAINED A SIGNIFICANT NUMBER OF COLOR PAGES WHICH DO NOT REPRODUCE LEGIBLY ON BLACK AND WHITE MICROFICHE.

The following notice applies to any unclassified (including originally classified and now declassified) technical reports released to "qualified U.S. contractors" under the provisions of DoD Directive 5230.25, Withholding of Unclassified Technical Data From Public Disclosure.

NOTICE TO ACCOMPANY THE DISSEMINATION OF EXPORT-CONTROLLED TECHNICAL DATA

1. Export of information contained herein, which includes, in some circumstances, release to foreign nationals within the United States, without first obtaining approval or license from the Department of State for items controlled by the International Traffic in Arms Regulations (ITAR), or the Department of Commerce for items controlled by the Export Administration Regulations (EAR), may constitute a violation of law.

2. Under 22 U.S.C. 2778 the penalty for unlawful export of items or information controlled under the ITAR is up to two years imprisonment, or a fine of $100,000, or both. Under 50 U.S.C., Appendix 2410, the penalty for unlawful export of items or information controlled under the EAR is a fine of up to $1,000,000, or five times the value of the exports, whichever is greater; or for an individual, imprisonment of up to 10 years, or a fine of up to $250,000, or both.

3. In accordance with your certification that establishes you as a "qualified U.S. Contractor", unauthorized dissemination of this information is prohibited and may result in disqualification as a qualified U.S. contractor, and may be considered in determining your eligibility for future contracts with the Department of Defense.

4. The U.S. Government assumes no liability for direct patent infringement, or contributory patent infringement or misuse of technical data.

5. The U.S. Government does not warrant the adequacy, accuracy, currency, or completeness of the technical data.

6. The U.S. Government assumes no liability for loss, damage, or injury resulting from manufacture or use for any purpose of any product, article, system, or material involving reliance upon any or all technical data furnished in response to the request for technical data.

7. If the technical data furnished by the Government will be used for commercial manufacturing or other profit potential, a license for such use may be necessary. Any payments made in support of the request for data do not include or involve any license rights.

8. A copy of this notice shall be provided with any partial or complete reproduction of these data that are provided to qualified U.S. contractors.

DESTRUCTION NOTICE

For classified documents, follow the procedures in DoD 5200.22-M, Industrial Security Manual, Section II-19 or DoD 5200.1-R, Information Security Program Regulation, Chapter IX. For unclassified, limited documents, destroy by any method that will prevent disclosure of contents or reconstruction of the document.

REPORT DOCUMENTATION PAGE

Public reporting burden for this collection of information is estimated to average 1 hour per response, including the time for reviewing instructions, searching existing data sources, gathering and maintaining the data needed, and completing and reviewing the collection of information. Send comments regarding this burden estimate or any other aspect of this collection of information, including suggestions for reducing this burden, to Washington Headquarters Services, Directorate for Information Operations and Reports, 1215 Jefferson Davis Highway, Suite 1204, Arlington, VA 22202-4302, and to the Office of Management and Budget, Paperwork Reduction Project (0704-0188), Washington, DC 20503.

1. AGENCY USE ONLY (Leave blank)	2. REPORT DATE	3. REPORT TYPE AND DATES COVERED
	January 1995	Final Report for May 1994 - January 1995

4. TITLE AND SUBTITLE

Leading Edge Material Thermal and Ablation Test Evaluations for Extended Range Reentry Missions

6. AUTHOR(S)

Henry L. Moody, Craig M. Graves, Daniel S. Moody, and James L. Deleget

5. FUNDING NUMBERS

Contract: F33615-89-C-5625
PE: 62102F
PR: 2417
TA: 01
WU: A3

7. PERFORMING ORGANIZATION NAMES(S) AND ADDRESS(ES)

Nichols Research Corporation
2201 Buena Vista SE, Ste 203
Albuquerque NM 87106-4265

8. PERFORMING ORGANIZATION REPORT NUMBER

9. SPONSORING / MONITORING AGENCY NAME(S) AND ADDRESS(ES)

Materials Directorate
Wright Laboratory
Air Force Materiel Command
Wright Patterson AFB OH 45433-7734

10. SPONSORING / MONITORING AGENCY REPORT NUMBER

WL-TR-95- 4032

11. SUPPLEMENTARY NOTES

Export control restrictions apply.

12a. DISTRIBUTION / AVAILABILITY STATEMENT

Distribution authorized to US Government Agencies and their contractors; critical technology, Jan 95. Other requests for this document shall be referred to WL/MLBC, Bldg 654, 2941 P St, Ste 1, WPAFB OH 45433-7750.

12b. DISTRIBUTION CODE

13. ABSTRACT (Maximum 200 words)

Arc-heater tests were conducted on candidate Air Force leading edge materials for extended range reentry applications. The objectives were to obtain thermal and ablation data on leading edge materials at a swept angle representative of the operational system. Model holders were designed and fabricated to allow the testing of leading edges at the desired 60° sweep angle and for comparison, 0° sweep. The NASA-Ames 60MW (IHF) facility was selected because of its unique ability to simulate both the pullout and glide phases of extended range in a single test.

A total of 23 arc-heater runs were made, 11 calibration and 12 model runs. Calibration involved using a replica configuration of the 60° sweep model to acquire heating and pressure data on the nosetip and leading edges. In the 12 model runs, 20 material samples were tested. The test variables included material type (223 Pan C-C, FWPF C-C, 40DO C-C, SAID C-C with Ultramet coating, Cercarb, and an MSNW impregnated carbon sock over Poco), weave orientation relative to the sweep angle (0°, 30°, 90°), angle of attack (0° and 10°), and trjactory sequence (i.e., glide only, pullout only, pullout and glide). The tests resulted in the generation of a data base for C-C leading edge material thermal and ablation responses during high altitude reentry flight. All pure C-C materials ablated in a well behaved laminar manner with no apparent mechanical ablation. The other materials appear to either have a thermostructural problem and/or underwent melt with resulting complex and irregular shaping. Weave orientation appeared to have little influence on ablation; the influence of angle of attack was as expected (the shape change was biased by the angle of attack).

14. SUBJECT TERMS

Carbon-Carbon Leading Edges, Swept Leading Edges, Thermal-Ablation Response, Ground Test Simulations, High Altitude Reentry

15. NUMBER OF PAGES

127

16. PRICE CODE

17. SECURITY CLASSIFICATION OF REPORT	18. SECURITY CLASSIFICATION OF THIS PAGE	19. SECURITY CLASSIFICATION OF ABSTRACT	20. LIMITATION OF ABSTRACT
UNCLASSIFIED	UNCLASSIFIED	UNCLASSIFIED	UL

NSN 7540-01-280-5500

COMPUTER GENERATED

Standard Form 298 (Rev. 2-89)
Prescribed by ANSI Std. Z39-18
298-102

Foreword

Henry L. Moody was the Principal Investigator for this Program. The Program technical effort was performed while both he and the co-authors were employed as consultants to Nichols Research Corporation. This effort was part of a NRC program with WL/MLBC for conducting advanced material development and material evaluations, Contract F33615-89-C-5625. Mr. Stanley Schulman and Mr. Rex Farmer were the MLBC personnel providing program management and technical support.

Mr. H. Moody was responsible for the test planning, facility interfacing, test article thermal design analyses, and actual testing. Mr. Craig Graves was responsible for the mechanical design and fabrication of all hardware and was supported by H. Moody and D. Moody in the design, fabrication, and assembly of the models-test articles. Jim Deleget conducted the hardware structural design analyses. The tests were conducted in the NASA-AMES Interactive Heating Facility (IHF). The facility is under the direction of Joe Hartman. The test engineer was Mr. Wendell Love who was assisted by Frank Hui and Vincent Meglio. Rex Farmer provided invaluable assistance in test planning, test matrix definition and support of post-test investigations.

Accesion For		
NTIS CRA&I	☐	
DTIC TAB	☒	
Unannounced	☐	
Justification		
By		
Distribution /		
Availability Codes		
Dist	Avail and / or Special	
C-2		

Table of Contents

List of Illustrations

List of Illustrations, cont'd

List of Tables

SUMMARY

Arc-heater tests were conducted on candidate Air Force leading edge materials for extended range reentry applications. The overall objectives of the tests were to obtain thermal and ablation data on leading edge materials at sweep angles representative of the operational system. To achieve this objective, a special model holder was designed and fabricated to allow the testing of leading edges at 60° sweep angles. To provide a comparison, a 0° sweep model (resembling a cylinder in cross flow) was fabricated. Selected materials were tested at both 60 and 0° sweep angles. The NASA-AMES 60MW (IHF) facility was selected for the tests because this facility has the unique ability to simulate both the pullout and glide phases of extended range in a single test.

A total of 23 arc-heater runs were made, 11 calibration runs and 12 model runs. The calibration runs involved using a replica configuration of the 60° sweep model, instrumented with calorimeters (5 total) and surface pressure ports (3 total). The calibration runs acquired data on the nosetip and leading edge surfaces for the conditions used in the material ablation tests. In the 12 model runs, 20 material samples were tested. The material samples and a summary of the results follow:

1)   One nosetip fabricated from SAIC C-C with an Ultramet coating was tested at the lowest heat flux obtainable in the NASA 60MW 6.0" nozzle. The material was exposed at a heat flux of 900 Btu/ft2-sec for 60 sec and underwent ablation almost immediately in the test.

2)   Three leading edge materials were tested at the pullout heat flux (630 Btu/ft2-sec) in the 0° sweep configuration for over 100 seconds each. The materials were: a) 223 C-C that underwent smooth laminar ablation with extreme uniformity along its impingement line, b) the SAIC C-C with an Ultramet coating which apparently underwent ablation early in the run, ablating through the coating and into the parent material, and c) a HfC impregnated C-C sock attached to a Poco graphite substrate that underwent ablation early in the run, ablating through the sock and into the Poco.

3)   Sixteen leading edge materials were tested in the 60° sweep configuration. The test involved glide only, pullout only, and combined pullout-glide. For these types of tests, the durations were 300, 90 and 390 seconds, respectively. Glide and pullout heating rates were nominally 220 and 620 Btu/ft2-sec, respectively. The materials were: a) 223 C-C that underwent smooth laminar ablation with extreme uniformity along its impingement line, b) FWPF C-C that ablated about the same as 223, c) 4DO C-C that also ablated about the same as 223, d) a SAIC C-C with an Ultramet coating which ablated through the coating (could have been caused by the upstream ablating C-C section), and e) the BP-Hitco Ceracarb which underwent significant ablation along the impingement line (could also have been caused by the upstream ablating C-C section).

1

In addition to material type, the test variables included weave orientation relative to the sweep angle, Angle-of-Attack (AoA), trajectory sequence (i.e., glide only, pullout only, pullout and glide), and test reproducibility. All C-C materials ablated just about the same, with the spread in data about equal to the test-to-test variations measured in the reproducibility evaluations. Also the influence of weave orientation was about equal to the measured test-to-test variations. The influence of AoA was as expected in that the shape change was biased by the AoA.

The tests resulted in the generation of a data base for C-C leading edge material thermal and ablation (or shape change) responses during high altitude reentry flight. The ablation performance of the Air Force C-C materials (FMI's 223, Textron's FWPF and GE's 4DO) is well behaved with no apparent mechanical modes of ablation. In all cases, the C-C materials ablate in a laminar behavior with no pits, divots or gouging evident from visual inspection. The other leading materials appear to either have a thermostructural problem and/or underwent melt, with resulting complex and irregular shaping during the ablation process. From these tests, the following conclusions can be made:

1) The ablation of all C-C materials are well behaved, with apparently no mechanical effects and no preferential oxidation or roughness development. The shapes appear to be caused by an all laminar boundary layer.

2) The thermal and ablation data generated for C-C materials appears to be of a quality sufficient for shape change codes to use as a data base for verification-demonstration.

3) The pullout heating levels appear to be too high for the SAIC and MSNW materials. The glide heating levels appear to be too high for the BP-Hitco material.

4) There appears to be little effect of weave orientation (relative to the sweep angle) on shape change.

5) There appears to be little effect of trajectory sequence on shape change (i.e., pullout only ablation + glide only ablation = combined pullout and glide ablation in a single test).

6) All the model hardware performed as designed and as expected. Some changes are recommended in the nosetip and thermal isolation of the leading edge's forward face. The test facility performed with no significant problems, allowing all tests to be conducted at the desired conditions.

1.0 TEST OBJECTIVES

WL/MLBC sponsored leading edge tests were conducted in the NASA-AMES 60MW arc-heater facility from 3 August through 6 Sept 94. The overall objectives of these tests were to obtain thermal and ablation (shape change) data on candidate leading edge materials at conditions simulating "extended range" reentry. These tests were to resemble the swept configuration that is anticipated for an advanced Air Force operational vehicle. A generic extended range vehicle configuration is presented in Figure 1. For this configuration, the nosetip and leading edges have nose radii of 0.50" and are swept back at an angle of 70° (angle leading edge impingement line is swept back from a plane perpendicular to vehicle axis). Sample extended range flight conditions are presented in Reference 1. Portions of the Reference 1 conditions are presented in Figure 2 for the vehicle nosetip and leading edges. The conditions for the IGRP-IIA trajectory are of prime interest to the Air Force and therefore these conditions were simulated in the tests.

The specific objectives of the tests are presented in Figure 3. These objectives were to simulate the supersonic regions and convective heating rates that are induced over the leading edge during flight. It was of particular interest to simulate the flight sweep angle and Mach Numbers (behind the bow shock) so that the flight supersonic regions in the vicinity of the leading edge's impingement line are duplicated. Variables in the tests were leading edge material, fiber orientation relative to the sweep angle, the sweep angle, Angle-of-Attack (AoA), and the simulation of different time segments of the extended range mission (i.e., glide only, pullout only and combined pullout-glide).

2.0 TEST FACILITY

2.1 Test Facility Review

A test facility review was made to select the best test facility for conducting the extended range simulations. The results of the review are summarized in Figure 4 wherein candidate facility capabilities are compared with the IGRP-IIA aerothermal conditions. As can be seen, the NASA-AMES 60MW does the best job of simulating the nosetip conditions for the pullout and glide portions of trajectory IGRP-IIA. Assuming that the model configuration can simulate the flight leading edge sweep angle, then the 60MW also does a good job in simulating leading edge pullout and glide conditions. For the terminal dive portion of IGRP-IIA, the 60MW's recovery enthalpy is too high to result in desired flight simulations.

The 60MW is capable of running for the desired extended range duration (over 800 seconds). The run time capability and the ability of the 60 MW to simulate pullout and glide conditions in a single test, resulted in the 60 MW being selected for conducting the leading edge evaluations described in this report. It should be noted that this facility was considered for conducting the nosetip extended range evaluations of Reference 1, but the facility was not available at that time (GFY 1992). Facility usage in 1994, however, did allow testing of the leading edges in GFY 1994.

3

2.2 Facility Conditions

The envelope of conditions that the 60MW can produce are presented in Figure 5. The 60MW has 5 different nozzles, with the conditions produced by 4 nozzles shown in the figure. The facility conditions required to produce the extended range heating rates are noted in Figure 5, wherein it can be concluded that the 6.0" nozzle is the only NASA nozzle for conducting the desired extended range leading edge tests. The points noted in the figure as "Moody pre-test pullout" and "Moody pre-test glide" were pre-test estimates of the facility operating conditions required to simulate the pullout and glide portions of extended range. To achieve the glide conditions, the 6.0" nozzle was estimated to require the addition of cold mixing air to reduce recovery enthalpy. NASA cold air mixing capability is reported to be a maximum of 50% of arc column air. At this 50% mixing ratio, the enthalpy (estimated as 4000 Btu/lb) is satisfactory for glide but too high (and the pressure too low, see Figure 4) to simulate the terminal dive portion of extended range. As noted in Figure 4, this condition is better simulated in AEDC's HEAT-H1 facility.

The actual facility conditions that were used in simulating the leading edge pullout and glide environments are presented in Figure 5. The actual pullout facility operating condition was slightly lower than the pre-test estimates because pre-test analyses were conducted with an approximate data base. The actual glide condition was higher than pre-test predictions because of the inability to add cold mixing air and obtain model calibration data. As will be discussed in Section 4.2, the 60MW arc-heater was capable of operating with the desired mixing air, but the arc induced extremely high electrical noise on all the calorimeter channels, making it impossible to acquire model heating rate data. Because the of this inability to define the leading edge conditions with mixing air, the lowest heating rate obtained in the 60MW (without cold air mixing and having good calibration data) was selected as the glide condition. This condition is noted in Figure 5.

It should be noted that the desired ratio of pullout heating-to-glide heating was 3.1 (pre-test value). The actual ratio that was used in the leading edge evaluations was 2.4. It was not possible to increase this ratio by lowering the glide heating (because, as noted above, of the inability to calibrate with cold mixing air) or increasing pullout heating. Although the facility could easily increase pullout heating by 30%, the internal cooled nosetip was estimated as being at its upper limit for survival (see Section 4.1 and 4.2 for discussion).

2.3 Facility Interfaces

A schematic of the 60MW's 6.0" diameter exit nozzle is presented in Figure 6. The nozzle has a 2.375" diameter throat, a 6.0" dia exit and is conical with a 10° cone half angle. The nozzle exit Mach number is reported by NASA to be between 2.8 and 3.8. The former number is assuming the flow is frozen aft of the sonic point, the later assumes the flow is in equilibrium throughout the entire nozzle. The outer portions of the test rhombus were inferred by using prior NASA data involving pitot pressure probe sweeps through the nozzle exit. These data are included in Figure 6 and represent the radial locations where the local pressure is 0.95

times the maximum value. As can be noted the test rhombus estimated using the lower exit Mach Number (M=2.8) appears to be in better agreement with the data than the higher value. This lower Mach Number inferred test rhombus was therefore used in designing the leading edge models.

As shown in Figure 6, the 6.0" dia exit plane is about 3.0" upstream of the forward most location that a model can be positioned in the flow and still rotate in and out of the flow without the use of axial drive. This nozzle feature causes a significant amount of unusable test rhombus. It is recommended that future improvements in the facility consider modifying the nozzle so that the 6.0" exit plane corresponds to the model insertion location. The use of axial drive to locate the model at the nozzle exit plane is not desired because the model is inserted at a position which makes camera coverage difficult and also induces a risk in that the model can become "stuck" up in the nozzle requiring the model to be in the flow during arc-heater shutdown.

A schematic of the test chamber is presented in Figure 7. The figure identifies the model insertion mechanism, the facility strut, the vacuum envelope (or test cell), water cooling supply-return for the model, instrumentation console, and the exhaust diffusor. The figure shows the model in two positions: 1) the test location (on nozzle centerline and 3.0" aft of the nozzle exit plane) and 2) the model location when it is out of the flow (i.e., during arc start-up and shutdown). Figure 8 presents two photographs of the nozzle exit. One photograph shows the model in the position corresponding to arc-heater start-up and termination (model "out of the flow"). The other photograph shows the model in the test location. The nozzle attachment hardware and facility strut can be noted in the photos.

Figure 7 shows the windows used for viewing the model and acquiring pyrometer data. The test cell has viewing windows on the ceiling and east and west walls as noted. In the leading edge tests, video coverage of the models was obtained from the window mounted in the ceiling. This view allowed the planform of both leading edges to be viewed at the same time. The east window is reserved for witnessing the tests and observing all the test cell hardware. This window was used to make real time decisions concerning arc-heater shutdown. For the leading edge tests, one window had optical properties suitable for acquiring pyrometer surface temperature data. This window and pyrometer are noted in Figure 7 and were used to obtain surface temperature data of the west leading edge. To acquire surface temperature data on the east leading edge, a pyrometer was mounted inside the test cell as noted in Figure 7. These pyrometers are described in more detail in Section 5. Also discussed in Section 5 is the pyrometer arrangements for the 0° sweep leading edge tests.

3.0 MODEL DESIGN

The key issues that dictated the design of the leading edge models included:

1) Swept Leading Edge. To simulate the supersonic flow field around the operational leading edges and the streamline orientation relative to the leading edge material fiber direction, the model had to be designed to accommodate swept leading edges, preferably

the 70° sweep angle inherent in the operational vehicle configuration. This feature dictated the complexity and cost of the model design. It would had been simpler to test the leading edges at 0° sweep as has been done in the past, however the importance of leading edge shape change on vehicle performance required testing of the swept configurations.

2)   Internal Cooling. Ablation analyses conducted on C-C materials showed that the nosetip will ablate over 1 inch causing significant nose blunting. This was found to cause large changes in the leading edge flow field; in fact, with the available test rhombus, over half of the leading edge would become the nosetip or a large part of the leading edge would have to be located out of the test rhombus to reduce nosetip shaping effects! Thus to minimize changes in leading edge conditions, an internal cooled nosetip was required. To transition the non-ablating nosetip to the ablating leading edge, it was necessary to incorporate a section that had the same ablating characteristics as the leading edge and extend far enough aft so that the leading edge conditions were not influenced by the non-ablating nosetip. Because most of the leading edge materials were C-C, this transition section was fabricated from FWPF C-C.

3)   Calibration. Because this was a first ever test of ablating leading edges at such a large sweep angle, a replica calorimeter model with pressure ports and calorimeters was required to characterize the flow and heating over the leading edge test articles.

4)   "Non-Ablating" Materials. Some of the leading edge material candidates were coated or impregnated with constituents that were to prevent or, relative to C-C, reduce ablation. The ablating transition section used to transition the non-ablating nosetip to the leading edge will cause a flow disruption at the forward edge of "non-ablating" leading edge test articles. It was not within program scope to redesign the nosetip so that the cooled nosetip extended aft to the leading edge. Thus, for testing materials that were not expected to ablate as much as C-C, it was decided to fabricate a 0° sweep model. The 0° model orients the leading edge stagnation line normal to the flow, thus leading edge ablation is not influenced by adjacent components.

The following subsections present the design details of the different models that were used in leading edge testing. This includes the swept model (60° model), the non-swept model (or 0° model) and the calorimeter model used to characterize the flow field and heating of the swept design.

3.1 Leading Edge Model Design, 60° Sweep

A schematic of the swept model design is presented in Figure 9. The figure shows the location and configuration of the main components. Figures 10 and 11 present photographs of the main components and a completely assembled model. A completely disassembled swept model is shown in Figures 11a and 12 and includes the following components:

6

1) An internally cooled copper nosetip, Figure 10b;

2) A C-C transition section to provide a transition between the non-ablating nosetip and ablating leading edge test articles, Figure 10c;

3) Two swept leading edge test articles, one on each side of the model, Figure 10d;

4) Two graphite end caps, located aft of the two leading edges to prevent heating of the leading edge aft face, Figure 10d;

5) Insulated retention for the leading edges and end caps, which include zirconia rods and an insulator pad, Figure 10d;

6) An upper and lower heatshield (silica phenolic) to protect the model's main structure, Figure 10a;

7) An internally cooled main structure for retention of the nosetip, two leading edges, end caps and upper-lower heatshields, Figure 11b & c;

8) An adaptor to enlarge the model base area so as to thermally protect the NASA sting, Figure 11a;

9) Adaptor upper and lower cooled covers, Figure 11a;

10) Upper and lower heatshields (silica phenolic) to the adaptor's cooled covers, Figure 11a; and,

11) A Sting mount (used to vary the Boomerang AoA and provide a structural attachment to the facility sting), Figure 11a.

The radii of the nosetip, leading edges and end caps are all equal and, with the swept leading edges located on both sides of the nosetip, the model resembles a "Boomerang". Thus, the model was dubbed the "Boomerang" model during the test series. The following paragraphs describe the trades that were involved in selecting the "Boomerang" configuration and present design summaries of the individual Boomerang model components.

Selection of the Boomerang Model Configuration

A trade study was conducted in selecting the Boomerang over other candidate configurations. Part of this trade study is reported in Reference 1 and the results are summarized in Table 1. In Reference 1, it was concluded that an aft facing strut design (shown in Table 1) would eliminate the need for a cooled nosetip and allow more leading edges to be tested in a single run (4 leading edges instead of two that results from the Boomerang configuration). The Reference 1 investigations were continued with NASA and it was eventually concluded that the

Boomerang configuration resulted in a simpler test with less risk. For example, the converging arrangement of the aft facing design could cause the flow to coalesce in the aft region, possibly causing a subsonic flow regime or flow complexities over the leading edge test articles. Cold flow testing was recommended to determine the nature of the flow field over the aft facing leading edges.

The reviews with NASA found that with the 6.0" nozzle and the support hardware needed for the aft facing struts, flow spillage into the test cell would occur in an unpredictable manner. For the 6.0" nozzle, the exit plane is 3.0" upstream of the model insertion plane (see Figure 6). The hardware supporting the aft facing struts would interact with the expanding nozzle flow and the flow would thus be distributed in an unknown manner around the test cell. Also, the aft facing strut support hardware would require thermal protection. The weight required for model support and insulation, together with the aft facing holder, was estimated to over-load the strut insertion mechanism. A review of flow spillage indicated that an extensive effort would be required to thermally protect facility components in the test cell and the strut insertion hardware would have to modified. Also, the acquisition of pyrometer data will require the use of mirrors which could over heat due to this spillage. Thus, too reduce risk in the leading edge tests, the "more conventional" Boomerang design was selected over the aft facing strut design.

The following paragraphs summarize the results of the trade studies that were involved in design and fabrication of the Boomerang leading edge test model.

Nose Radii

The nosetip and leading edge radii were selected to be 0.375". This radius is what was used in the prior nosetip tests, Reference 1. Any larger radius would have caused a reduction in the amount of leading edge that can be located in the test rhombus.

Definition of Sweep Angle

A trade study was conducted to identify the leading edge sweep angle that could be accommodated in the facility. Sweep angle was found to have a large influence on the ability to cool the nosetip and retain the leading edges. Large sweep angles left little room in the forward region of the model for routing the nosetip coolant supply-return lines and providing leading edge retention with sufficient insulation so that the leading edge temperatures were not influenced by the model holder. The influence of sweep angle on restricting coolant supply and leading edge retention can be observed in Figure 12, an exploded view of the Boomerang design finally selected for fabrication (detailed parts shown in Figure 11a). The larger the sweep angle, the more cramped the forward region becomes requiring small coolant lines. The 70° sweep angle used in the operational design restricted the coolant line diameter so that not enough coolant flow could be delivered to the nosetip. With a sweep angle of 60°, the nosetip's coolant pressure drop flow rate is about 50% in the supply-return lines and 50% in cooling the nosetip. This is close to undesirable because in designing a cooling system it is a goal to have the majority of the pressure drop used in cooling or metering coolant and not in the coolant supply-

return lines. Thus, there is a trade in the amount of thermal-structural margin that exists in the cooled nosetip design and the amount of leading edge sweep that is possible to simulate the flight configuration. This trade resulted in a sweep angle of 60° and the nosetip having no thermal margin and about a 1.5 structural margin. Also at the 60° sweep, provision could be made to retain the leading edge so that radiation rather than conduction dominated the leading edge heat loss.

Using the Mach 2.8 freestream flow (minimum exit Mach value estimated for the 6.0" nozzle), the 60° angle results in a 1.4 Mach number flow normal to the leading edge and Mach 2.4 flow along the impingement line. Thus, at 60° sweep, the leading edge impingement region is supersonic, satisfying the main objective of the tests, the nosetip can be cooled and the leading edges can be sufficiently insulated and retained. Thus, in the Boomerang model, a 60° sweep rather than the flight 70° was used to test the leading edge materials.

Test Article Size and Design

The 60° Boomerang model and the way it "fits" into the nozzle test rhombus, is illustrated in Figure 13. The expansion lines induced by the two Mach numbers estimated for the nozzle (2.8 for frozen aft of the throat and 3.8 for full equilibrium flow) are shown in Figures 13 and 6. Figure 6 shows the edges of the test rhombus as inferred by data acquired from a stagnation point probe swept through the nozzle's exit plane. As can be noted, the Mach 2.8 test rhombus size appears to be in better agreement with the pressure data than does the 3.8 Mach number inferred test rhombus. Thus in sizing the length of the leading edge test articles, the smaller test rhombus resulting from the 2.8 Mach flow was used. This resulted in a leading edge length of 2.25". In the actual tests, the test rhombus appeared to have impinged on the end caps, and the entire leading edge appeared to be in the test rhombus.

The engineering drawing for the leading edge test article is presented in Figure 14. The design is a plug and as noted above, the length is 2.25" and the nose radius is 0.375". To miss the nosetip coolant lines, the forward region is cut at a bias as noted. The shank is designed to accommodate the retention design described in the following paragraph. Figure 14 was the engineering drawing for machining all test articles.

Leading Edge Retention and Plug vs Shell

A trade was made of using a shell vs a plug leading edge design. The plug design and the manner in which it is retained are presented in Figures 14, 15 and 16. The plug is retained along its shank by two insulator rods and a backing plate. These components extend along the length of the test article. The assembly is loaded by a set screw located in the back so that the insulator rod and backing plate are in compression. Leading edge pitch strains are countered by the set screw load (i.e., any pitch movement requires the set screw to move aft, which requires compression failure of the Zircar insulator pad). To obtain leading edge backface temperature, Type K thermocouples (TC) are placed between the leading edge back and insulator pad as noted on Figure 16. The set screw compression loads the TC junction in place.

9

A 994 graphite end cap is located downstream of the leading edge and has the same shape and retention as the leading edge. The end cap prevents the aft face of the leading edge from being heated. Thermal expansion along the leading edge and end cap impingement lines are accommodated by a grafoil spacer and Zircar insulator pad contacting the aft face of the end cap. The screw that loads this end cap assembly is noted in Figure 15.

The leading edge insulator rod and pad are sized so that the conduction losses through these components are less than the radiation loss from the shank. The rods were fabricated from Zycron H (95% zirconia) and the pads from Zircar FBD.

The shank is sized to so that the core of material that Lockheed is proposing for their "Stay Sharp" design is well within the shank's external dimensions. That is, Lockheed is proposing a central core of material that has a diameter that is 0.4 times the nose diameter. This material is reported to maintain a sharp leading edge shape during ablation, but has a low strength relative to the adjacent C-C. Thus, in the plug design, the shank width is 0.540". For a nose radius of 0.375", this leaves 0.120" of C-C material on either side of the central core for retention.

Relative to the plug, a shell design has inferior structural retention capability and the maximum amount of ablation is less. For the shell design, a central core of structure is required for retention. The central structure therefore can either 1) push against the central part of the leading edge or 2) connect to the two outer shells and the backfaces of the shell are loaded for shell retention. Relative to the plug, these options result in inferior leading edge retention because the shell's walls do not have the thickness that the plug shank has for shear load retention. Also, the ablation depth at which the substructure is exposed to the flow is less for the shell than the plug.

Boomerang Holder

The main structural member of the Boomerang model is the central copper holder presented in Figure 11b &c. The cooled nosetip is bolted to the holder's front and the nosetip coolant lines are routed to the back through two grooves located on the top and bottom surfaces of the holder. The swept edges of the holder are used to retain the leading edges (see Figures 15 and 16 for a cross-section of the retention concept). The holder's upper and lower surfaces are insulated with silica phenolic heatshields. Because of the long run duration and the proximity of the hot leading edge test articles, the holder is internally cooled.

Cooled Nosetip Design

Most of the leading edge design analyses were performed on the internally cooled nosetip. A Photograph of the nosetip is presented in Figure 10b. A cross-section of the nosetip is presented in Figure 17. The nosetip consists of an outer copper shell and an inner copper structure. The two copper parts are separated by a water passage that cools the nosetip. The

10

cooling schematic is shown in Figure 17 and involves a central water supply that impinges on the back side of outer copper shell. Water then flows around the annulus to a metering section. The metering section is used to equalize the flow so that the entire backface of the outer shell receives equal cooling. The two copper parts are structurally attached by threads and sealed by a silver braze.

The thermal design used water at a 600 psia supply pressure, which on arrival to the test was actually 480 psia. This reduction in pressure left no thermal margins in the design. Although no problems occurred with the nosetip, the outer edges of the nosetip did approach, but did not reach melt. A during test of the model and a post test photograph of a sample nosetip are presented in Figure 18. Note in the Figure 18 post-test photographs the dark region at the lateral sides. These are the regions that had very little thermal margin in the design.

Transition Section, Nosetip to Leading Edge

As noted in Figure 9, there is a C-C transition section that is placed between the nosetip and leading edge test articles. This section provides a transition between the non-ablating nosetip and ablating C-C leading edges. The transition section was designed to extend far enough downstream so that any flow separation coming off the nosetip would reattach on the transition section and not on the leading edge. The length of the transition section was selected to be 0.50" (distance along the impingement line). From video coverage of the tests, this length was observed to be sufficient to prevent reattachment on the leading edge.

A photograph of a typical transition section is presented in Figure 10c. This is a view of the face that interfaces with the nosetip. As can be noted, the thinnest section occurs at about 1:00, 5:00, 7:00 and 11:00 o'clock around its circumference. The material thickness at these locations is 0.090". This thickness dictated the run time of the Boomerang model. The selected 390 second trajectory simulation of pullout and glide was found to leave (post test) about 0.025" of C-C at these locations. Longer run times were not recommended as the transition section could have uncovered part of the copper nosetip, forming a forward facing step and "unzipping" the transition section. This "unzipping" could cause significant implications to the leading edge shape change data.

The transition sections were fabricated from FWPF C-C. For those leading edge materials that were to ablate less than C-C, the ablating transition section will cause the forward region of the leading edge to become a forward facing step. The forward step will cause augmented heating on this part of the leading edge and possibly result in an unfair test of the leading edge material. As will be described in Section 7.0, the forward facing step did occur with SAIC's and BP-Hitco's leading edges which were designed to ablate less the C-C. To test the special materials, program scope was not sufficient to supply a cooled nosetip that extended aft to the leading edge section or modify the design so the "non-ablating" leading edge could be extended up to the cooled nosetip. Thus, to test the "non-ablating" materials, the 0° sweep model described in Section 3.2 was designed and fabricated.

11

It should be pointed out that in the "actual" flight design, the nosetip experiences surface temperatures that are too high for the "non-ablating" materials to prevent, or, relative to C-C, retard ablation. Thus, the actual flight nosetip will most likely use C-C and for "non-ablating" leading edge materials, there will always be a transition from an ablating C-C nosetip and the "non-ablating" leading edge; just like there is in the Boomerang model. Thus, the Boomerang model with the ablating transition section will simulate some of the flight forward facing step phenomena. However, the Boomerang causes the leading edge test articles to be closer to the stagnation point than does the flight designs and therefore the augmented heating induced by the Boomerang on the "non-ablating" leading edge could be higher. To provide a test method for evaluating the "non-ablating" leading edge materials without the forward step, the 0° sweep model of Section 3.2 was used. The 60° Boomerang model does result in an indication of how the "non-ablating" materials will perform with the step and both the 60° and 0° model configurations were used to evaluate selected leading edge materials.

Adaptor, Boomerang to Facility Strut

An adaptor is used to install the Boomerang model on the facility sting. The adaptor is designed to serve the following functions: a) provides thermal protection to the facility strut by enlarging the Boomerang base area to cover a 3.0" dia strut, b) provides excess to disconnect the nosetip water lines, and c) routes water to and from the internally cooled main holder.

The adaptor, shown in Figures 9 and 12, consists of a copper body, two cooled plates, two silica phenolic heatshields and a sting mount. The two plates and heatshields are placed on the upper and lower adaptor surfaces. Three sting mounts were made so that the Boomerang could be canted to 0, 10 or 20° relative the nozzle centerline. These three stings were used to change the leading edge Angle-of-Attach (AoA).

Boomerang Assembly

All the components to the Boomerang were designed so that the leading edge test articles could be easily removed and installed. NASA's pre-test goal was to run a maximum of two models in one day. This required the use of two sets of Boomerang holders and model assembly procedures that allowed a Boomerang model to be turned around in a minimum of one day. To simplify model disassembly, the main Boomerang holder, the adaptor and the adaptor's upper and lower plates were all water cooled. This eliminated costly passive thermal protection that might have to sacrificed after each run. The silica phenolic heatshields were sized to last at least three runs without refurbishment. RTV60 was used as a sealant and a bonding agent (rather than epoxy). The model design and assembly procedures resulted in the ability to run two models in one day and provided excellent leading edge test results. However, because of the problems that can arise with hurry-up testing, the two runs per day were to changed to one test per day.

3.2 Leading Edge Model Design, 0° Sweep

A schematic of the 0° sweep model design is presented in Figure 19a. A photograph of all the 0° model components are presented in Figure 19b. The same exact leading edge test articles, end caps, and retention hardware used in the 60° Boomerang model are also used in the 0° design. The only differences are in the leading edge sweep angle, the model holder, and heatshield configurations. As noted above, the 0° sweep model was designed to evaluate leading edge materials with ablation rates that are lower than C-C. The 0° sweep model eliminates the forward facing step that occurs with the 60° Boomerang model when "non-ablating" leading edges are to be evaluated.

The 0° sweep model can also provide an indication of the uniformity in enthalpy and pressure that exist laterally across the test rhombus. That is, the 0° model's test article can be a "witness bar" whose ablation profile along the stagnation line can provide an indication of the uniformity of the heating across the nozzle plane at which the model is placed. Using C-C as the "witness bar" will result in an indication of the uniformity of pressure but not necessarily enthalpy. That is, when carbon ablation is dominated by carbon combustion (i.e., B' independent of temperature) then ablation will be independent of enthalpy and dependent only on pressure. Analyses will be conducted on the 223 C-C ablation test that was conducted in Run 59-021 to determine the validity of using the test results to indicate enthalpy uniformity.

Another reason for constructing the 0° sweep model was to acquire an indication of how useful the nozzle's test rhombus is in acquiring heatshield thermal and ablation test data. As will be shown in Section 7, Run 59-021, the test indicates that excellent heatshield thermal and ablation data can be acquired on wedge models tested in the 6.0 nozzle.

3.3 Calorimeter Model Design, 60° Sweep

This test series is the first time that leading edges, with significant sweep, have been tested in arc-heaters. The aerothermal conditions on the swept configuration are therefore uncertain. In comparison, the 0° sweep model conditions can be derived from the prior arc-heater calibration data base acquired on hemispherical nosetips. Laminar stagnation point boundary layer theory (Reference 2) shows that a hemisphere has 1.41 times higher heating than a cylinder with the same nose radii (cylinder in cross flow, or 0° sweep). These correlations have been confirmed by prior wind tunnel and arc-heater data. For swept leading edges, no similar arc-heater calibration data base exists, only a lot of "unverified" theory. Thus, for the 60° sweep model, it was required that a calibration model be designed and tested to quantify the leading edge aerothermal conditions and help evaluate existing theories.

The objectives of the 60° swept calorimeter model were to measure the nosetip stagnation point and leading edge impingement line pressures and heating rates for the conditions that were to be used in the material evaluations. To achieve these objectives, the calorimeter model configuration was the same as the 60° Boomerang model. The calorimeter model was instrumented for the measurement of wall pressure and convective heating rate. The

13

instrumentation locations and gage identifications that were incorporated in the model are presented in Figure 20.

In designing the calorimeter model, a compromise was required because of program scope. For the nosetip to be instrumented, program scope did not allow the nosetip to be water cooled and therefore the model could not undergo a dwell in the test section. Thus, the model had to be designed to be swept through the test section to prevent overheating, especially the nosetip calorimeter. This sweep operation prevented use of the NASA pressure transducers because of the long line lengths between the model and the pressure transducers. The lines were over 10' long and therefore slow time responses could be expected. Thus, it was desired to use miniature Kulite transducers so that pressures could be measured in the model. Program scope did not allow the purchase of the Kulite transducers and therefore AEDC was requested to loan their Kulites transducers for the test series. AEDC supplied 4 Kulite transducers. The Kulites were located in the adaptor section of the model, see Figure 21a. The lowest range of Kulites that could be obtained from AEDC were for 0-50 psia. The maximum stagnation pressures were about 14 psia, thus all measurements occurred at the low end of the transducer scale.

In the actual use of the cal model, NASA was not able to sweep the model through the test section fast enough to prevent over heating of the nosetip's calorimeter. NASA's fastest sweep resulted in the model being exposed to high heating for about 1.2 seconds. At the peak pullout heat flux, this resulted in burnout of the nosetip calorimeter.

The calorimeters used in the model included Gardon gages procured from Thermogage and Null-Points procured form Medtherm. The baseline calorimeter was the Gardon gage because of its ability to be laboratory calibrated before installation into the model and its ruggedness. Both calorimeters have response times on the order of a few milliseconds. In the assembly of the calorimeters into the model, the lead wires of the Medtherm calorimeter failed up in the lead wire sheath. Attempts to repair the leads were unsuccessful. All the Thermogage calorimeters operated as expected during the calibration runs.

Photographs of the calorimeter model are presented in Figures 8 and 21. In the cal model design, assembly was very difficult because of the amount of instrumentation and size of the model. The space available for connecting the pressure lines and routing the calorimeter leads can be noted in Figure 21a. This compactness required that the pressure lines be soldered at both ends prior to assembly. Thus, in the disassembly of the models, it was not possible to un-solder the pressure lines without overheating the calorimeter lead wires. Thus, in repairing the nosetip calorimeter after Run 59-008 (see Section 4.0), it was required to cut the two leading edge pressure lines. Therefore, leading edge pressure data were not obtained after Run 59-008.

14

4.0 TEST CONDITIONS AND MODEL CALIBRATIONS

4.1 Desired Test Conditions

The leading edge flight aerothermal conditions are presented in Figures 2 and 4. For reference, the corresponding nosetip conditions are also presented in Figure 2. The Figure 2 predictions were obtained from SPARTA, Reference 1. In Reference 3, LMSC made a comparison of the analysis techniques used by LMSC, SPARTA and TRW to predict leading edge conditions. These comparisons for the laminar portion of flight are summarized in Figure 22 wherein it can be seen that the LMSC enthalpy and convective coefficients are both about 15% lower than SPARTA's. Figure 22 presents the SPARTA aerothermal conditions for the pullout and glide portions of the extended range trajectories. At the time the test series conditions were defined, it was not known which prediction technique was most applicable and therefore the SPARTA conditions were arbitrarily selected.

In selecting the NASA-AMES 60MW conditions, the Figure 22 scaling law was used to account for the differences in the flight and Boomerang leading edge sweep angle (70° vs 60°). Because NASA has an extensive data base on hemispherical nosetip heating and the corresponding facility conditions required to obtain them, the nosetip conditions of Figure 22 were adjusted to obtain the flight heating rates on the 60° swept Boomerang model. That is, to obtain the flight pullout leading edge heating rate of 1020 Btu/ft2-sec (flight sweep angle is 70°) on the 60° swept Boomerang leading edges, the corresponding nosetip heating rate is 2325 Btu/ft2-sec [=3400 x (cos70°/cos60°)]. Likewise, to obtain the flight glide leading edge heating rate of 240 Btu/ft2-sec on the 60° swept Boomerang leading edges, the corresponding nosetip heating rate is 550 Btu/ft2-sec [=800 x (cos70°/cos60°)].

To achieve these leading edge heating rates, NASA estimated that the pullout conditions could be obtained with the arc operating at 2820 amps, 6700 volts and an arc column supply pressure of 85 psia (and no cold mixing air). For glide, the arc parameters were estimated as 200 amps, 2700 volts, 55 psia arc column pressure (which includes about 50% cold mixing air).

In order to simulate the heating transients of flight (see Figure 2), it was decided that simulating both the ramping up to peak pullout heating rate and the ramping down to the glide value was risky as all this had to done manually. In discussions with the facility engineers, it was decided to only simulate the ramping down from pullout to glide. The planned facility mode of operation for simulating the flight heating rates _and_ transients is presented in Figure 23. This includes starting the arc and reaching the facility conditions corresponding to the peak heat rate of pullout (on the leading edge). After the arc was stabilized, the model is inserted into the test section. After 45 seconds of dwell at this condition, the arc column supply pressure and the arc current are decreased, in the steps noted in Figure 23, so that at 90 seconds the desired glide heating rate is achieved. The run is terminated after a 390 second exposure. The 45 and 90 second time periods in the test result in the integrated heat load occurring in flight at the end of peak pullout heating and at the start of glide, respectively. The 390 second period was dictated

15

by transition section ablation. As noted in Section 3.1, the transition section can be expected to fail for dwells longer than 390 seconds because of burn through.

4.2 Test and Model Condition Calibrations

Calibration Runs

The objectives of the calibration runs were: 1) to verify the facility conditions that produce the desired pullout and glide leading edge heating rates, 2) determine the validity of the leading edge aerothermal analyses in predicting swept leading edge pressures and heating and 3) to determine the ability and reproducibility of ramping down from pullout to glide. A summary of all the calibration runs is presented in Table 2. This figure presents the time average facility conditions and the time averaged calibration model pressure and heating rates. The detailed plots of all these data as a function of time are presented in Appendix A.

In all the calibration runs, the Boomerang calibration model shown in Figures 20 and 21 was used. No facility models were used. The stagnation point data obtained from the Boomerang model agreed with the NASA data base and the added expense of modifying the facility to accommodate both the NASA and Boomerang calibration model was not justified.

The calibration runs started out by characterizing the glide conditions. This involved stabilizing the arc at the lowest achievable conditions (without mixing air) and rotating the calibration model in and out of the test section to obtain data. This in and out operation resulted in having the calibration model exposed to the test section heat load for 1.2 to 1.5 seconds, depending on how the actuator was set. After this first exposure, the conditions were changed by adding mixing air. The arc column air flow valve was not changed and therefore the change in arc column pressure noted in Figure 23 is a result of adding the mixing air (the mixing air is introduced aft of the arc anodes, in the nozzle entrance section). With the mixing air condition stabilized, the model was re-inserted back into the test section. Upon re-insertion the noise level on all calorimeter instrumentation channels was extremely high, not allowing the calorimeter responses to be identified. However, the output of the Kulite pressure transducers had, in most cases, low noise allowing pressure data to be acquired. This noise was obtained in all cases where cold mixing air was used. Calibration runs 59-001, -002, -003, and -007 were attempts to obtain calibration data with cold mixing air. In all these runs, changes were made in the instrumentation setup, filtering and signal conditioning in an attempt to obtain data with mixing air. As noted in Table 2, no data could be obtained with mixing air. Thus, the lowest condition that the 60MW could be reliably operated without mixing air and we had good calibration data on the Boomerang model was selected as the glide condition.

It was uncertain what cased the excessive noise during cold mixing air injection. NASA operates with the model and instrumentation leads all ungrounded (or electrically floating). AEDC operates with the model grounded and the other side of the instrumentation leads ungrounded. The AEDC logic is that the arc will usually decide how and where the model will be grounded and this occurrence can be unstable. The unstable behavior is postulated to be due

16

to changes in the degree of grounding and the grounding location. During the tests, NASA was willing to try model grounding but was worried about causing failure of the instrumentation signal conditioning. The program scope was not sufficient to warrant this risk and, therefore, the glide condition was selected as not having cold mixing air.

In attempting to correct the instrumentation noise, Runs 59-001 through -004, the nosetip's stagnation point calorimeter gradually became oxidized (or over heated) and finally on Run 59-006, experienced a burn through. Changing this calorimeter, however required cutting the two leading edge pressure port lines (see Section 3.3) and therefore it was decided to obtain leading edge heating and pressure data before this operation was attempted. Thus, in Runs 59-007 and -008, the nosetip calorimeter was not functional but all the leading edge instrumentation were. After run 59-008, the nosetip calorimeter was replaced and calibrations were made to obtain nosetip and leading heating rates. Because the leading edge pressure lines had to be cut to replace the nosetip calorimeter, no leading edge pressure data was acquired after Run 59-008. Also, because of the severity of the peak pullout heating rate on the nosetip calorimeter, measurement of this condition was not attempted again (the attempt in Run 59-006 resulted in calorimeter failure). Rather, 0.7 times the peak pullout value was measured in Run 59-012. This condition also represents a point in the ramp down sequence in going from pullout to glide.

Calibration Results

The results of the calibration runs are summarized in Figure 23. Sample plots of the pressure and heat flux data as a function of time are shown in Figure 24. The figure presents representative plots of the calibrations conducted for the glide, 0.7 times the pullout, and the pullout conditions. All the calibration data that was acquired in the test series (and the facility conditions that existed during these measurements) is presented in Appendix A.

Important features to note in the Figure 23 data are the time responses of the calorimeters and pressure transducers. Referring to Figure 20, the calibration model was rotated so that the east side entered the test section first and therefore the east side exited last. Thus, measurements on the east side responded before the nosetip and west side instrumentation and then lasted longer. Also, the instrumentation transient responses are fairly uniform, except for the nosetip calorimeter. The nosetip is exposed to the highest heating rate. Therefore, the decay noted for the 0.7 time pullout heating (called "intermediate" in the figure) is probably due to calorimeter over heating. Calorimeter calibration is valid for temperatures less than 500°F. This temperature was exceeded in both the intermediate and pullout calibrations. In fact, for the pullout condition, the nosetip calorimeter failed, possibly causing the noted transient behavior.

A comparison of the measured data and predicted conditions are presented in Figure 25. As can be noted, the measured stagnation point pressures were in exact agreement with NASA pre-test predictions. The measured stagnation point heating rates were within 20% of NASA's pre-test predictions. The predictions derived by LMSC and SPARTA are presented in Figure 25 as ratios of leading edge-to-nosetip heating and pressure values. The ratios are compared rather than the absolute values because the predictions did not necessarily correspond, exactly to the

17

arc calibration conditions. From Figure 25, it can be concluded that the LMSC leading edge predictions are in closer agreement with the data than SPARTA's.

Comparing the measured leading edge conditions of Figure 25 to the flight (or desired) conditions of Figures 2 and 22, it is concluded that the pullout heating is lower than desired and the glide value is about correct. Even through the facility can increase the arc current and pressure to result in higher pullout heating, this could not be done because of the cooling limitations of the Boomerang nosetip. Referring to Figure 5, it can be seen that the facility can increase arc power and pressure to result in a net increase in nosetip (and therefore leading edge) heating of about 30%. This increase, however, cannot be accommodate by the nosetip which was designed to operate at a maximum heat flux of 2320 Btu/ft2-sec with a water supply pressure of 600 psia. This inability is partly due to the fact that the SPARTA predicted conditions were used to design the Boomerang model. As noted in Figure 25, the SPARTA predicted ratio of leading edge-to-nosetip heating is higher than measured and that predicted by LMSC. Thus, to obtain the desired leading edge heating, the nosetip heating has to be increased above the 2320 Btu/ft2-sec that was used in the nosetip cooling design. Also, the facility water supply pressure is 480 psia rather than the 600 psia value used in the nosetip design. Thus, in the leading edge tests, the pullout value was about 620 Btu/ft2-sec, lower than the SPARTA predicted flight heating of 1020 Btu/ft2-sec. It should be noted, that the LMSC predicted flight conditions may be lower than SPARTA's because of their lower ratio of leading edge-to-nosetip heating. Thus, the LMSC flight leading edge heating rates may be in more agreement with the 620 Btu/ft2-sec that was actually used in the tests.

The glide heating rate that will be used in the tests is about 220 Btu/ft2-sec as noted in Figure 25. This compares to the 240 Btu/ft2-sec predicted by SPARTA. Since this SPARTA value may be too high, the 220 Btu/ft^2-sec glide value actually used in the tests may be correct for the LMSC flight values also.

It is recommended that further leading edge boundary layer analyses be conducted on the calibration runs of Table 2 and flight to evaluate the validity of the analysis techniques and calibrations.

5.0 TEST SETUP AND INSTRUMENTATION

5.1 Test Facility Setup and Facility Instrumentation

A schematic of the facility test cell is presented in Figure 7. The figure identifies the model insertion mechanism, the facility strut, the vacuum envelope (or test cell), water cooling supply-return for the model, instrumentation connection panel, and the exhaust diffusor. The figure shows the model in the test location (on nozzle centerline and 3.0" aft of the nozzle exit plane). The location of the pyrometers and video camera for making during test measurements are presented in Figure 7 for the 60° sweep Boomerang model. The video and pyrometer arrangements for the 0° sweep model are presented in Figure 26. In both cases, video coverage of the models was obtained from the window mounted on the ceiling of the test cell. For the

18

Boomerang model, this allowed the planform of both leading edges to be viewed at the same time. For the 0° sweep model, the video covers the planform of the leading edge; but because the camera is offset slightly aft of the model, it is difficult to view the stagnation line.

For the leading edge tests, one window had optical properties suitable for acquiring pyrometer surface temperature data. This window and pyrometer are noted in Figure 7 and were used to obtain surface temperature data. Note that the image of the leading edge is reflected off a gold plated mirror, through the test cell window and onto the pyrometer's aperture. For the Boomerang model, this pyrometer viewed the west leading edge test article about normal to the impingement line. For the 0° sweep model, this pyrometer viewed the leading edge's stagnation line but at a angle of about 80° off normal. To acquire surface temperature data on the east side, a pyrometer was mounted inside the test cell. This pyrometer viewed directly the leading edge. For the Boomerang model, this pyrometer viewed the east leading edge test article about normal to the impingement line. For the 0° sweep model, this pyrometer viewed the leading edge's sonic line. The pyrometer orientations relative to the test articles and the pyrometer spot sizes are presented in Figures 7 and 26 for the 60° sweep Boomerang and the 0° sweep model, respectively.

The west pyrometer was a Mikron instrument (Model M90V). NASA had verified vendor supplied calibration for this instrument. The instrument operates at a wavelength of 0.65 microns and is reported to "saturate" at temperatures above 5430°F. For this pyrometer, the vendor supplied calibration data, a test cell window transmissivity and a mirror reflectivity product (τ x r) of 0.9, and a leading edge emissivity of 0.85 were used in the data reduction.

The east pyrometer was a Mikron instrument (Model M668). NASA had vendor supplied calibration constants for this instrument. The instrument operates over a wavelength range of 0.78 to 1.06μ and is reported to "saturate" at temperatures above 4720°F. For this pyrometer, the vendor supplied calibration data and a leading edge emissivity of 0.85 were used in the data reduction.

The facility instrumentation entailed that which was needed to monitor the health and conditions of the facility. Facility instrumentation that were important in denoting the actual delivered nozzle freestream conditions were the arc current, arc voltage and arc column pressure. The facility instrumentation sampling rate was 1 Hz for the leading edge tests and 20 Hz for the calibration runs.

5.2 Model Instrumentation

The model instrumentation included two backface thermocouples (TCs) on each leading edge test article and TCs on the nosetip water inlet-outlet lines. TC numbers T4 and T6 were mounted in the forward region of the leading and T5 and T7 in the aft region. T6 and T7 were on the east leading edge and T4 and T5 on the west. In all cases, the TCs were Type K (chromel-alumel). These TCs are limited to about 2300°F, considerably lower than that expected for the leading edge backface. Relative to Type K's, higher temperature TCs mean more cost

19

and/or less ruggedness. Because of the large number of leading edge test articles and the need to turn around each model in 1 day, it was decided to stay with the Type K.

The manner in which the leading edges were instrumented with TCs, is shown in Figure 16. Thermal contact between the TCs and the leading edge backface is insured by loading an insulator pad from the back with a set screw. TCs conduction losses through the lead wires is minimized by having the junction and a portion of the lead wires, in contact with the leading edge backface (junction and about 0.10" lead wires in isothermal zone, wire diameter is 0.003"). A near adiabatic condition on the leading edge backface and TC was insured by using a Zircar insulator pad.

The water inlet-outlet lines were instrumented with TCs by either soldering or epoxy bonding the junction to the line. In both cases, neither resulted in good data. Maintaining thermal contact during the run was probably the reason for the unsatisfactory data.

5.3 Model Assembly and Facility Installation Procedures

Model assembly involved first measuring the weight and initial thickness of each test article. Referring to Figure 12, model assembly then involved inserting the transition section on the nosetip and the nosetip was then installed on the main structure. The leading edge backing plate, insulation pads and TCs were installed in the main structure and the leading edge test articles inserted in the retention cavity. The two retention pins were then inserted and the back set screw tighten to pre-load the leading edge. The end caps and their respective backface pad, retention rods and aft end insulation were then installed. The axial screw at the base of the Boomerang was used to load the end cap and leading edge against the C-C transition piece. RTV60 was used to bond the upper and lower heatshield on and seal all joints between the leading edges and heatshields. The heatshields fasteners were then tightened and the screw heads filled with RTV60.

Between the leading edges and C-C transition section (see Figure 15), a trade was made as to using grafoil to insulate the leading edges from the transition section. The use of grafoil would form a gap between these two pieces and with the possible orientation of the flow streamlines in the region, this gap could cause a forward facing step. Because the heating associated with this gap could be high, it was decided not to insulate the leading edges from the transition section. In reviewing the test videos, conduction cooling of the forward edge of the leading edge was found to be high and the use of grafoil insulation would probably have been a better decision.

In installing the model onto the facility sting, it was important to connect the correct nosetip water line to the inlet. As noted in Figure 17, nosetip cooling occurs by the impingement of a centralized water jet (inlet) on the stagnation region. Reversing the water lines so that the central jet is now the outlet will reduce the cooling capability and cause possible overheating. After the model was installed on the sting, the model's stagnation point was centered on the nozzle centerline and all pitch and yaw angles nulled to zero. For Run 59-019, which has a pitch

20

angle of 10°, this was the exception. For this run, the nosetip was pitched down so that the nosetip stagnation point was 0.44" below nozzle centerline. This resulted in the axial center of each leading edge (Station 2.5" from the nosetip stag pt) to be on the nozzle centerline plane. Thus the forward half of the leading edge impingement line is below the nozzle centerline and the aft half is above.

After the model was aligned, the video camera and pyrometers were aligned and the instrumentation was connected. Instrumentation, pyrometers and video were then checked in the control room to insure the data acquisition system was functioning properly. The model's water cooling system was finally pressure checked by operating the pumps. If the instrumentation was working properly and no leaks were observed in the test cell, the run was initiated.

6.0 TEST MATRIX

Tests were conducted in the NASA-AMES 60MW from 3 August through 6 Sept 94. There were a total of 23 runs involving the following model configurations:

1) Eleven (11) calibration runs (see Section 4.2 and Table 2);

2) Eight (8) leading edge runs at 60° sweep (= 16 leading edge test articles);

3) Three (3) leading edge runs at 0° sweep (= 3 leading edge test articles), and

4) One (1) nosetip run (using the model holder used in the GFY93 LCAT tests, Reference 2).

The test variables, test article materials and conditions for each of the runs are summarized in Figure 27. The leading edge test variables included:

a) Sweep Angle. Leading edge sweep angles of 0 and 60° were tested;

b) Material Type. The materials included FMI's 223 PAN, Textron's FWPF; GE's 4DO; SAIC's 4D in-plane HFC-HfB$_2$ filled C-C with an Ultramet HfC-SiC coating, Hitco's Ceracarb; and an MSNW HfC impregnated carbon "sack" over Poco graphite.

c) Fiber Orientation. The "Z" fibers were oriented parallel or perpendicular to the leading edge impingement line and/or normal to the Boomerang's bases. For 223 and FWPF, the Z fibers were either parallel of perpendicular to the impingement line. For the 4DO material, the Z fibers were perpendicular to the model base (i.e., intersected the impingement line at the sweep angle.

d) Model AoA. The model Angle-of-Attack was nominally 0°. One run was conducted at 10°;

21

e)   Trajectory Sequence. This involved testing at glide only, pullout then ramp to glide (and then stop), or combined pullout-ramp down-glide;

f)   Test Reproducibility. The same material was repeat tested on the same side of the Boomerang and also on the opposite side (effects of test and model holder side).

The 223 and FWPF C-C materials (including the FWPF transition section) were obtained from MK21 nosetips, except for one of the 223 leading edges (FMI #12) which was purchased from FMI. All C-C were qualified to MK21 specs. All C-C leading edges and transition sections were machined by FMI using the same machining tolerances and processes as were used in the GFY92 and GFY93 nosetip tests, Reference 2. The Hitco, SAIC and MSNW leading edges were machined by the respective suppliers. The SAIC nosetip was the nosetip that was already tested in the GFY93 LCAT tests and did not experience any ablation in that test. This nosetip was retested in Run 59-015.

The test matrix for the 3 August through 6 Sept 94 test series is summarized in Table 3. The table summarizes for each run, the model configuration, the test material, the fiber orientation, the heat flux history that was simulated in the run, the post test weight loss, the impingement line dimensional changes, and the inferred surface temperature. The test series started out by running the glide only condition first (Run 59-009) in order to check the model design at a low heating condition. With the design performing as expected, the next run involved the pullout and transition to glide condition (Run 59-013). The results of these two runs were used to determine what the dwell should be for the combined pullout and glide runs that followed. As expected, the C-C transition section ablation was found to dictate the dwell time for the remaining models. The combined dwell of 390 seconds was concluded to leave sufficient margin so that transition section failure would not occur.

7.0 TEST RESULTS

This section presents an overview of the tests results followed by a discussion of each individual test. The individual test discussions are presented in the sequence in which the test were run. Table 3 summarizes the test sequence and also summarizes the test results. The ablation measurement locations denoted as "Fore" and "Aft" are defined in Figure 14. Video coverage was provided for each run. Table 4 summarizes the quality of the video and phenomena that can be observed in the video.

7.1 Summary of Test Results

Overall, the test series was very successful in achieving all test objectives. The facility performed very well and all tests were completed on time and on budget. Leading edge material thermal and ablation responses were measured in a "well" characterized and reproducible environment. All indications show that very little contamination (or particle impingement from arc column copper) occurred and the test core that influences the leading edge ablation is nearly uniform in both pressure and enthalpy. One definite particle impingement was observed and this

occurred on the copper nosetip in Run 59-013. Possible copper contamination may have occurred in Run 59-022 as a copper colored residue was observed in the melt zone of the SAIC leading edge. The uniform ablation profile that occurred along the 0° sweep test of a 223 leading edge (Run 59-021) indicates uniform pressure and maybe enthalpy. That is, in certain regimes of carbon ablation in air, the ablation of carbon can be independent of surface temperature (and therefore recovery enthalpy). Therefore the ablation regime of the Run 59-021 test article needs to be checked in order to determine if the measured uniform ablation also indicates enthalpy uniformity. The heatshields located in the upper and lower surfaces of the model also experienced uniform ablation. Silica ablation is extremely dependent on surface temperature, thereby possibly inferring uniform pressure and enthalpy.

The repeatability of the test conditions appears to be acceptable. The FWPF leading edges of Runs 59-014 and -018 were repeatability tests and the weight losses are within 1.3% of one another. The 4DO tests of Runs 59-016 and -017 were repeatability and effect of side tests. The weight losses are within 1.3% of one another. This is considered excellent test repeatability. It should be noted that the 60MW is not really designed to operate at the low pressure and current levels required for glide condition. At this condition it was sometimes difficult to maintain that condition for the entire test sequence (pressure fluctuations of about 15% were observed in some runs). The pullout condition and the manual ramp down from pullout to glide both appeared to be fairly reproducible.

Calibrating the leading edge aerothermal conditions was satisfactory, although some problems occurred in obtaining calorimeter data with cold mixing air. After reviewing how the mixing air is injected into the arc flow, it is probably for the best that calibration data was not obtained at this condition and, therefore, this condition not used in the glide simulations. That is, the manner in which cold mixing is added appears to add a gradient in the enthalpy that occurs across the test section flow. This is not desired for the Boomerang tests.

Also, the facility sweep rate did not allow calibration of the nosetip heating rates at the pullout condition because of calorimeter overheating. This is, however, not a significant issue because of the large facility data base that can be used to infer the actual nosetip condition. What is sacrificed without the direct measurement of nosetip heating, is the determination of the ratio of leading edge-to-nosetip heating that occurred in the tests. The direct measurements of both in the same run are probably more accurate than the measurement of one and NASA's prediction of the other.

Overall, everything fit, everything worked and there were no serious problems. Flow spillage occurred for the 0° sweep model which caused the facility actuator arm to fail and cause early termination of the run (Run 59-021). Also, the 600 psia water pressure used in the design of the nosetip was actually 480 psia, preventing the Boomerang from being able to be run at the maximum possible facility condition. Also, after Run 59-017, one of the water pumps failed causing a 10% reduction in water supply pressure for the remaining runs. The reduction in water pressure did not cause any problems.

23

In reviewing all the test data, the test hardware performed very well with little changes recommended for future improvement. The only design feature that is recommended to be changed is that a thin piece of Grafoil be placed between the C-C transition section and the leading edge to reduce the conductive interchange. In all cases but one, the supplied leading edge test articles were of excellent dimensional quality. For the test article of Run 59-023, the leading edge was not even close to the Figure 14 dimensions, resulting in the stagnation line of the model being proud by over 0.10" relative to the adjacent end caps. Also a large gap existed beneath the leading edge outer sock and Poco graphite substrate that could not be covered by the 994 end caps.

The test variable results are presented in Table 5 and can be summarized as follows:

a) Sweep Angle. The differences between the 0 and 60° were as expected. For the 60° sweep there is a variation of ablation along the impingement line that appears to correspond to the measured difference in heating obtained from the calibration model. The maximum recession is in the forward location (except the region in contact with the transition section), tapering off towards the aft end. From the post test ablation profiles, there appears to be no test rhombus intersection with the leading edges or end cap. However, the video inferred temperatures appear to indicate that the test rhombus intersects about in the middle of the end cap. The 0° sweep ablation profile for the C-C material (Run 59-021) appears to be very uniform along the stagnation line, as do the two 994 end caps. Both the 0 and 60° leading edge ablation profiles denote fully laminar flow but the nose blunting that occurred in the GFY93 LCAT nosetip tests is not as severe in the leading edges.

b) Material Type. As indicated in the LCAT nosetip tests, the FWPF ablates slightly less than the 223 but the difference is insignificant. The 4DO ablates about the same as the other C-C materials. From preliminary post test observation, no divots are indicated on any of the C-C materials. The SAIC C-C material underwent, essentially, immediate ablation on entry into the test section for all conditions tested. This was evident from the sparks that were observed downstream from the test articles, which appeared to be originating from the impingement line region. This immediate ablation may be due to thermostructural failure of the coating or the occurrence of melt. Further examination is recommended. Hitco's Ceracarb was tested at the glide condition only, and appeared to behave extremely well early in the run, but after about 90 seconds into the dwell, the middle portion (axial center) of the impingement line appeared to undergo melt. This melt persisted throughout the run. The melt appeared to flow at a bias angle relative to the impingement line and appeared to terminate at about the initial sonic point. The MSNW material appeared to have survived the initial thermostructural loads but under went ablation after about 10 seconds of dwell, as evident by the formation of downstream sparks. Failure of the entire "sock" occurred after about 90 seconds of dwell.

c) Fiber Orientation. Ablation and shape change appeared not to be significantly influenced by the "Z" fiber orientation. For 223, the Z fibers aligned ⊥ to sweep ablated 1.3% more

24

than $\parallel$ to sweep (Run 59-014 and -016, respectively). For FWPF, just the reverse was found; the Z fibers aligned $\perp$ to sweep ablated about 3% less than $\parallel$ to sweep (Run 59-014 & -018 vs -017, respectively). These variations are within the test-to-test variation and fiber orientation is concluded to have little effect.

d) Model AoA. The AoA appears to influence shape change as expected. The location of maximum recession appears to move about as much as the AoA moves the impingement line location. For both 223 and FWPF, the 10° AoA models ablated about 2% less than the 0° models (based on weight loss). The biggest AoA effect is observed to occur in the downstream heatshield. The strength and number of vortices shed off the leading edges onto the downstream heatshield appear to increase with AoA. This occurrence should be further evaluated for future heatshield ablation testing.

e) Trajectory Sequence. The addition of the ablation and weight losses that were measured for glide only and pullout-ramp down are about 8% less than the leading edges that underwent the entire trajectory sequence in one test. that is, add Run 59-009 ablation to Run 59-013 ablation and compare to Run 59-014 ablation.

f) Test Reproducibility. Test reproducibility was excellent. There appeared to be no effect of which side the model was tested on or in which run. The ability to repeat the ramp down from the pullout condition to the glide condition appeared to be satisfactory.

Surprises that occurred in the test can be summarized as follows:

1) For the Boomerang model, the thermal contact between the C-C transition section and leading edges appeared to be excellent as evident from video inferred temperatures. Conduction from the forward region of the leading edge to the transition section appeared not to have influenced C-C leading edge ablation but it did the coated material (SAIC Run 59-018) and Ceracarb material (Run 59-020). In subsequent leading edge tests with the Boomerang model, a thin piece of Grafoil should be place between the transition section and leading edges to reduce conduction cooling of the leading edges.

2) The actual ratio of leading edge-to-nosetip heating rate was lower than the Reference 1 pre-test predictions.

3) The 60MW cooling water is supplied to the test cell at 480 psia and not 600 psia. This partly influenced the inability to increase facility operating conditions to increase the leading edge heating rate during pullout.

4) The calorimeter model did not acquire heating data when cold mixing air was injected into the arc air. This may be eliminated if the model is grounded and not allowed to "float". The model grounding procedures used by AEDC are recommended in the future if calibration problems should again become an issue.

5) Vortices occurred in the adaptor heatshield that resulted in higher than expected ablation. This was especially true of the test at 10° AoA (Run 59-019). This did not result in any test compromises, but it did require using all the spare heatshields.

6) The nozzle exhaust impinged on the nosetip water lines that were routed external from the strut (especially with the model out of the flow). This caused the facility to wrap the lines with insulation to prevent heating of the nosetip cooling water. Also with the 0° sweep model in the flow, the nozzle exhaust was diverted down onto the test cell floor causing certain facility components to over heat. This was solved by covering the floor with insulation blankets.

7) For the leading edges that were not C-C and tested on the Boomerang model, some surprises occurred. After the C-C transition section underwent ablation, the flow separated off the cooled nosetip, as expected, and impinged on the forward part of the leading edge. This impingement induced a recirculation flow over the entire portion of the C-C transition section. This recirculation caused leading edge material (not carbon but possibly oxides from the SAIC and Hitco materials) and some of the silica from the heatshield to be deposited on the transition section. This was observed not only on the Boomerang side that tested the SAIC and Hitco materials (Runs 59-018 and -020) but on the other side that tested C-C. No similar deposits were observed on Boomerang models that tested C-C on both sides.

8) The Hitco Ceracarb material underwent ablation phenomena that was not expected before the run. On examining the video and post test specimen the ablation phenomena is postulated to be: a) the transition section cools the Ceracarb so that the forward portion of the leading edge can resist the augmented heating at this forward facing step, b) the Ceracarb that does not benefit from transition section cooling, undergoes melt, c) this melt flows along the impingement line flow up to the sonic region along a bias, d) as the melt flows to a lower heating region, the melt becomes very viscous (slows down) and may freeze, and e) this melt flow and resolidification causes the "gouge" observed along the impingement line of the post test model. This explanation was selected over another that involved the formation of a shock at the forward facing step (caused by the ablating transition section), and shock reflection off the expansion region of the test rhombus, back toward the model. From plotting the shock and reflected expansion lines, this postulate does not appear reasonable because of model size in relation to the test rhombus.

9) The fact that the SAIC material underwent almost immediate ablation at all conditions tested in the arc, was a surprise based upon the data reported by Ultramet. In this test series, the SAIC material was exposed to heating rates of 620, 630 and 900 Btu/ft2-sec in the 60° Boomerang (Run 59-018), the 0° sweep model (Run 59-022), and the nosetip model (Run 59-015) configurations, respectively. In the Progress review at LMSC (Nov 93), Ultramet indicated that the material has survived heating rates of over 700 Btu/ft2-sec with no problem. In this test series, the SAIC material underwent significant ablation.

26

10) For the 0° sweep model, the gaps and channels that existed between the end caps and the SAIC and MSNW materials appeared to be the reason for the severity of aggravated ablation that was observed in the respective tests (Runs 59-022 and -023). These gaps and channels caused significant aggravated ablation and early termination of both tests.

7.2 Discussion of Individual Test Results

The following paragraphs discuss the individual tests in the order that they were ran. Table 3 should be referred to denote the material and test variables. For each test, the facility conditions and model data are presented. Also for each run, post test photographs are presented of the assembled model and each disassembled leading edge. The leading edge photographs show the front (impingement line is in the center of the view), planform and the profiles of each end. To scale the photos, initially all model lengths were 2.250" (±0.002") and the distance from backface to impingement line was 1.010" (±0.002"). This was not true for the MSNW model as these measurements could not be made for that model.

Run 59-009. The objectives of this run were to a) obtain glide only ablation data and b) evaluate the performance of the Boomerang design. The facility and model performed as expected. Both leading edges appeared to have laminar shape change. The test data and model photographs are presented in Figure 28. The two pyrometers viewing the two leading edges are in excellent agreement indicating a steady state temperature (at the impingement line) of 3550°F. The backface thermocouples (TCs) performed in a well behaved manner with the two forward TCs (T4 & T6) reading higher than the two aft TCs (T5 & T7). The surface and backface thermal responses for 223 and FWPF were essentially identical. There was no indication of the test rhombus intersecting the test articles (seen either as a change in temperature in the video or ablation profile along the impingement line). As the transition section ablated, the flow appeared to separate off the cooled nosetip and reattach in the forward part of the transition section (separation inferred as the dark region of the transition section in the video). At the end of the test, the separation region appeared to cover the forward 25% of the transition section.

Run 59-013. The objectives of this run were to a) obtain pullout and transition to glide (but not glide) ablation data and b) evaluate the performance of the Boomerang design at high heating rates. The facility and model performed as expected. Both leading edges appeared to have laminar shape change. The test data and model photographs are presented in Figure 29. The two pyrometers viewing the two leading edges are in excellent agreement indicating a peak temperature (at the impingement line) of 4300°F and following the heating decay to the glide condition. The backface TCs did not respond in a well behaved manner, indicating some kind of thermal contact problem. In measuring the transition section ablation and comparing it to the ablation depth from Run 59-009, it was concluded that a total dwell time of 390 sec for the pullout-transition-glide runs would not result in burn through. There was no indication of the test rhombus intersecting the test articles (seen either as a change in temperature in the video or ablation profile along the impingement line). As the transition section ablated, the flow appeared to separate off the cooled nosetip and reattach in the forward 25% of the transition section (separation inferred as the dark region of the transition section in the video).

Run 59-014. The objectives of this run were to a) obtain pullout-transition-glide ablation data and b) evaluate the performance of the Boomerang design in a long duration test at both high and low heating. The transition section had about 0.030" of material left after the test, indicating that slightly longer dwells could cause model problems. Both leading edges appeared to have laminar shape change. The test data and model photographs are presented in Figure 30. The two pyrometers viewing the two leading edges are in excellent agreement indicating peak pullout and steady state glide temperatures (at the impingement line) of about 4300 and 3600°F, respectively. The backface thermocouples (TCs) performed in a well behaved manner up to burnout. Type K TCs are reported to fail at about 2500°F which is what apparently occurred in the run. As the transition section ablated, the flow appeared to separate off the cooled nosetip and reattach on the transition section (separation inferred as the dark region of the transition section in the video). The separation region was concluded to cover about 75% of the transition section's length at the end of the run. Thus, for the testing of leading edges, the influence of the non-ablating nosetip appeared to be handled by the transition section, with apparently minimal influence on the leading edge test articles, at least for the C-C leading edge materials.

Run 59-015. The purpose of this run was to obtain ablation data on the SAIC nosetip that was tested in the FGY93 glide tests at MDC's LCAT facility. In LCAT (Reference 2), the nosetip was exposed to a cold wall heat flux of 410 Btu/ft2-sec and recovery enthalpy of 3200 Btu/lb for 400 sec with no measurable ablation. The objective of this test was to increase the heat flux to about 900 Btu/ft2-sec (the lowest value in the test series) for 60 seconds to determine its ablation performance. The test data and model photographs are presented in Figure 31. The two pyrometers viewing the nosetip are in good agreement indicating gradually increasing temperature to about 4500°F (emissivity assumed 1.0). The model was not instrumented with TCs. As noted in the post test photograph the nosetip experienced shape change. From the video, sparks were evident about 10 sec after entry, indicating the onset of ablation.

Run 59-016. The purpose of this run was to obtain pullout-transition-glide ablation data on 4DO and 223 with the Z aligned along the impingement line (parallel to sweep). In the above tests the 223 Z was aligned perpendicular to the impingement line. The test data and model photographs are presented in Figure 32. This test was very similar to 59-014. The two pyrometers viewing the two leading edges are in excellent agreement indicating peak pullout and steady state glide temperatures (at the impingement line) of about 4300 and 3500°F, respectively. The backface thermocouples (TCs) performed in a well behaved manner up to burnout. The surface and backface thermal responses for 223 and 4DO were essentially identical.

Run 59-017. The purpose of this run was to obtain pullout-transition-glide ablation data on 4DO (a repeat of 59-016 except on the opposite side) and FWPF with the Z aligned along the impingement line (parallel to sweep). The test data and model photographs are presented in Figure 33. This test was very similar to 59-014 and -016. The two pyrometers viewing the two leading edges are in excellent agreement indicating peak pullout and steady state glide temperatures (at the impingement line) of about 4400 and 3600°F, respectively. The backface thermocouples (TCs) performed in a well behaved manner up to burnout. The surface and backface thermal responses for FWPF and 4DO were essentially identical. The streamline flow

over the leading edge can be partially observed from the video by noting the flow behavior of the RTV melt runoff.

Run 59-018. The purpose of this run was to obtain pullout-transition-glide ablation data on FWPF (a repeat of 59-014) and the SAIC leading edge material. The test data and model photographs are presented in Figure 34. The performance of the FWPF was essentially the same as in 59-014. The FWPF pyrometer indicate peak pullout and steady state glide temperatures (at the impingement line) of about 4500 and 3700°F, respectively. The SAIC pyrometer is not as well behaved as the FWPF pyro. The steps in the pyro data may mean mechanical erosion as the video coverage revealed sparks and melt flow on the SAIC leading edge. As expected, the ablating C-C transition section caused a forward facing step to develop at the forward edge of the SAIC leading edge. The excessive ablation observed in the video and post test photograph of Figure 34 may have been caused by the aggravated heating induced by this step. The 994 end cap adjacent to the SAIC leading edge ablated about double the amount that its twin did on the other side. The melt flowing off of the SAIC material may have reacted with the 994 causing the observed high ablation. Except for T4, the backface TCs appeared to have contact problems with the leading edges. Some indication of the streamlines in the vicinity of the leading edges is evident in the video by noting the flow of the heatshield melt runoff.

Run 59-019. The purpose of this run was to obtain pullout-transition-glide ablation data at a 10° AoA. This test used 223 and FWPF leading edges. The test data and model photographs are presented in Figure 35. This test was very similar to 59-014, except for the AoA. The two pyrometers viewing the two leading edges are in excellent agreement indicating peak pullout and steady state glide temperatures (at the impingement line) of about 4400 and 3600°F, respectively. The backface thermocouples (TCs) performed in a well behaved manner up to burnout. The surface and backface thermal responses for 223 and FWPF were essentially identical. The separated region over the transition section appeared to be similar to 59-014. The biggest difference between Runs 59-014 and -019, was the heatshield ablation performance. For 59-019, the windward heatshield had considerably higher ablation (as expected) and also more vortices than 59-014.

Run 59-020. The purpose of this run was to obtain glide only ablation data on BP-Hitco's Ceracarb. Exposing the material to pullout heating was not attempted because it was felt that the SiC portion of the material could cause problems. Note that for pullout, temperatures over 4400°F were measured on previous runs. For glide only, temperatures over 3500°F were measured (see Run 59-009). The upper limit for SiC is about 3000°F, so the glide test was considered as a good test of the Ceracarb material. To occupy the other test space, the FWPF leading edge from Run 59-013 was installed on the other side. This FWPF leading edge experienced pullout and transition to glide, but not glide. A new C-C transition section was used. Therefore an attempt to compare the FWPF ablation data from this run with the other materials may not be valid as the new section caused a separated flow over part of the leading edge (see video coverage). The test data and model photographs are presented in Figure 36. As noted in Section 7.1 (Item 8), the Ceracarb did not ablate as expected, but formed a deep cavity along the impingement line as noted in the post test photographs . The postulated reason for this behavior

is noted in Item 8 above and is based upon the upper temperature limit of SiC (that is only in those region with high heating and temperatures above 3000°F would the Ceracarb be expected to ablate). Also as noted in Section 7.1 (Item 1 above), deposits were noted upstream of the Ceracarb, on the transition section.

Run 59-021. The objectives of this run were to 1) obtain ablation data on 0° swept leading edges at the pullout heating rate, 2) obtain an estimate of the enthalpy profile across the test rhombus, and 3) estimate if the nozzle produces a good test section for future heatshield testing. The 0° sweep angle allows the leading edge test article to be tested by itself, without the effects of upstream material ablation that occurs in the 60° sweep tests. The model orientation relative to the nozzle is presented in Figure 26. From this figure it can be seen that the west pyrometer (M90V) is viewing the leading edge at about a 5 to 10° angle of incidence. At this angle the temperature could be questionable. The test data and model photographs are presented in Figure 37. The East pyro and TC data are well behaved with the East pyro measuring about 4700°F (the "questionable" West pyro measured about 4800°F). The post test ablation contour of the leading edge, its end caps and downstream heatshield all ablated in a very smooth, well behaved manner. The appearance of the ablated surfaces indicate that, laterally, the heating was uniform over the entire model. This may also indicate that the enthalpy is uniform laterally across that portion of the test rhombus that the model occupied. As noted in Section 3.2, because C-C ablation is independent of surface temperature in the carbon combustion regime of ablation, that this conclusion may not be correct. The ablation pattern of the downstream silica phenolic heatshield is uniform, which maybe more indicative of the enthalpy profile than C-C because of the high dependency of silica melting ablation on surface temperature. The video coverage indicates something strange on the east side, but when the model is extracted from the flow, apparently debris was on the window was in the field of view. This run was terminated early because of the failure of a facility actuator line caused by flow deflection from the 0° model.

Run 59-022. The purpose of this run was to obtain ablation data on the SAIC leading edge material without the influence of ablating upstream materials. This material was tested in Run 59-018 in the 60° sweep configuration. In 59-018 it was postulated that the material performed poorly because of the upstream ablating C-C transition section. Thus, in this run, the SAIC leading edge is exposed to only the flow from the nozzle and not influenced by upstream ablating components. This run was designed to produce the pullout heating rate of Run 59-018, except at 0° sweep. The test data and model photographs are presented in Figure 38. On entry into the test rhombus, the leading edge appeared to have underwent almost immediate ablation. This is evident from the sparks that can be seen in the video. The rate at which ablation started makes one think that some kind of thermostructural failure occurred. On post inspection of the model, copper colored specks were evident in the melt layer of the leading edge. The source of this residue is unknown except possibly copper from the arc electrodes. Model "dusting" by electrode copper was only evident on one other model in the entire test series (Run 59-013). An item to note about the pre-test model is that a large "gouge" existed on the lateral face of the leading edge as noted in Figure 38, "pre-test nose on view". This "gouge" appeared to be caused by a C-C fiber that was apparently pulled out during machining. The entire front and lateral two surfaces were coated, including the "gouge", indicating the gouge occurred before application of

the Ultramet coating. This gouge was the source of the problem that caused the model to be extracted early in the run. Freestream gas appeared to have flowed through the gouge, causing aggravated ablation of the downstream heatshield. During the run it was not known if this flow was ablating the holder, so the test was terminated.

Run 59-023. The purpose of this run was to obtain ablation data on the MSNW leading edge material without the influence of ablating upstream materials (just like the above SAIC Run). This leading edge test article had problems on delivery. The external shape of the test article was not even close to the Engineering Drawing (Figure 14). The overhang (backface to impingement line) was at least 0.1" longer than Figure 14 and there was a substantial gap between the braided external layer and the Poco graphite substrate. The impingement line and gap extended out further than the adjacent 994 end caps, causing some concern about freestream flow into the gap. Delivery of the model from MSNW was at the last moment and assembly of the model at NASA-AMES was accomplished late at night without excess to photographic coverage and weight measurements. The test data and model photographs are presented in Figure 39. From the video and real time observation, the leading edge appeared to start ablating about 10 sec from entry into the test rhombus. This is evident from sparks that can be seen in the video. The excessive ablation that occurred on one edge of the leading edge (see post test photo of Figure 39) was the reason the run was terminated early.

8.0 SUMMARY, CONCLUSIONS AND RECOMMENDATIONS

Arc-heater tests were conducted on candidate Air Force leading edge materials for extended range reentry applications. The overall objectives of the tests were to obtain thermal and ablation data on leading edge materials at sweep angles representative of the operational system. To achieve this objective, a special model holder was designed and fabricated to allow the testing of leading edges at 60° sweep angles. To provide a comparison, a 0° sweep model (resembling a cylinder in cross flow) was fabricated. Selected materials were tested at both 60 and 0° sweep angles. The NASA-AMES 60MW (IHF) facility was selected for the tests because this facility has the unique ability to simulate both the pullout and glide phases of extended range in a single test.

A total of 23 arc-heater runs were made, 11 calibration runs and 12 model runs. The calibration runs involved using a replica configuration of the 60° sweep model, instrumented with calorimeters (5 total) and surface pressure ports (3 total). The calibration runs acquired data on the nosetip and leading edge surfaces for the conditions used in the material ablation tests. In the 12 model runs, 20 material samples were tested. The material samples and a summary of the results follow:

1)   One nosetip fabricated from SAIC C-C with an Ultramet coating was tested at the lowest heat flux obtainable in the NASA 60MW 6.0" nozzle. The material was exposed at a heat flux of 900 Btu/ft2-sec for 60 sec and underwent ablation almost immediately.

31

2)   Three leading edge materials were tested at the pullout heat flux (630 Btu/ft2-sec) in the 0° sweep configuration for over 100 seconds each. The materials were: a) 223 C-C that underwent smooth laminar ablation with extreme uniformity along its impingement line, b) the SAIC C-C with an Ultramet coating which apparently underwent ablation early in the run, ablating through the coating and into the parent material, and c) a HfC impregnated C-C sock attached to a Poco graphite substrate that underwent ablation early in the run, ablating through the sock and into the Poco.

3)   Sixteen leading edge materials were tested in the 60° sweep configuration. The test involved glide only, pullout only, and combined pullout-glide. For these types of tests, the durations were 300, 90 and 390 seconds, respectively. Glide and pullout heating rates were nominally 220 and 620 Btu/ft2-sec, respectively. The materials were: a) 223 C-C that underwent smooth laminar ablation with extreme uniformity along its impingement line, b) FWPF C-C that ablated about the same as 223, c) 4DO C-C that also ablated about the same as 223, d) a SAIC C-C with an Ultramet coating which ablated through the coating (could have been caused by the upstream ablating C-C section), and e) the BP-Hitco Ceracarb which underwent significant ablation along the impingement line (could also have been caused by the upstream ablating C-C section).

In addition to material type, the test variables included weave orientation relative to the sweep angle, Angle-of-Attack (AoA), trajectory sequence (i.e., glide only, pullout only, pullout and glide), and test reproducibility. All C-C materials ablated just about the same, with the spread in data about equal to the test-to-test variations measured in the reproducibility tests. Also the influence of weave orientation was about equal to the measured test-to-test variations. The influence of AoA was as expected in that the shape change was biased by the AoA.

8.1 Conclusions

The tests resulted in the generation of a data base for C-C leading edge material thermal and ablation (or shape change) responses during high altitude reentry flight. The ablation performance of the Air Force C-C materials (FMI's 223, Textron's FWPF and GE's 4DO) is well behaved with no apparent mechanical modes of ablation. In all cases, the C-C materials ablate in a laminar behavior with no pits, divots or gouging evident from visual inspection. The other leading materials appear to either have a thermostructural problem and/or underwent melt, with resulting complex and irregular shaping during the ablation process. From these tests, the following conclusions can be made:

1)   The ablation of all C-C materials are well behaved, with apparently no mechanical effects and no preferential oxidation or roughness development. The shapes appear to be caused by an all laminar boundary layer.

2)   The thermal and ablation data generated for C-C materials appears to be of a quality sufficient for shape change codes to use as a data base for verification-demonstration.

32

3)   The pullout heating levels appear to be too high for the SAIC and MSNW materials. The glide heating levels appear to be too high for the BP-Hitco material.

4)   There appears to be little effect of weave orientation (relative to the sweep angle) on shape change.

5)   There appears to be little effect of trajectory sequence on shape change (i.e., pullout only ablation + glide only ablation = combined pullout and glide ablation in a single test).

6)   All the model hardware performed as designed and as expected. Some changes are recommended in the nosetip and thermal isolation of the leading edge's forward face. The test facility performed with no significant problems, allowing all tests to be conducted at the desired conditions.

8.2 Recommendations

The tests resulted in an excellent data base for C-C leading edge material thermal and ablation responses during high altitude reentry flight. It is recommended that these data (including the calibration data) be analyzed to determine the data quality and ability of current computer analyses to predict the heating and material thermal and ablation responses. These and other recommendations are summarized below.

1)   An analytical effort should be conducted on the heating and pressure data acquired by the calorimeter model to determine data quality, test condition reproduction and the ability of existing analysis techniques to correlate the data.

2)   An analytical effort should be conducted on the C-C material thermal and ablation responses to determine the ability of the analyses to predict leading edge aerothermal performances in high endo-reentry environemtns.

3)   Detailed post test inspection and investigations should be conducted to determine the depth of oxidation, quantitative shape change contours, during test shape change transients, and surface roughness.

4)   The test evaluation of extended range reentry should be continued by conducting terminal dive simulations on the leading edges tested this test series at the pullout and glide phases of extended range.

5)   If sweep leading edges are to be tested in the future, the following changes to the hardware designed in this effort are recommended: a) a piece of Grafoil should be placed between the leading edge and upstream transition section to reduce the conductive interchange and b) the cooled nosetip should be machined so the aft face is not flat but angled forward so that the two ends of the nosetip, along the impingement line, are better

33

cooled. This latter change will require that the transition section forward face has two bevels to match the nosetip.

9.0 REFERENCES

1. Hirvo, D., "Representative Aerothermal Environments for Maneuvering Hypersonic Systems", SPARTA, NRC Bi-monthly, October 1992.

2. Deleget, J.L., "Nosetip Material Testing for Extended Range Missions", AFWAL-TR-95-TBD, April 1994.

Figure 1. Generic Range Extension Vehicle and Trajectories

Control Surfaces

A

Antenna Windows

Leading Edges

Heatshields

Nosetip

Antenna Windows

Antenna Window

INU

A-A

° **HP-MaRV**

- GPS and Data Link on Leeward

- SAR on Leeward with 180° Vehicle Role for Acquisition

- Configuration Drivers:
  L/D, Payload / INU Packaging, Yaw Stability, Heatshield

° **MOODY'S INTERPRETATION OF "NEW" GOALS**

- No roll = Continuous GPS Data Link and
  SAR (if necessary) on Windward

TRAJECTORIES / ANTENNA TEMPERATURES

° HP-MaRV and Current BMT Goals = CONUS Launch with Dual Mission Use

- Extended Range

ALTITUDE (kft)   ANTENNA Tw (°C)

Tw (Windward)

Tw (Leeward)

Altitude

TIME (sec)

- Ballistic With Evasion

ALTITUDE (kft)   ANTENNA Tw (°C)

Altitude

Tw

TIME (sec)

2259412c.drw

35

NOSETIP (Rn = 0.50")

LEADING EDGE (Rn = 0.50", SWEEP = 70°)
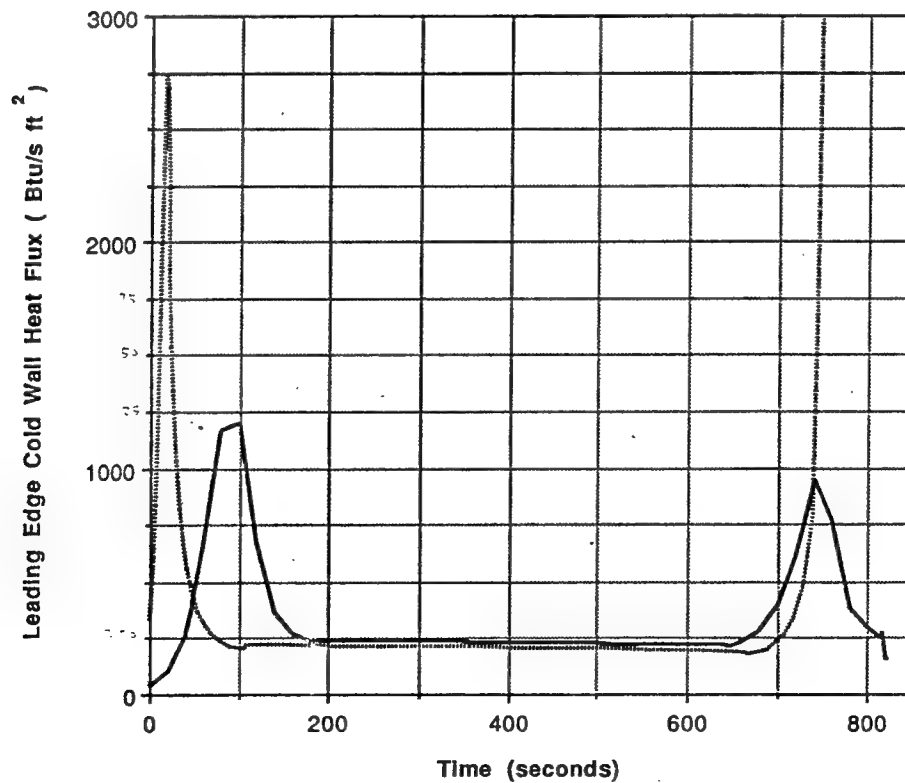
Figure 2. Extended Range Flight Environments
(From Reference 1)

TEST OBJECTIVES, PULLOUT-GLIDE

o ASSESS ABLATION AND ROUGHNESS DEVELOPMENT PRIOR TO TERMINAL DIVE

o MEASURE SHAPE CHANGE, RECESSION RATES AND TEMPERATURE HISTORIES
  AT REPRESENTATIVE CONDITIONS

  - SIMULATE FLIGHT SUPERSONIC REGIONS ON LE

  - LAMINAR ABLATION ? STREAMLINE FLOW BEHAVIOR

  - FORMATION OF DIVOTS, SURFACE POROSITY ?

  - MATERIAL STRUCTURAL IMPLICATIONS, RETENTION

  - RELATIVE FIBER-MATRIX-COATING (if present) ABLATION

  - FIBER ORIENTATION RELATIVE TO VELOCITY VECTOR

  - ANGLE-OF-ATTACK INFLUENCES

  - DOES INITIAL PULLOUT INFLUENCE SUBSEQUENT ABLATION BEHAVIOR ?

  - ASSESS KINETIC/CATALYTIC WALL IMPLICATIONS, DO THEY CHANGE DURING GLIDE

  - ANY SURPRISES FOR PULLOUT-GLIDE ?

Figure 3. Leading Edge Test Objectives
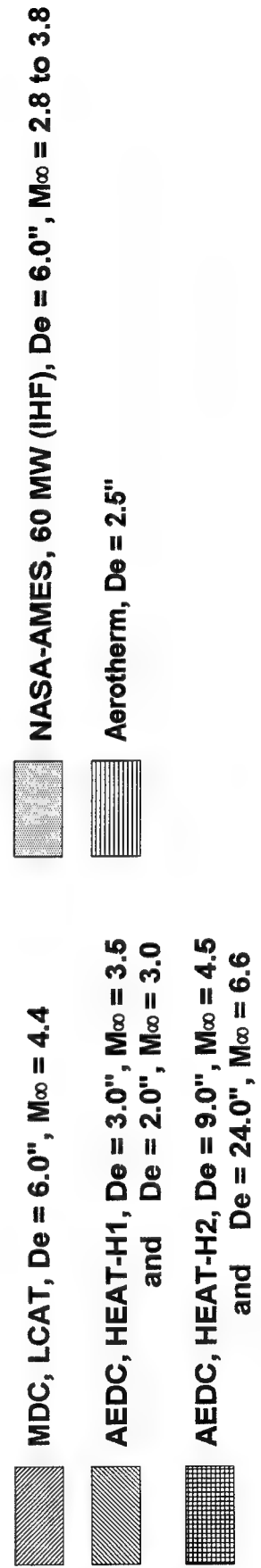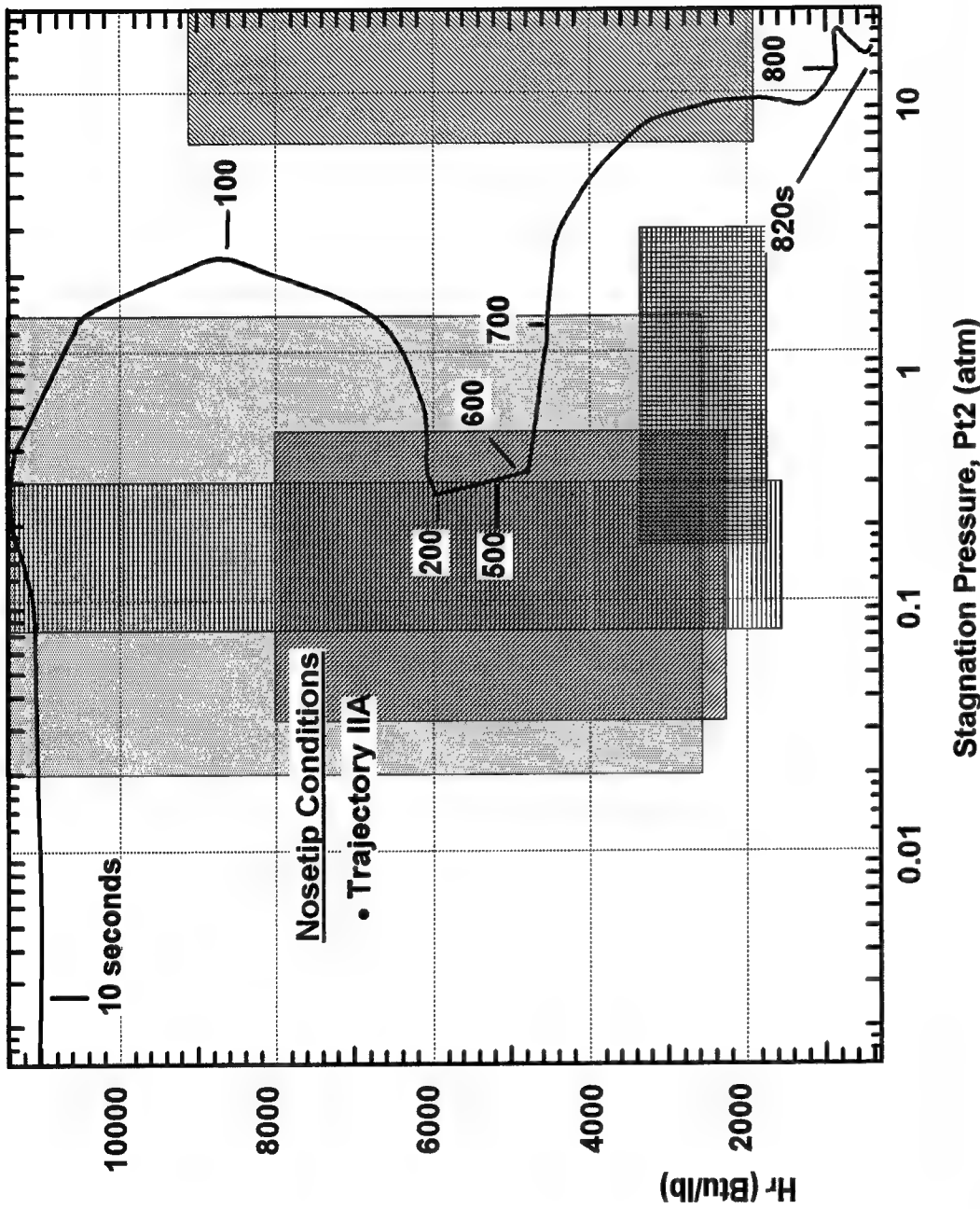
Figure 4. Arc-Heater Simulations of Nosetip Aerothermal Loads for Extended Range Missions

38

2249414b.drw
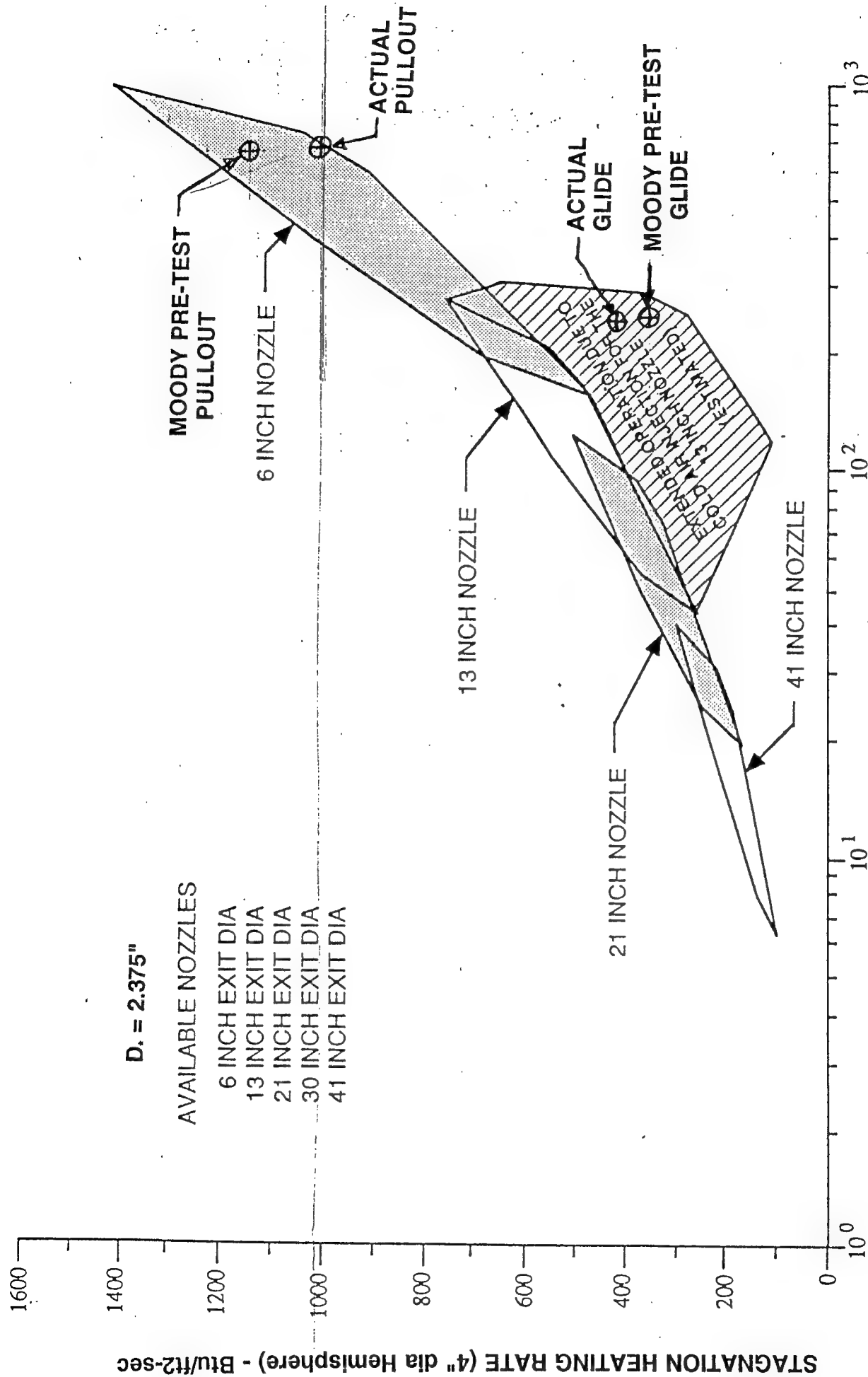
Figure 5. NASA-AMES 60MW Operating Envelope and Actual Leading Edge Test Conditions

WLL - 9/6/91

39
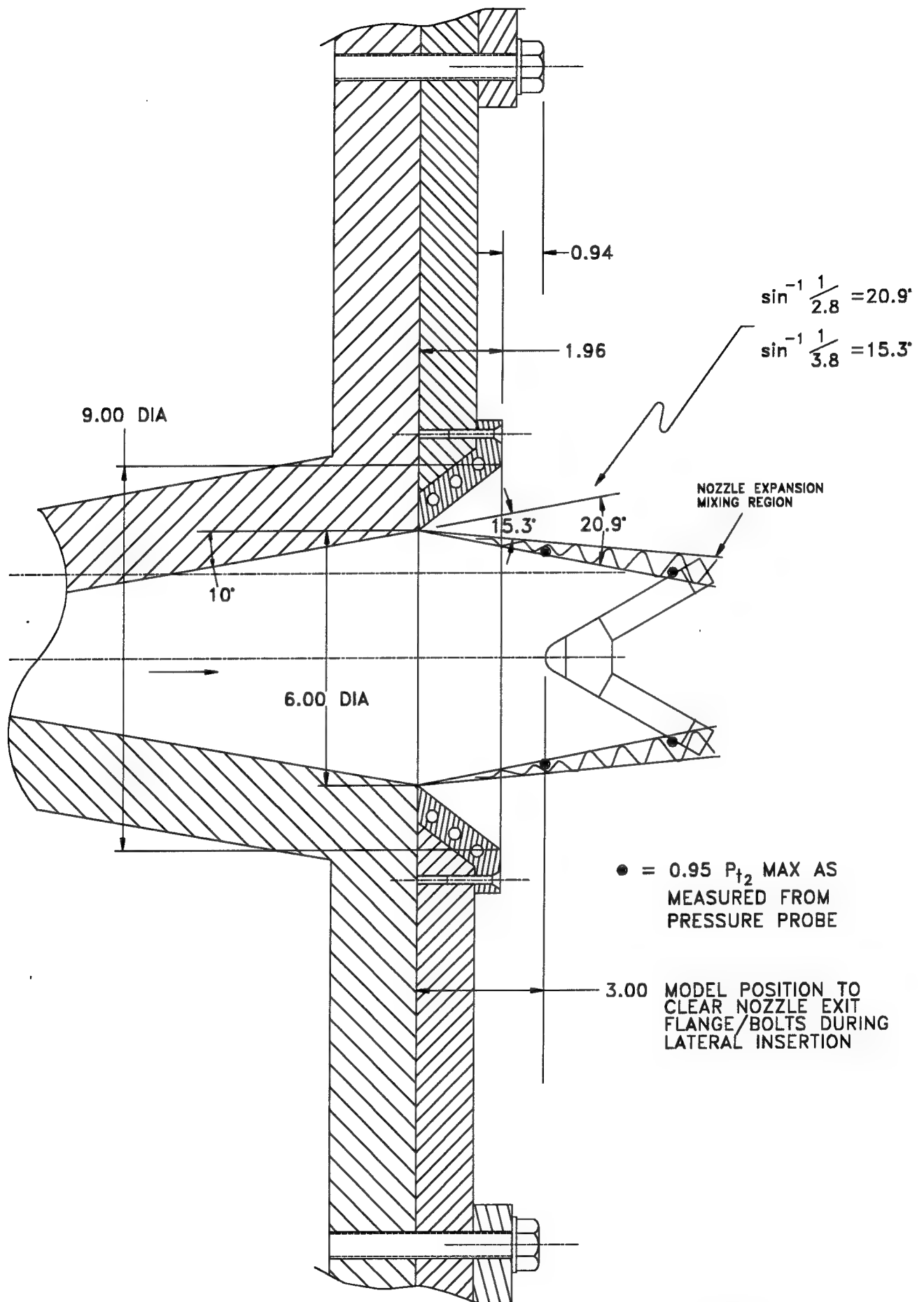
Figure 6. Schematic of 6.0" Diameter Nozzle Exit, NASA-AMES 60MW

Figure 7. NASA-AMES IHF Test Cell

Pyro View ①

-0.30' dia FoV

2.25'

1.1'

Pyro View ②

-0.12' dia FoV

2.25'

1.1'

East Pyro (M668)
Near Normal View of LE
Impingement Line

South

North

90°

90°

②

①

West Pyro LoS

Gold Mirror
for West Pyro

East

East Observation Window

Door

B

B

Model Out of
Flow Position

West

Two Observation Windows

West Pyro (M90V) Near Normal View of LE Impingement Line

Overhead Video Camera

Fused Silica
Pyro Window

Ceiling Window

Section A-A

Overhead Video Camera

East Pyro (0° Sweep Model)

East Pyro
(60° Boomerang)

Vest Pyro

Water
Cooling
Manifold

Instrumentation
Console

32

Section C-C

To Diffuser

A

Ceiling

C

C

Test
Model

Strut

0.1'
3.0'

9.0'

East Observation
Window

Arc
Column

A

Floor

Section B-B

nasacell.dwg

41

NASA-AMES 6.0" NOZZLE EXIT AND CALORIMETER MODEL

- PHOTOS TAKEN IN TEST CELL
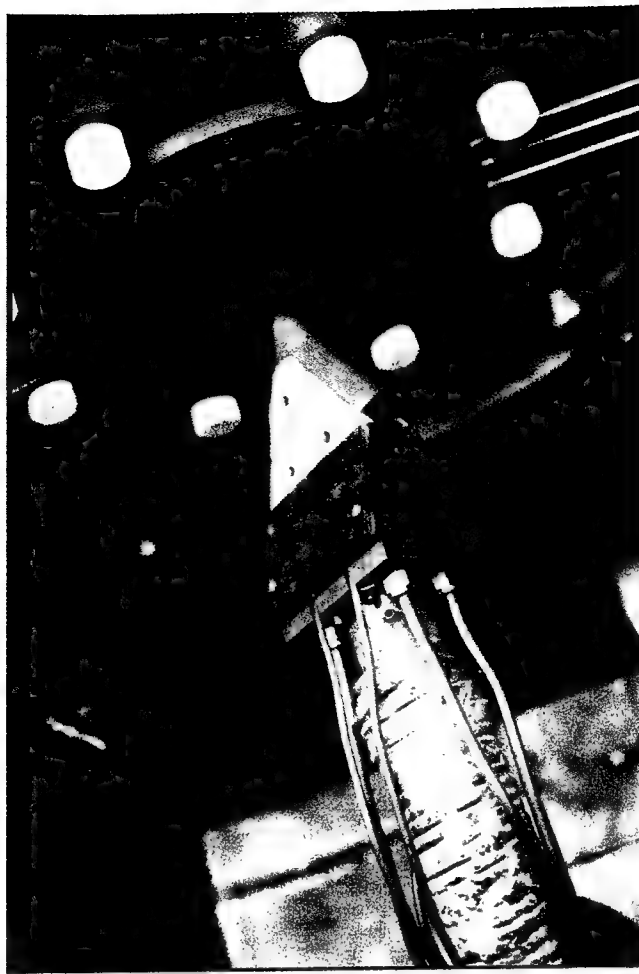
Figure 8. View of NASA-AMES Test Cell, 6.0" Nozzle with Leading Edge Calorimeter Model Installed on Strut

HEATSHIELD PANELS (SP)

ADAPTOR TO NASA STING

994 GRAPHITE END CAPS

LEADING EDGE TEST ARTICLE

$R_N = .375$

INTERNAL COOLED NOSETIP

C-C TRANSITION SECTION

2.25"

60° Sweep

$R_N = .375$

SCALED LAYOUTS
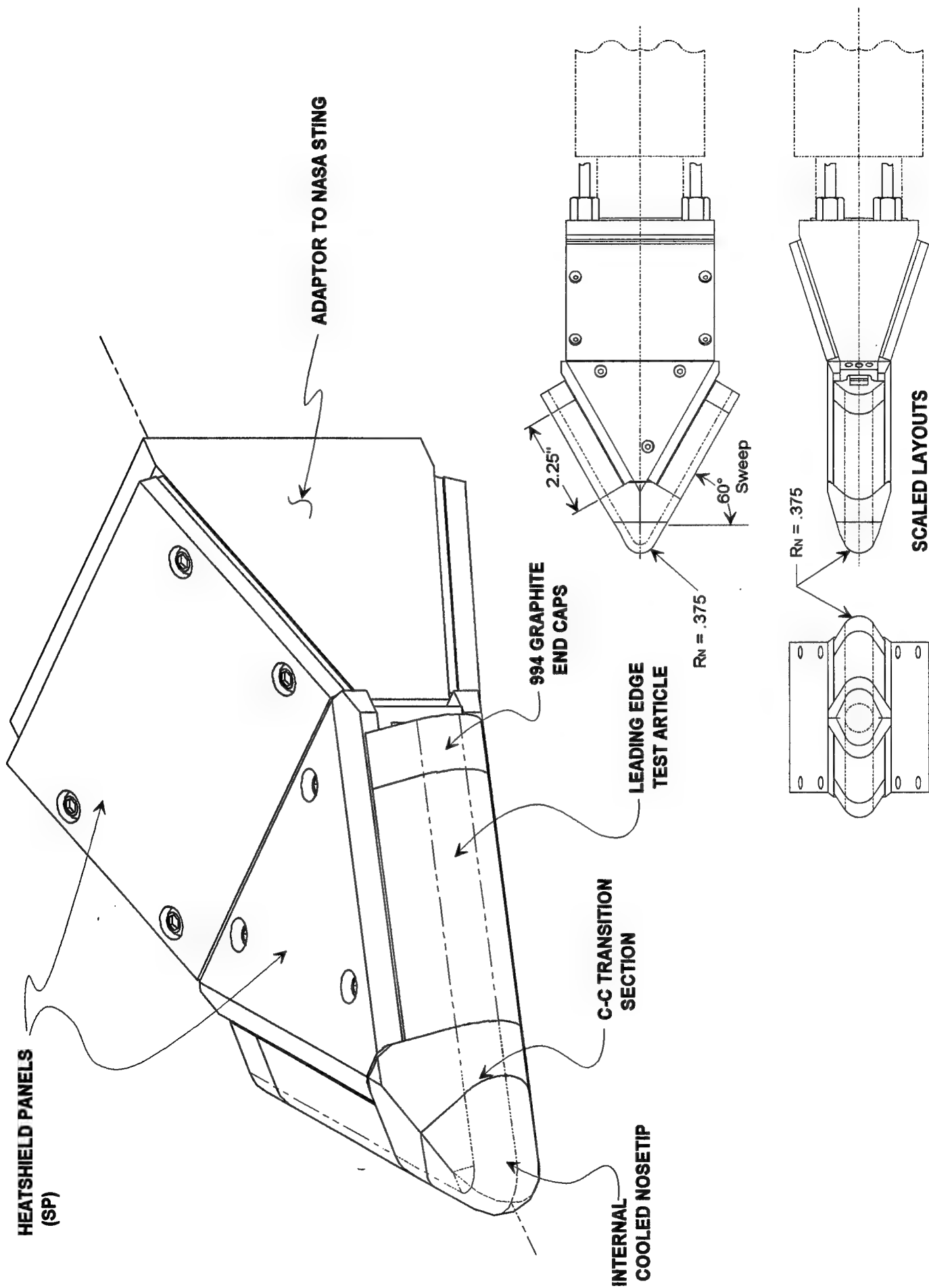
Figure 9.   Schematic of Leading Edge Test Model

9189415a.drw

43

BOOMERANG ASSEMBLY

a) ASSEMBLED MODEL

W L / M L B C
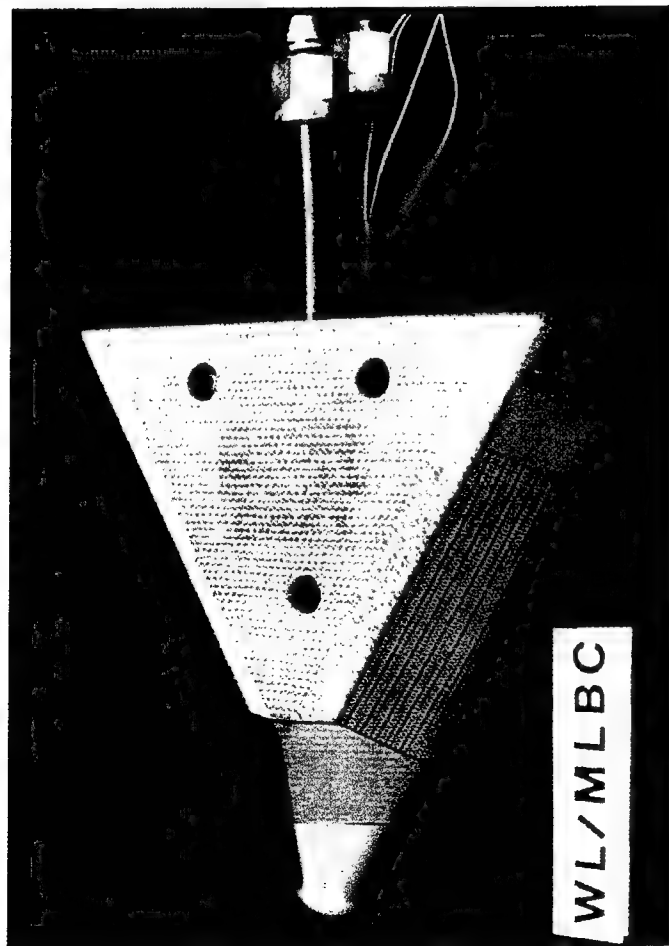
b) INTERNAL COOLED NOSETIP
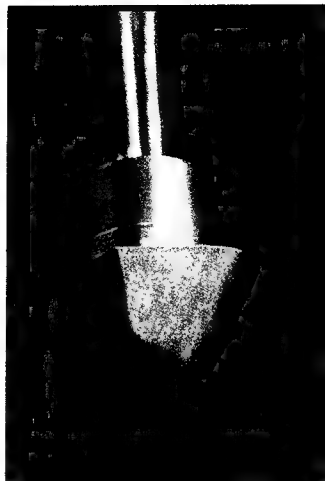
c) C-C TRANSITION SECTION

d) C-C LEADING EDGE, 994 END CAP AND INSULATION / RETENTION HARDWARE
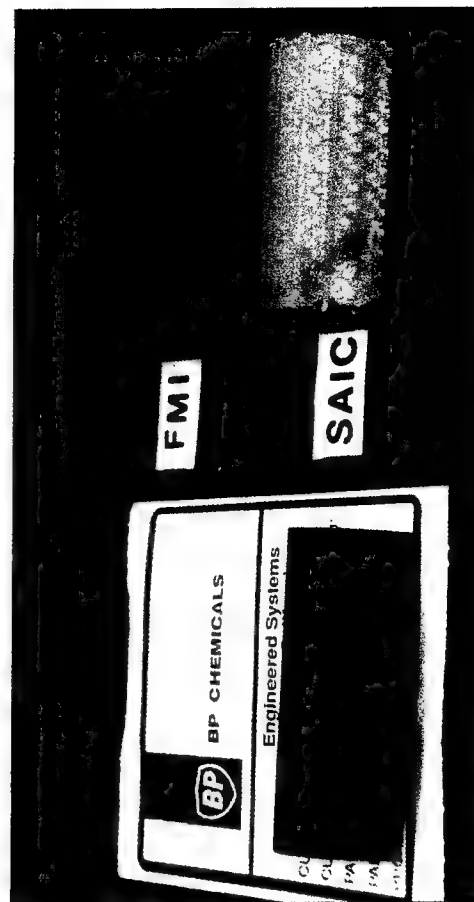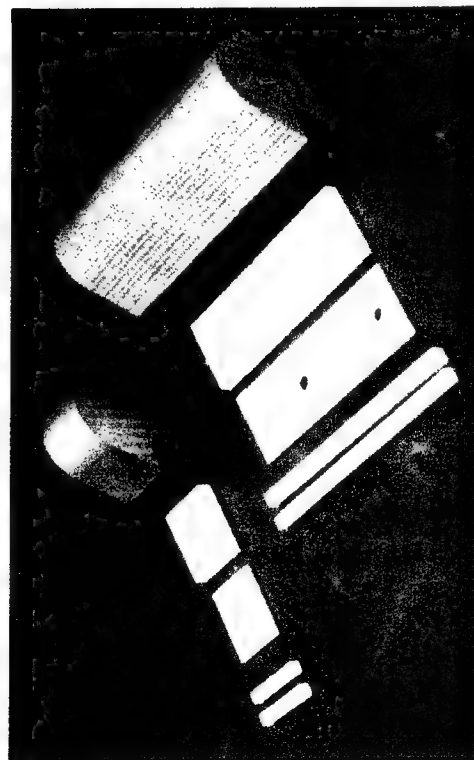
e) SAMPLE LEADING EDGES: BP = CERACARB, FMI = 223 C-C, SAIC = C-C WITH ULTRAMET COATING

Figure 10. Leading Edge 60° Sweep Model Hardware ("Boomerang" Model)

44

m9
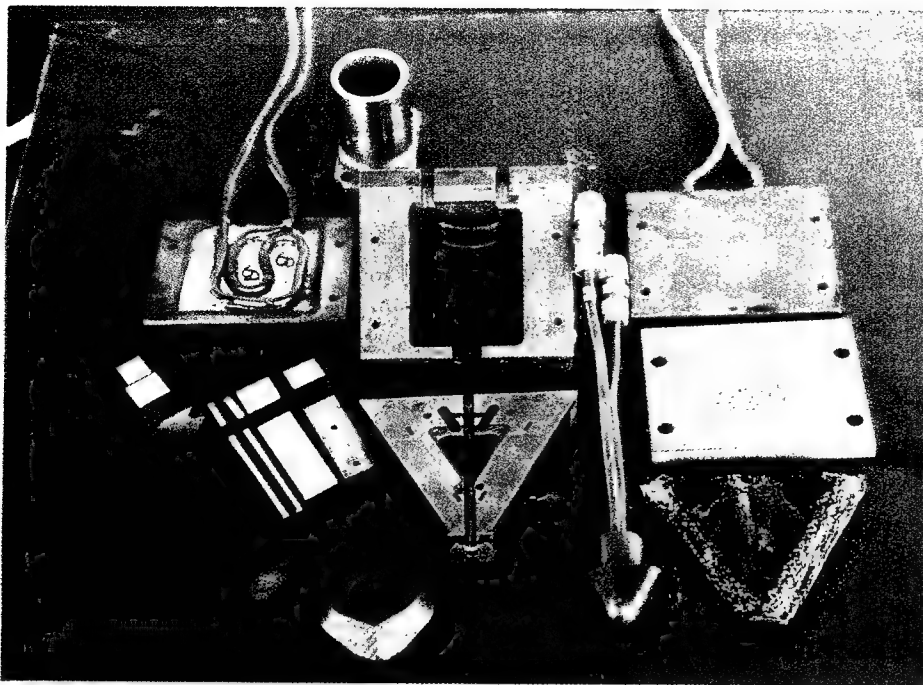
a) Boomerang Hardware Components and Aft adaptor, Disassembled
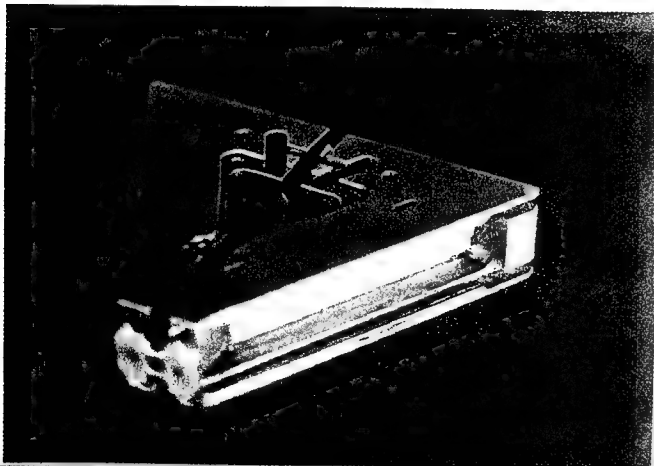
b) Cooled Boomerang Main Structure
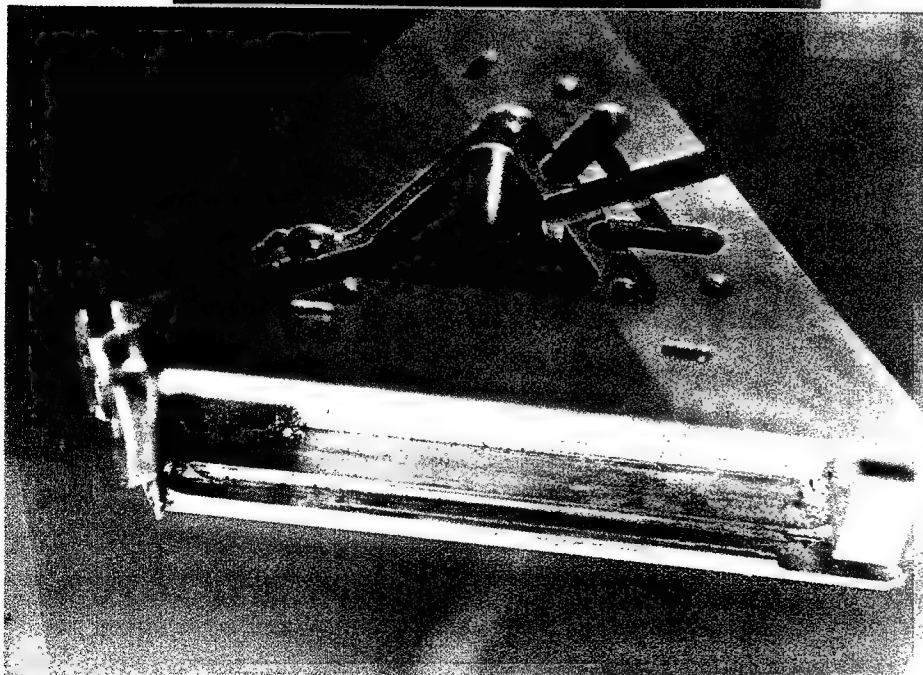
c) Closeup of Boomerang Main Structure Showing Leading Edge Retention Cavity

Figure 11. Boomerang Hardware

45
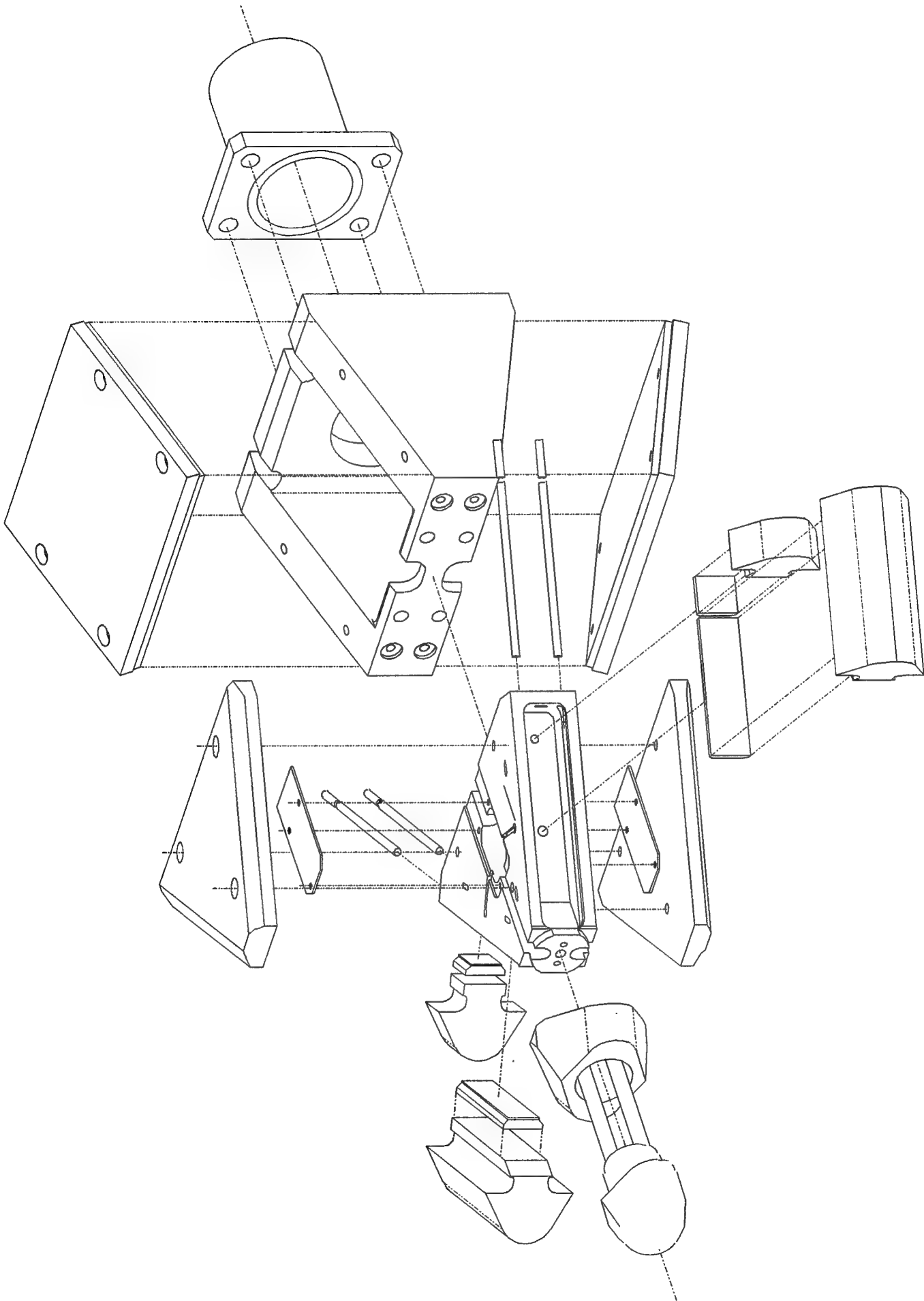
Figure 12. Exploded View of Leading Edge Test Model and Facility Interface Hardware

4159413b.drw

ESTIMATED RHOMBUS
IMPINGMENT ON MODEL (Pretest)

ESTIMATED TEST RHOMBUS
BOUNDARIES (Pretest)

3.25 "Witness Bar" Span

20.9°

15.3°

3.000"

1.9

4.1

NOZZLE

REQUIRED CLEARANCE
FOR MODEL LATERAL
INSERTION

BOOMERANG

1"

SCALE

ADAPTOR

FACILITY STING
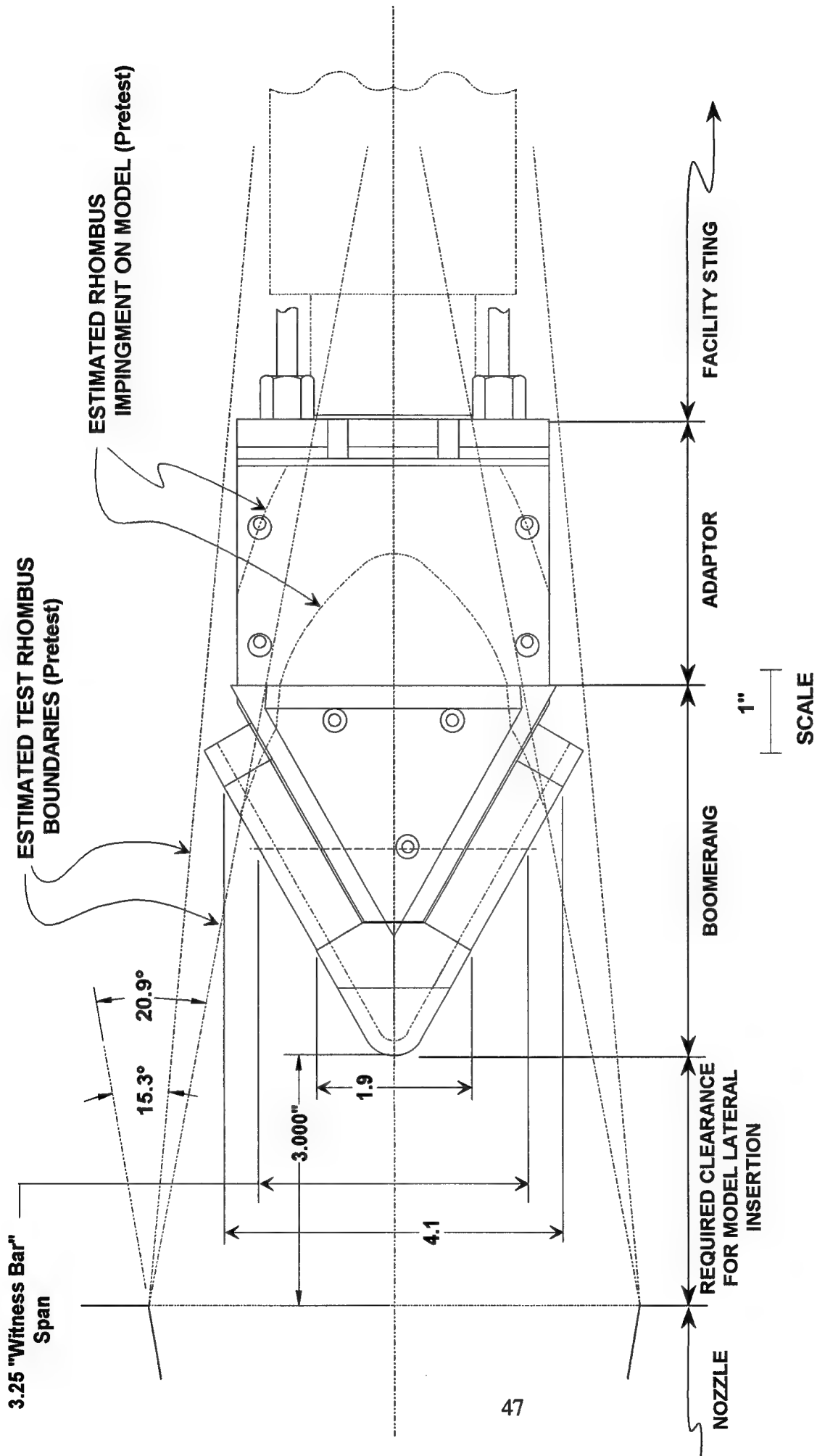
• NASA-AMES 60 MW WITH 6.0" DIA EXIT NOZZLE

Figure 13. Leading Edge Test Section

47

Post Test "Forward" Ablation
Measurement Location

Post Test "Aft" Ablation
Measurement Location

.644

0.854 $^{0.000}_{-0.005}$

.85

0.150±0.005

R0.125

0.640 $^{0.000}_{-0.004}$

⊕ | 0.004 Ⓜ | A Ⓢ

R0.375 | A Ⓢ

⊕ | 0.004 Ⓢ | A Ⓢ

.29

30°
REF

1.177 $^{0.000}_{-0.004}$

⊕ | 0.005 Ⓛ | A Ⓢ

A—A

MAX 0.030 RAD
Fillet

0.210±0.005

0.540 $^{0.000}_{-0.004}$

-A-

1.004 REF

A

0.235

30°

A

1.177 REF

2.250
②

GENERAL NOTES

1. ALL DIMENSIONS PER ANSI Y14.5M-1982

② DIMENSION CAN BE REDUCED PER APPROVAL FROM H. MOODY

48

UNLESS OTHERWISE SPECIFIED DIMENSIONS ARE IN INCHES TOLERANCES ARE:		DFTR: CRAIG M. GRAVES	4/1/94
		CHKR: H.M. MOODY	4/1/94
DECIMALS	ANGLES	DSGNR: H.M. MOODY	4/1/94
.x ±.1	±0°30'	PROG MGR: H.M. MOODY	
.xx ±.010		CONTRACT NO.	
.xxx ±.005			
MAT:SEE MATRIX			

DETAIL, LEADING EDGE

SIZE: A | DRAWING NO. MTE01-01 | REV: A

SCALE: NONE | SHEET: 1 OF 1

Figure ·14. Leading Edge Detail Drawing

RETENTION DETAILS

+ TWO ZYCRON H (ZrO_2) RODS RETAIN PLUG LEADING EDGES. ASSEMBLY LOADED BY ZIRCAR (FBC) BLOCK ON BASE OF LE SHANK

+ 994 GRAPHITE ENDS CAP OFF AFT FACE OF TEST ARTICLES. 994 CAPS LOADED FROM SIDE WITH GRAFOIL-ZIRCAR-SS TO ACCOMMODATE TRS ALONG IMPINGEMENT LINE.

+ TCs CAPTURED AND LOADED BETWEEN LE BASE AND ZIRCAR (2 places).

SCREW FOR LOADING ALONG STAG LINE

D-D

x THERMOCOUPLE LOCATIONS

SP HEATSHIELD

994 END CAP

LEADING EDGE TEST ARTICLE

LEADING EDGE AND TRANSITION SECTION IN DIRECT CONTACT

DETAIL B

ZrO_2 RODS

ZIRCAR INSULATION PAD

SS STRONG BACK

TC LEADS

SCREW FOR SHANK LOADING

C-C

COOLING PASSAGE

4139416b.drw

49
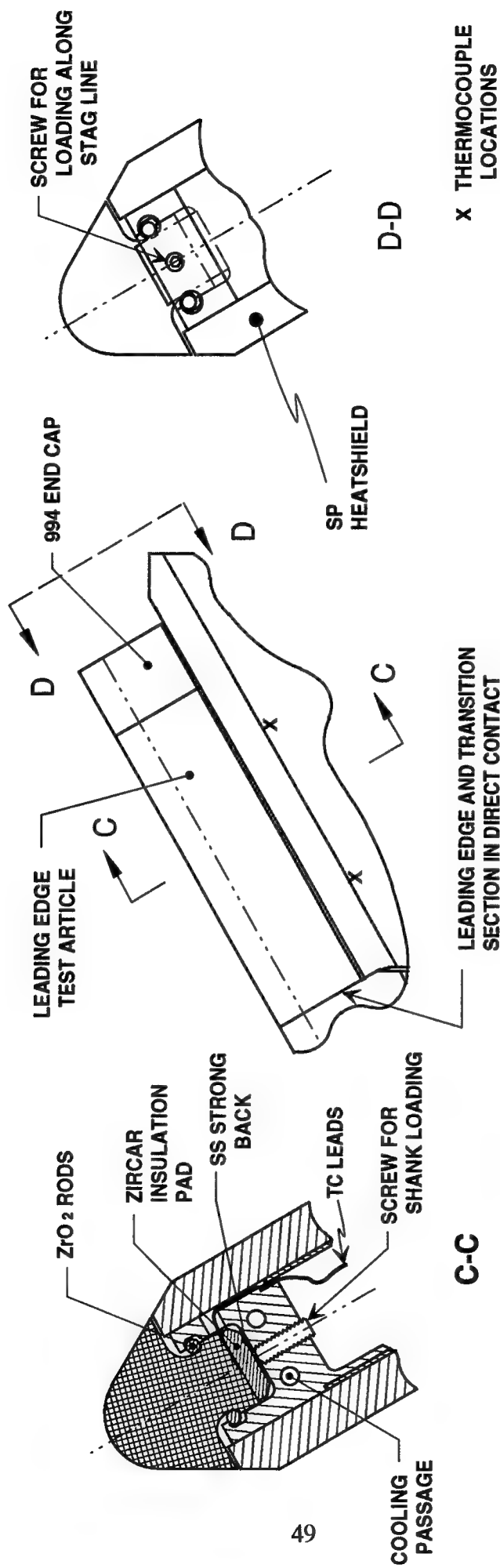
SPECIAL CONSIDERATIONS

+ Considered placing Grafoil between C-C transition and LE for thermal isolation of LE. Rejected because gap may produce forward facing step because of postulated flowfield. However, should be tried in the future.

Figure 15. Leading Edge Retention and Isolation
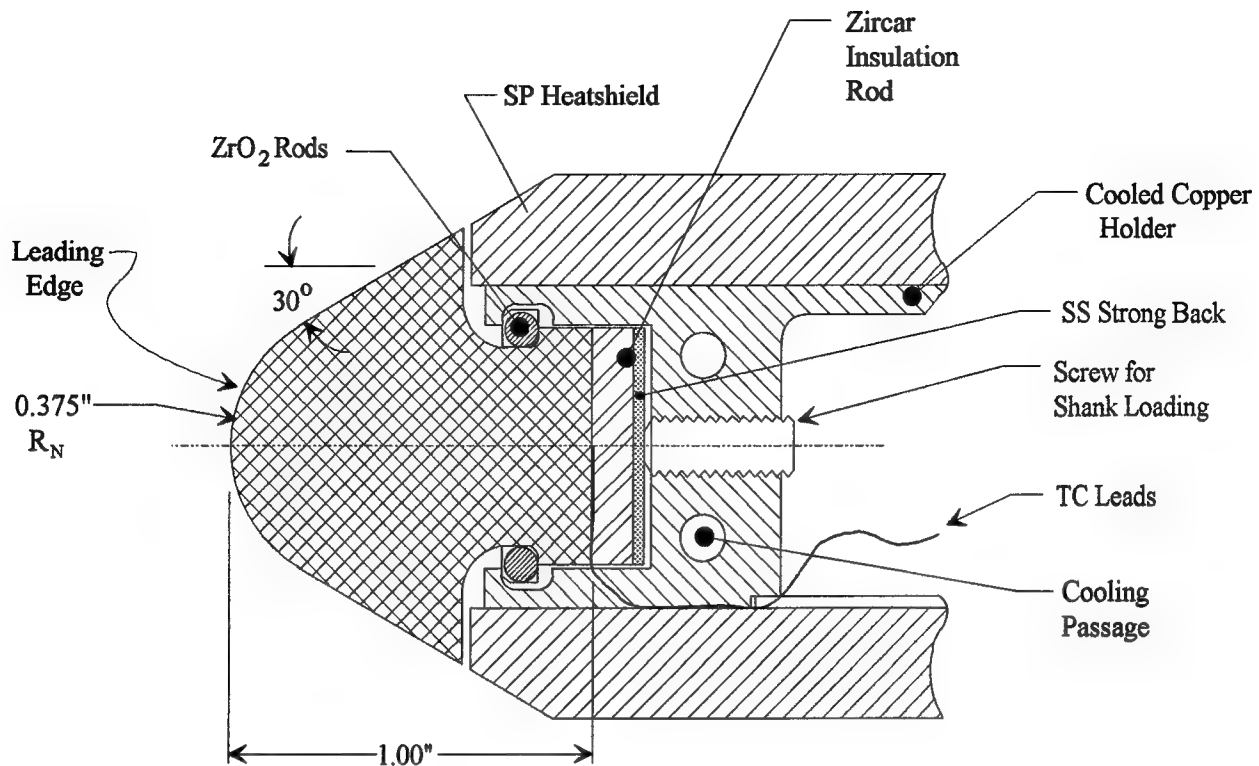
Figure 16. Leading Edge Retention and Thermal Isolation for Extended Range Testing
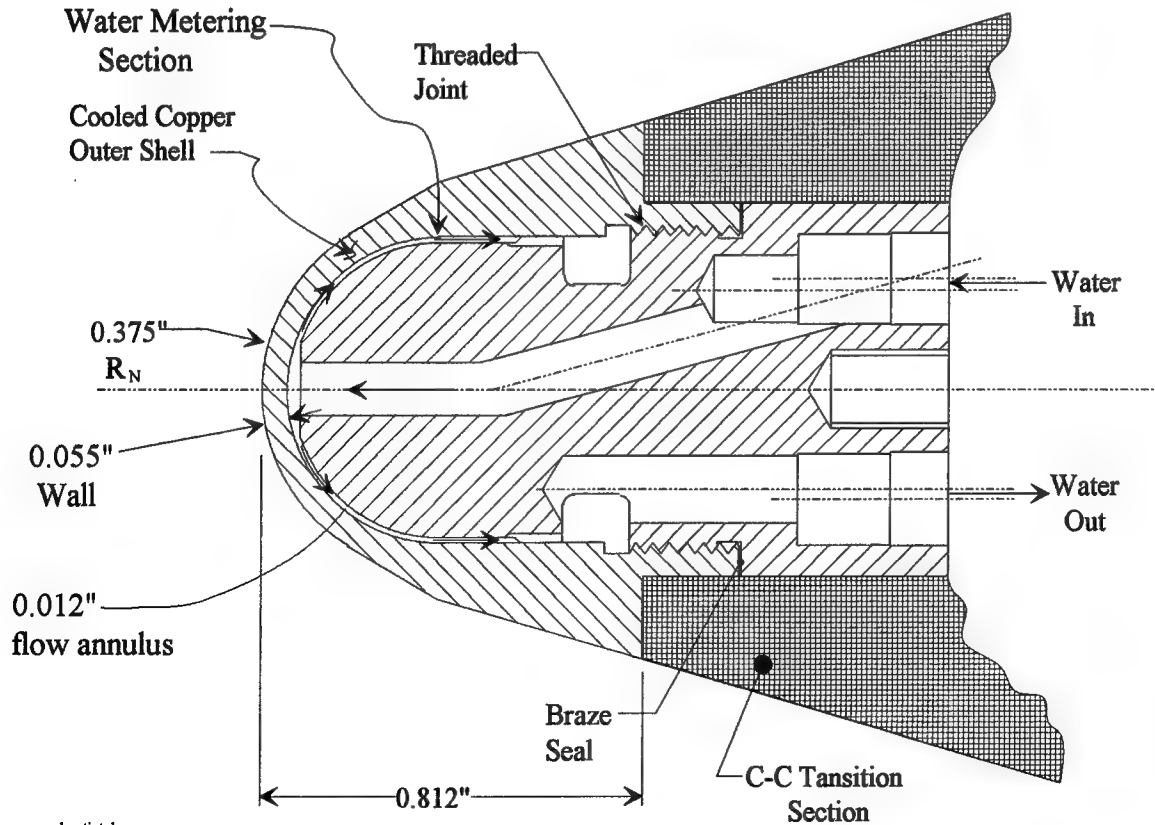
Figure 17. Internally Cooled Nosetip for Leading Edge Extended Range Testing

50

POST TEST PHOTO

o NOSETIP AFTER 3 RUNS,
EACH RUN = 390 sec

DURING TEST PHOTO, PLANFORM

o RUN 59-018
o PHOTO TAKEN AFTER 5 sec Dwell
o Stag Pt Qcw = 2320 Btu/ft2-sec
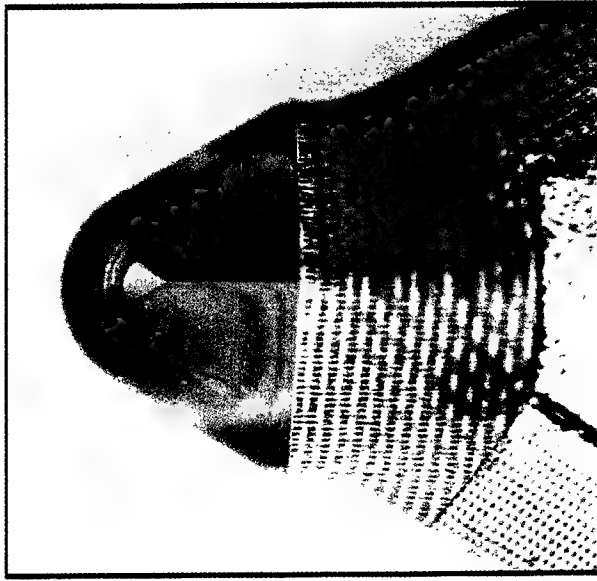
Figure 18. During Test Photo of Boomerang Model
and Post Test Photo of Cooled Nosetip

51
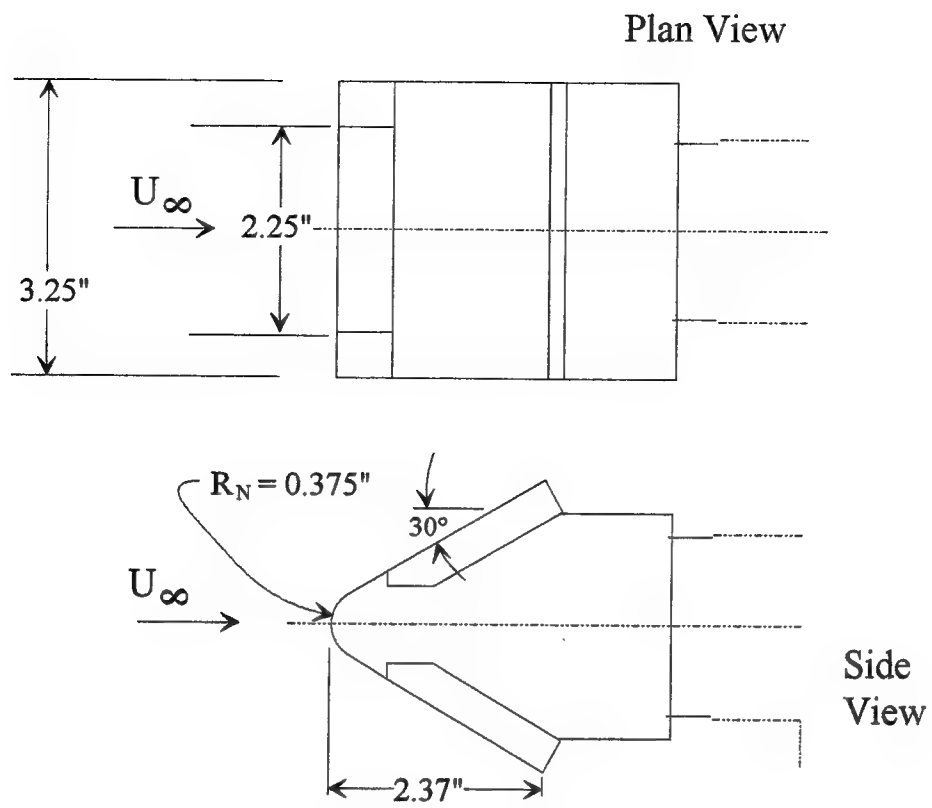
a) Design Schematic

b) Model Components, Post Test

Figure 19.   0° Sweep Leading Edge Model

- **All Cal and Pressure Ports at Stag Pt (NT) or Impingment Line (LE), Except P1 (See B-B)**

NO.	TYPE
Q4	Thermogauge 5776, Replaced with 5818 after Run 08.
Q5	Thermogauge 5774
Q6	Thermogauge 5773
Q7	Thermogauge 5775
Q8	Null Point, Medtherm 11409
P1	0.050" dia port, 0.112" above Q4
P2	0.050" dia port
P3	0.050" dia port

9189412A.DRW
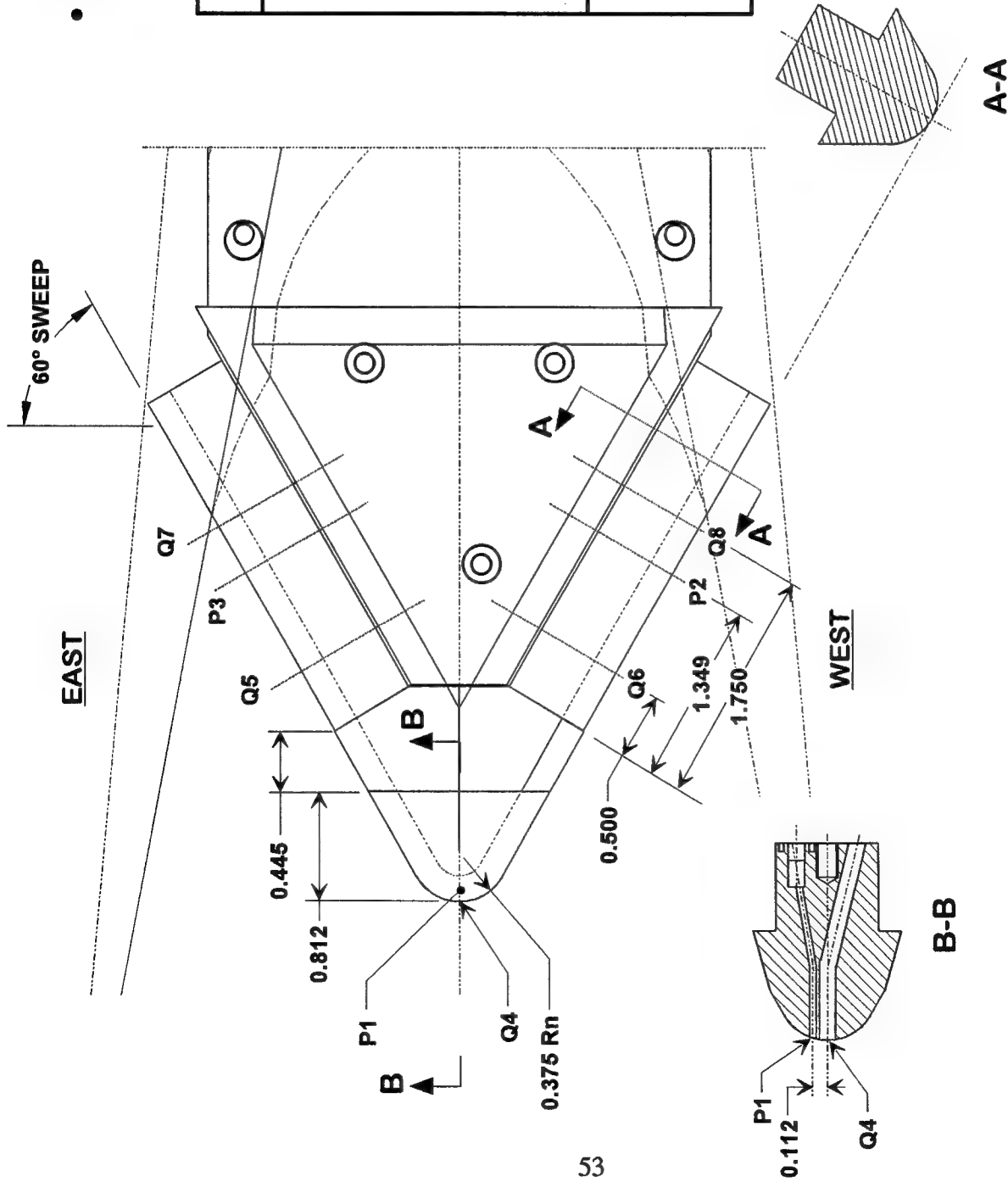
Figure 20. Calorimeter and Pressure Locations, Boomerang Cal Model

53

CALORIMETER MODEL

a) CALORIMETER MODEL WITHOUT HEATSHIELDS
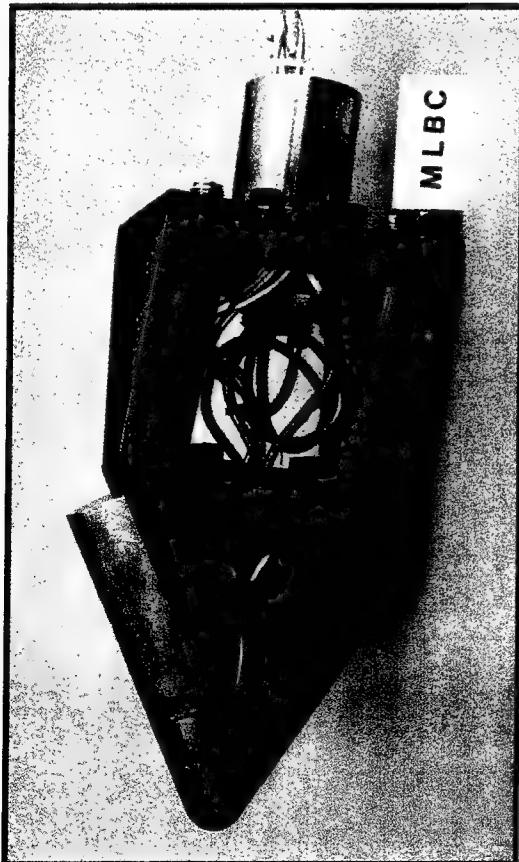
b) ASSEMBLED CALORIMETER AND AFT WEDGE

c) CALORIMETER INSTALLED ON FACILITY STRUT
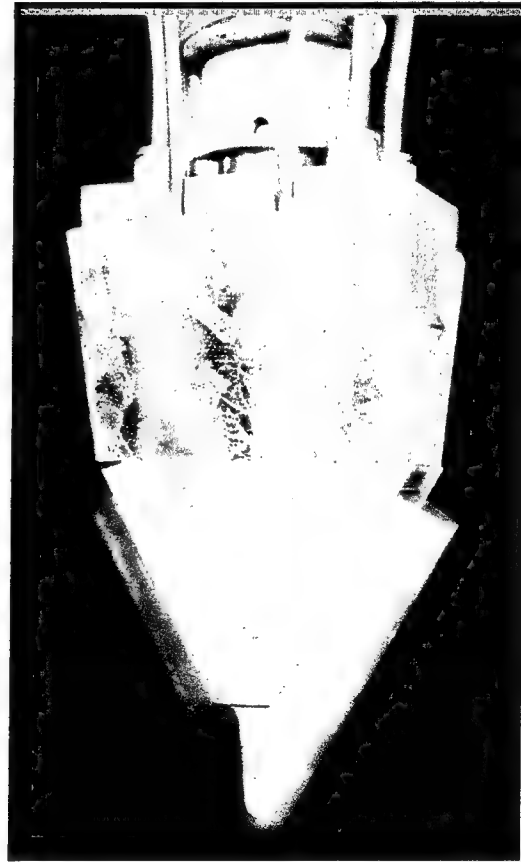
Figure 21. Boomerang Calorimeter Model

54

m18

EXTENDED RANGE FLIGHT ENVIRONMENTS

SPARTA PREDICTIONS

o NT AND LE RADII = 0.50" and LE SWEEP ANGLE = 70°
o FOR HEATING TRANSIENTS, SEE NEXT CHART
o NT STAG PT AND LE IMPINGEMENT LINE CONDITIONS:

Trajectory	Max Pullout Phase		Ave Glide Phase	
	Nosetip	Leading Edge	Nosetip	Leading Edge
AF-OPV	Qcw = 8000 Hr = 9000 P_{T2} = 10 atm	Qcw = 2510 Hr = 9000 Pstag = 1.6 atm	Qcw = 700 Hr = 7500 to 5000 P_{T2} = 0.20 atm	Qcw = 210 Hr = 7500 to 5000 Pstag = 0.030 atm
IGRP IIA	Qcw = 3400 Hr =9000 P_{T2} = 2.5 atm	Qcw = 1020 Hr = 9000 Pstag = 0.45 atm	Qcw = 800 Hr = 7000 to 5000 P_{T2} = 0.30 atm	Qcw = 240 Hr = 7000 to 5000 Pstag = 0.040 atm

* Units: Qcw = Btu/ft2-sec, Hr = Btu/lb

COMPARISON OF LMSC AND SPARTA PREDICTIONS (Preliminary)

o NT:

- Qcw, Hr and Pt_2 AGREE

o LE:

- LMSC's Hr is 0.85 x SPARTA's
- LMSC's CONVECTIVE COEFFICIENT IS 0.83 x SPARTA's
- LMSC AND SPARTA USE SAME SWEEP ANGLE SCALING: COS^2 for Pressure and COS^1 for Heating

Figure 22. Extended Range Flight Predictions

FACILITY PROCEDURE FOR PULLOUT-GLIDE SIMULATIONS

o **ARC STARTUP AND STABILIZATION. CHANGE ARC CURRENT AND PRESSURE TO PULLOUT**

o **WITH ARC STABILIZED AT PULLOUT CONDITION, INSERT MODEL.**

o **AT 40 sec FROM MODEL INSERTION, MANUALLY START RAMP DOWN TO GLIDE (5 sec Response Time of Control System Results in desired 45 sec at Pullout):**

     - **REDUCE PRESSURE THEN CURRENT;**
     - **WAIT 15 sec, REDUCE PRESSURE THEN CURRENT;**
     - **WAIT 15 sec, REDUCE PRESSURE THEN CURRENT (Current now at Glide Value);**
     - **WAIT 15 sec, REDUCE PRESSURE (Pressure now at Glide Value)**

o **KEEP PRESSURE AND CURRENT AT GLIDE VALUES, REMOVE MODEL AFTER 390 sec DWELL**

TYPICAL TRAJECTORY SIMULATION
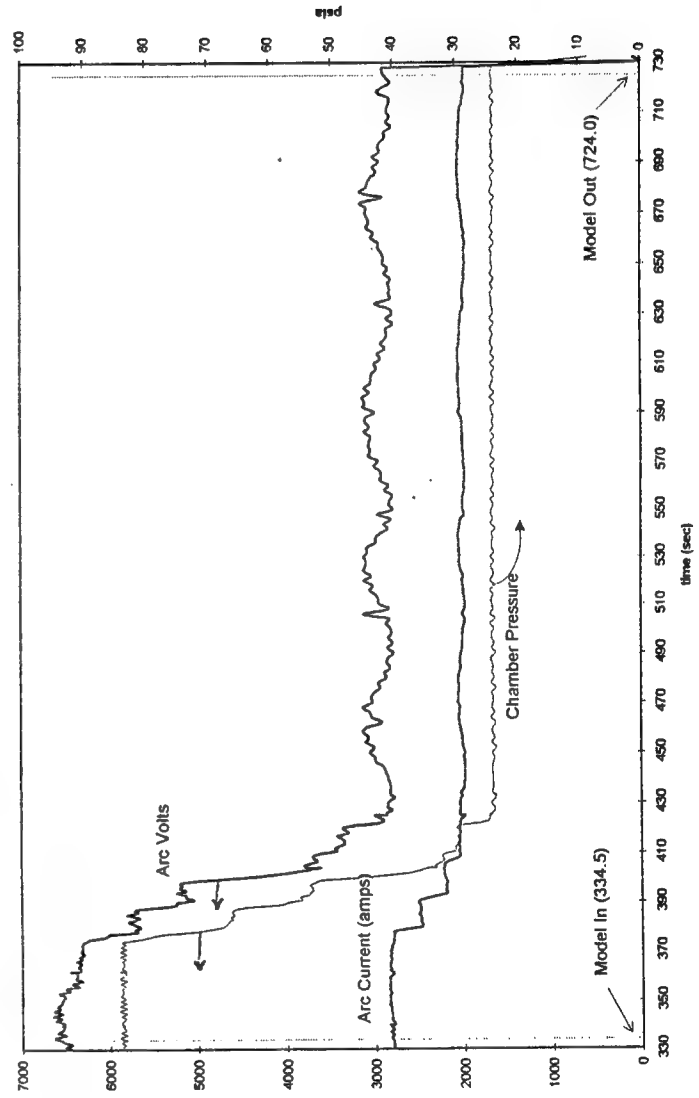
Figure 23. Test Method for Simulating Flight Trajectory Transients

GLIDE

Run 59-010, Cal & Pressure data

INTERMEDIATE

Run 59-012, Cal & Pressure data

PULLOUT

Run 59-006, Cal & Pressure data
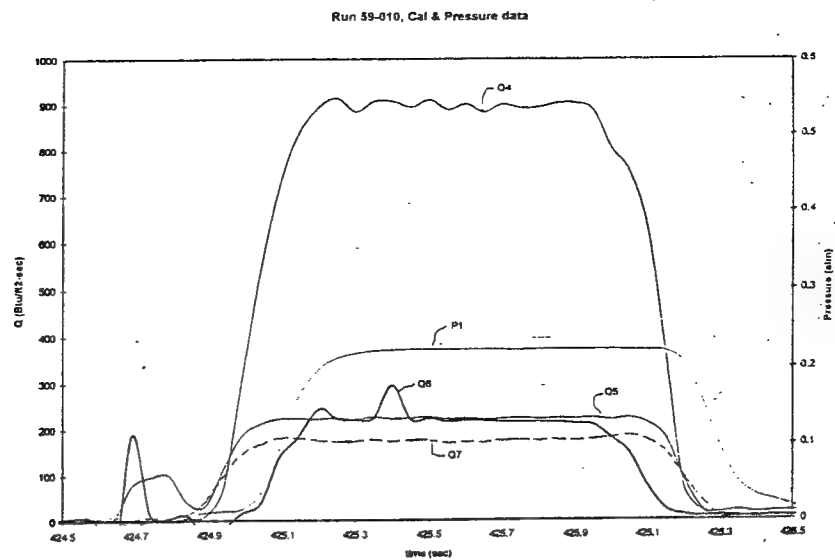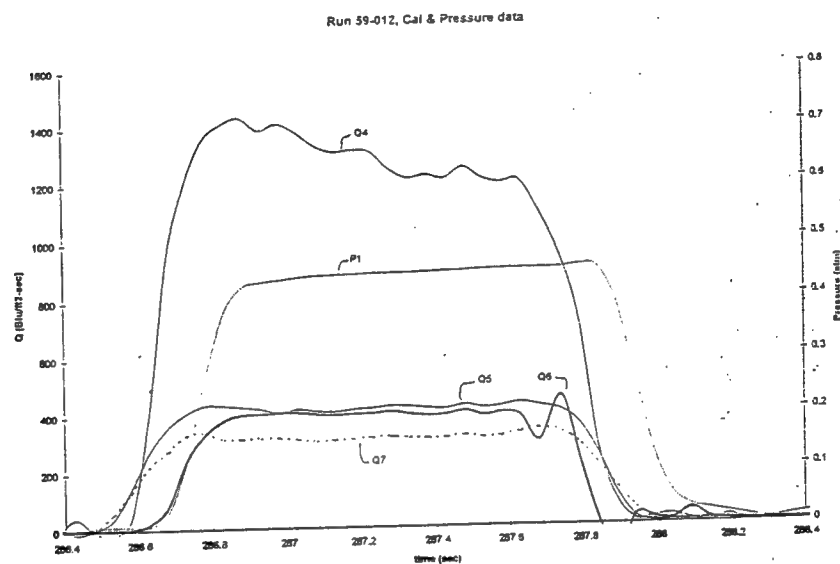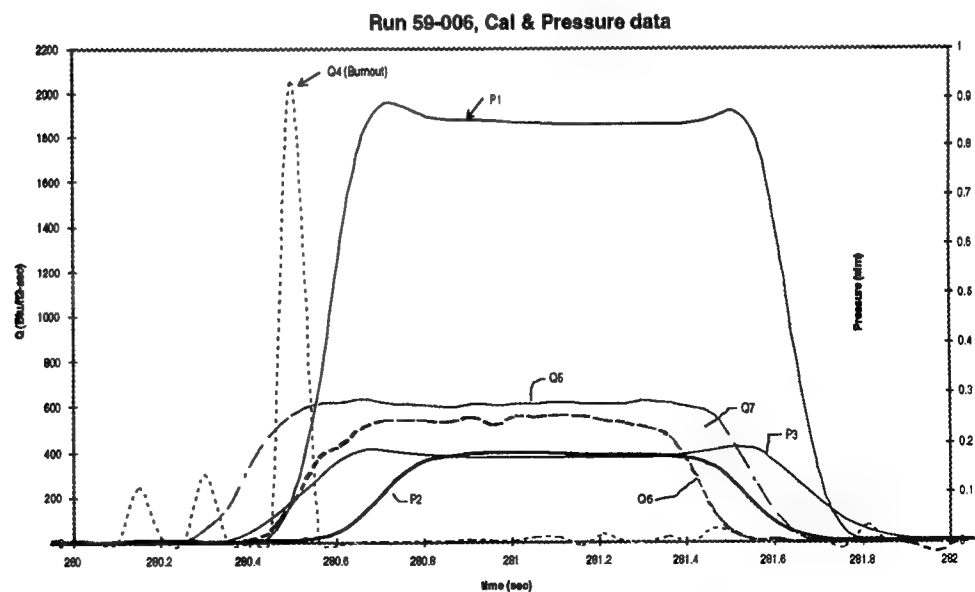
Figure 24. Typical Calorimeter and Pressure Response Data

57

o **SUMMARY OF "BOOMERANG" CALORIMETER MEASUREMENTS (Qcw = Btu/ft²-sec, P = atm, Ht = Btu/lb)**

- NOSETIP (Rn = 0.375")

Condition	Measured			NASA Pre-Test	Predicted
	Qcw	Pt₂	Inferred* (Ht-Hw)	Qcw	Pt₂
Glide	890 to 950	0.21 to 0.23	8,100	1100	0.23
0.7 x Pullout	greater than 1400, Cal overheat	0.41 to 0.46	10,200 (using NASA Qcw)	1600	0.44
Pullout	greater than 2000, Cal melt	0.87 to 0.92	10,300 (using NASA Qcw)	2300	0.90

- LEADING EDGE (Rn = 0.375", SWEEP = 60°)

Condition	Measured Along	Impingement Line	Measured	Ratios
	Qcw	Pe	Q$_{LE}$/Q$_{NT}$	P$_{LE}$/P$_{NT}$
Glide	190 to 225	0.04 to 0.05	0.23	0.23
0.7 x Pullout	400 to 430	0.09 to 0.10	less than 0.30, 0.26 using NASA predicted Q$_{NT}$	0.22
Pullout	560 to 620	0.18	0.26 using NASA predicted Q$_{NT}$	0.21

o **PREDICTED LEADING EDGE HEATING AND PRESSURES (SWEEP = 60°)**

- SPARTA: $Q_{LE}/Q_{NT} = 0.44$, $P_{LE}/P_{NT} = 0.28$ (FOR BOTH PULLOUT and GLIDE)

- LMSC: $Q_{LE}/Q_{NT} = 0.30$, $P_{LE}/P_{NT} = ?$ (FOR BOTH PULLOUT and GLIDE)

* $Qsp = 0.0417 (Pt_2/Rn)^{0.5}(Ht-Hw)$, Rn = ft, P = atm, H = Btu/lb, Qsp = Btu/ft2-sec

Figure 25. Summary of Test Calibrations and Comparison with Predictions

Figure 26.   Test Setup for 0° Sweep Model

Overhead
Video LoS

East Pyro View (30° to
40° off Stag Pt)

30°

0.375" R$_N$

Side View

East Pyro

East Pyro Spot

5 to 10 ° (West Pyro View)

Plan View

45°

0.12" 0.30"

3.25"

East Pyro
Spot Size

West Pyro
Spot Size

Nose-On View

59
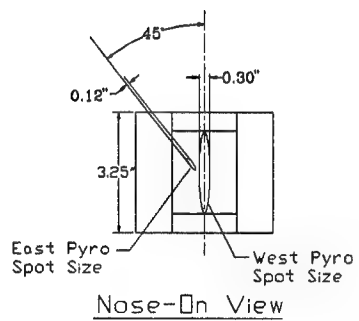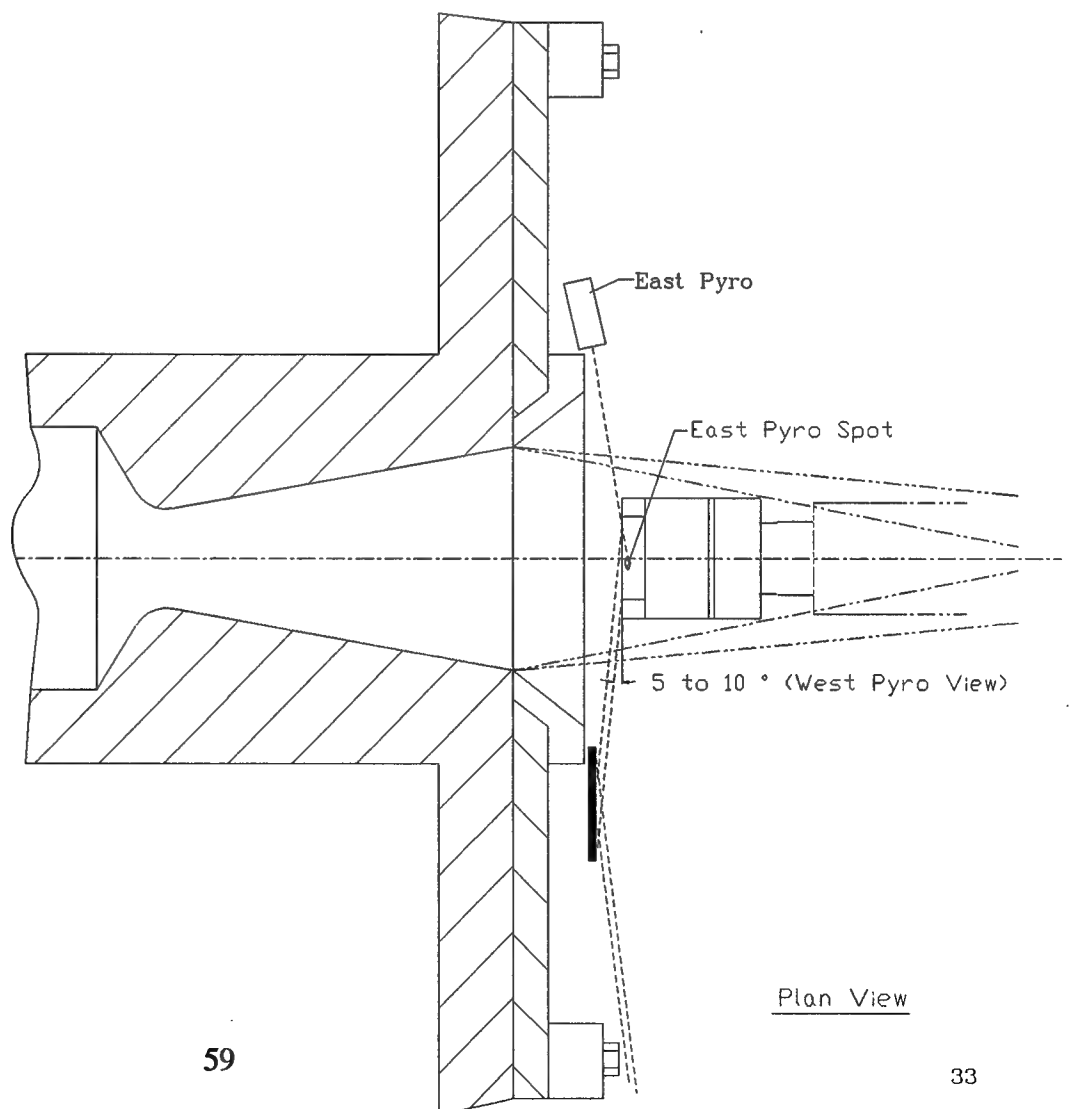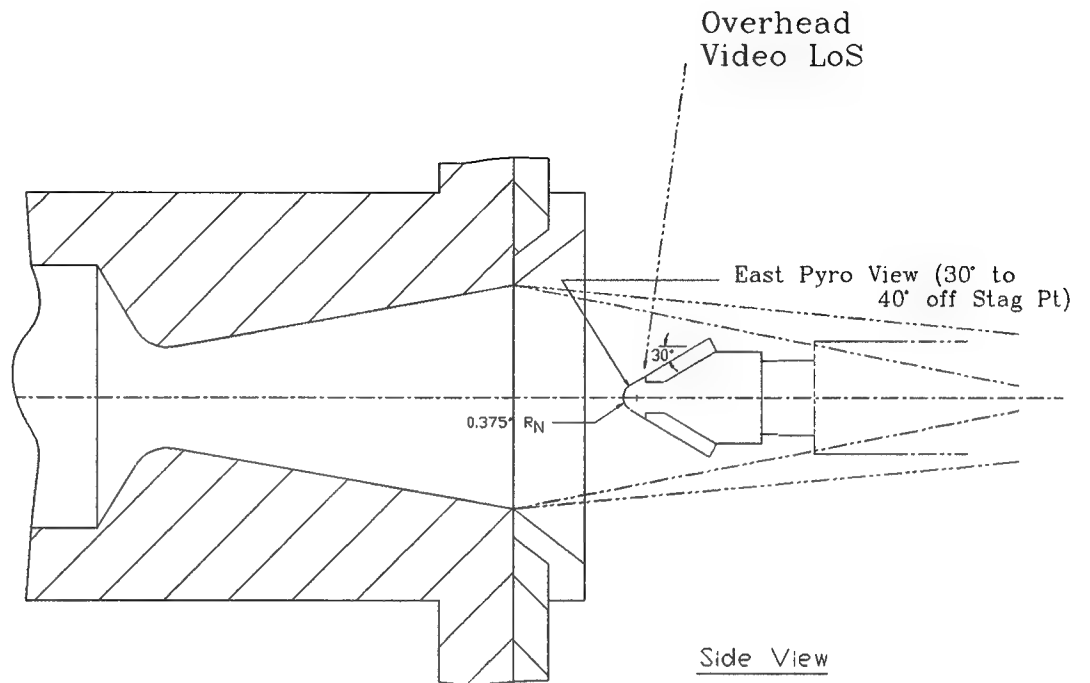
o **ONE (1) NT TEST**

  - MATERIAL: SAIC C-C with ULTRAMET COATING, MODEL TESTED IN LCAT (GFY93) at Qcw = 415 and Hr = 3200 and Experienced No Ablation
  - CONDITION: LOWEST Qcw OBTAINABLE IN 6.0" NOZZLE, Qcw = 900 Btu/ft2-sec for 60 sec (per SAIC recommendation)

o **THREE (3) LE TESTS AT 0° SWEEP**

  - MATERIALS: FMI 223(Pan), SAIC C-C with ULTRAMET COATING, MSNW "SOCK" OVER POCO
  - CONDITION: LOWEST Qcw OBTAINABLE IN 6.0" NOZZLE, Qcw = 630 Btu/ft2-sec for a Planned 160 sec Dwell. Qcw same as LE Pullout on 60° Boomerang, duration gives integrated heating of Boomerang Trajectory Simulation.

o **EIGHT (8) LE TESTS AT 60° SWEEP (= 16 Samples)**

  - MATERIAL: FMI 223(Pan), TEXTRON FWPF, GE 4DO,
            SAIC C-C with ULTRAMET coating, HITCO Ceracarb
  - TEST VARIABLES:
    + WEAVE ORIENTATION: and   to impingement line
    + AoA: 0° AND 10°
    + TRAJECTORY SEQUENCE: PULLOUT ONLY, GLIDE ONLY, and PULLOUT and GLIDE (single test)
      + TEST REPRODUCIBILITY
      + EFFECT OF BOOMERANG SIDE

  - CONDITIONS:
    + PULLOUT: Qcw = 620 for 45 sec, then ramp down to Glide (at 90 sec, Qcw = 220). Dwell = 90 sec
    + GLIDE: Qcw = 220 for 300 sec Dwell
    + PULLOUT and GLIDE: sum of PULLOUT and GLIDE, Dwell = 390 sec

Figure 27. Summary of Leading Edge Test Matrix

60

Run 59-009, Arc data
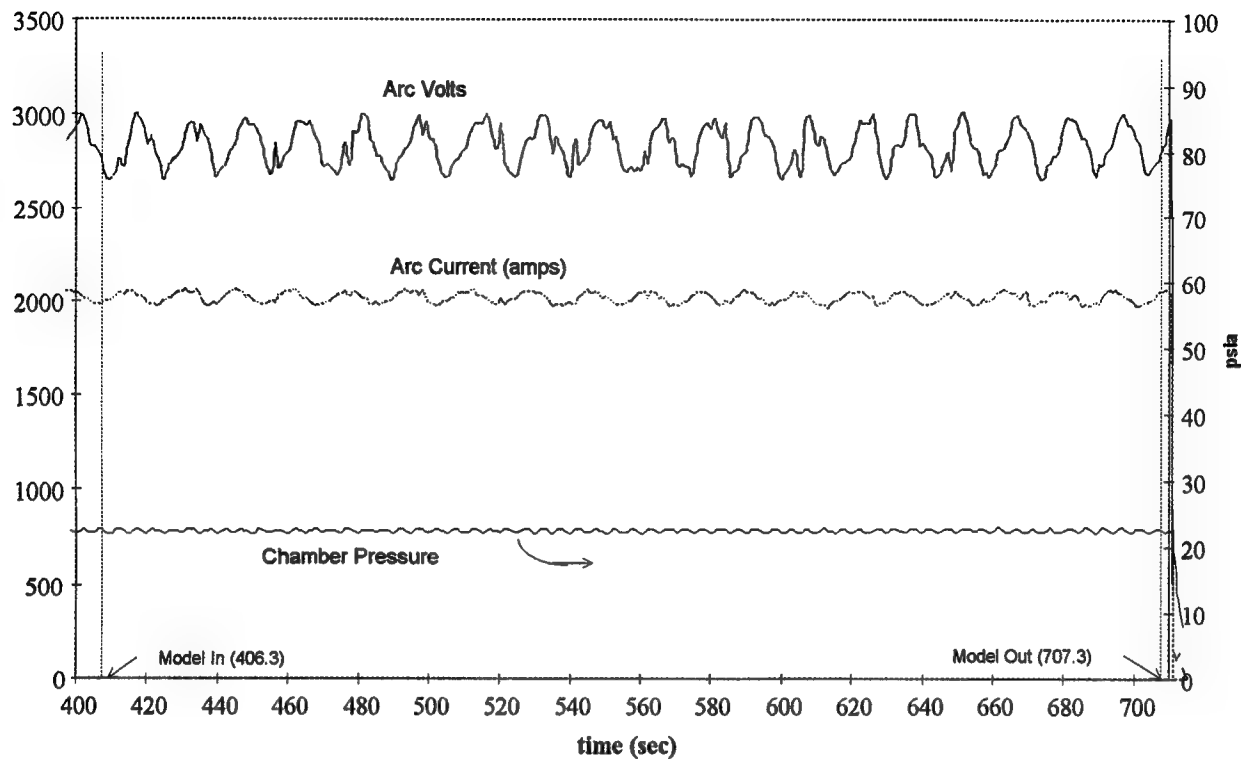
Run 59-009, TC & Pyro data
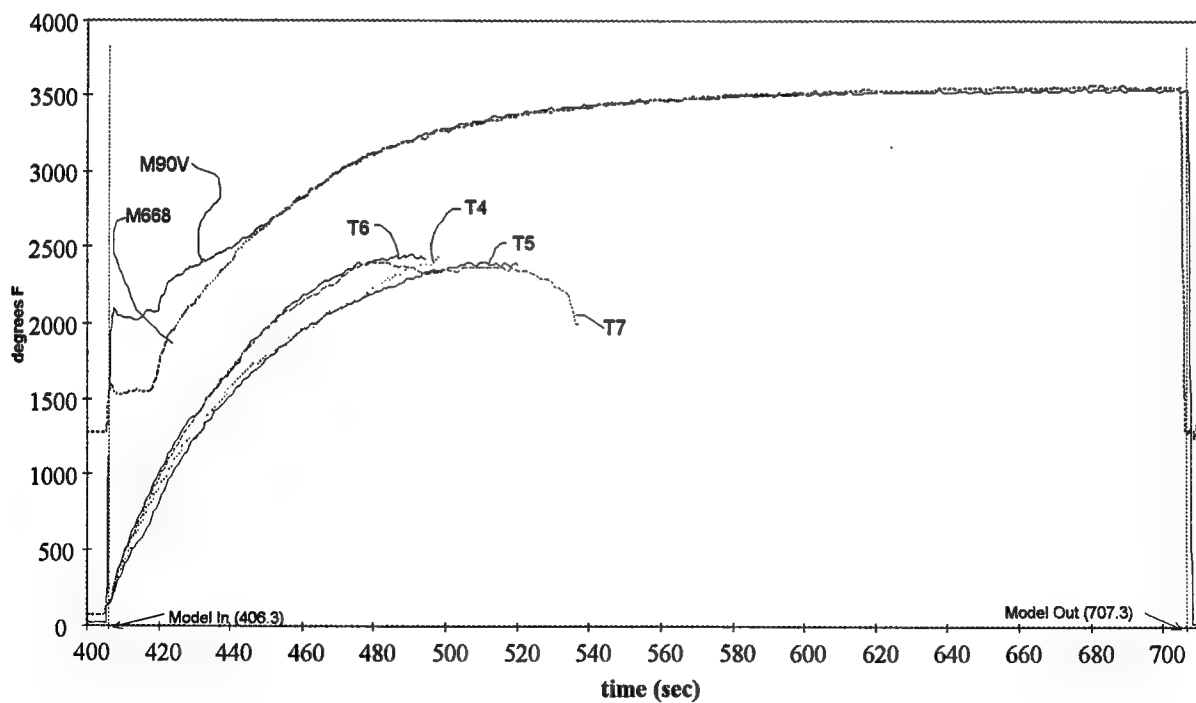
Figure 28. Run 59-009 Facility and Model Data

61

RUN 59-009, GLIDE. FWPF (WEST) AND 223 (EAST) AT 0° AoA

b) POST TEST PLAN VIEW (EAST ON TOP)

c) NOSE ON VIEW (EAST ON LEFT)

a) PRE-TEST (WEST ON TOP)
Note: Gaps Not Yet Filled with RTV
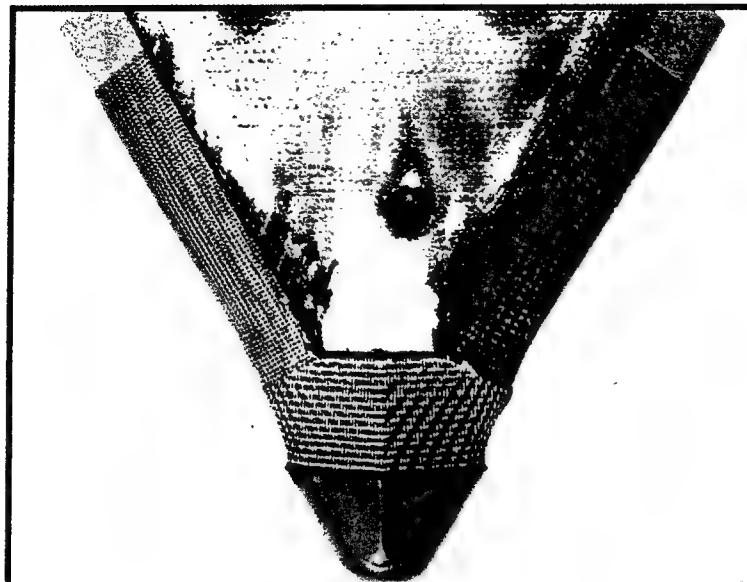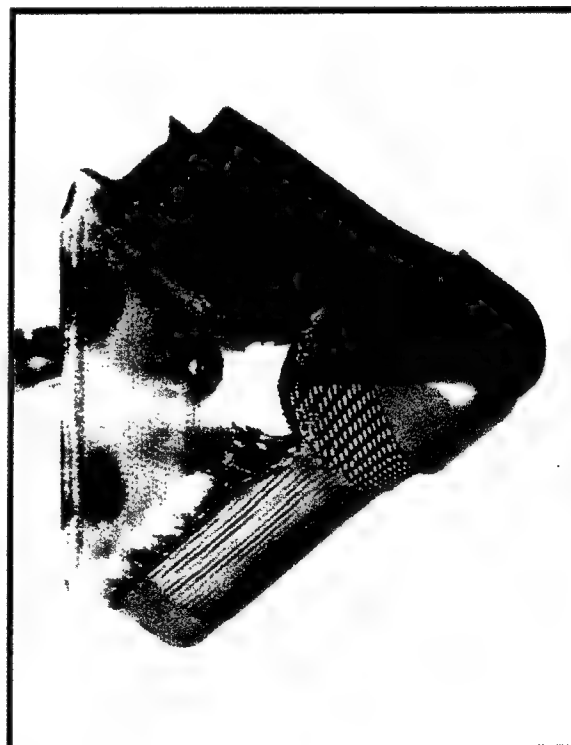
Figure 28 cont'd. Model Photographs

62

Run 59-009, FWPF Leading Edge

Fore

Aft
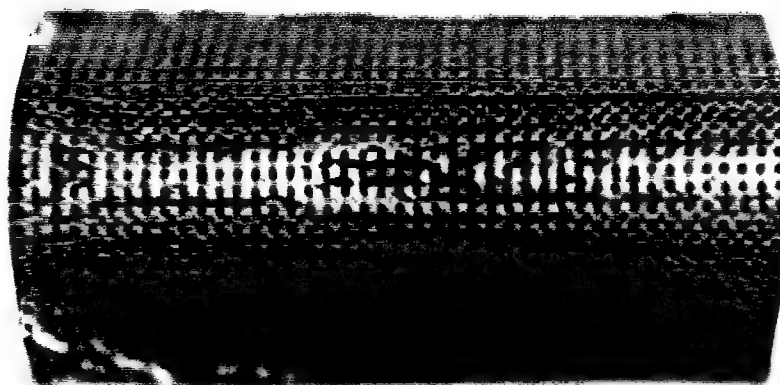
a) Front View
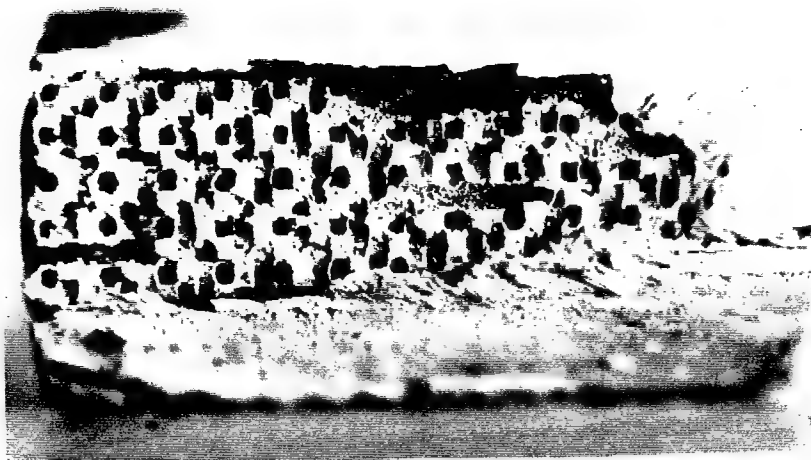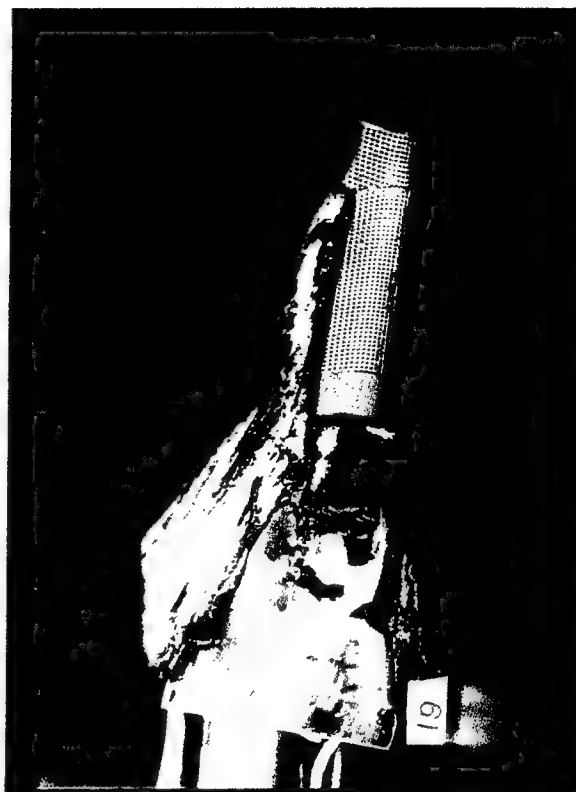
Fore

Run 09,
FWPF

Aft
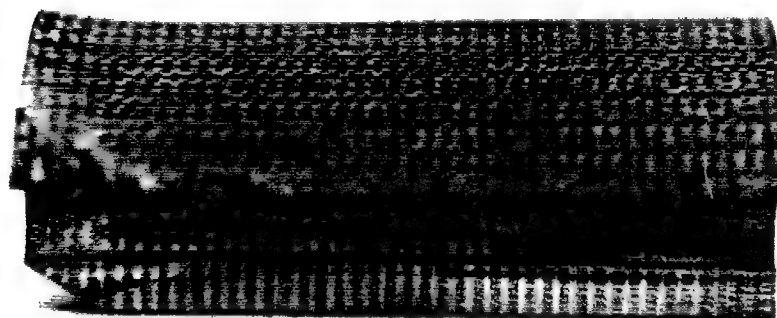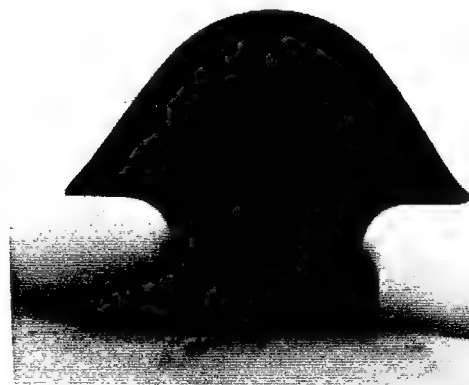
b) Planform View

Run 09,
FWPF

Run 09,
FWPF

c) Profile, Fore

d) Profile, Aft

Figure 28 cont'd. Run 59-009 Post Test Ablation Contours
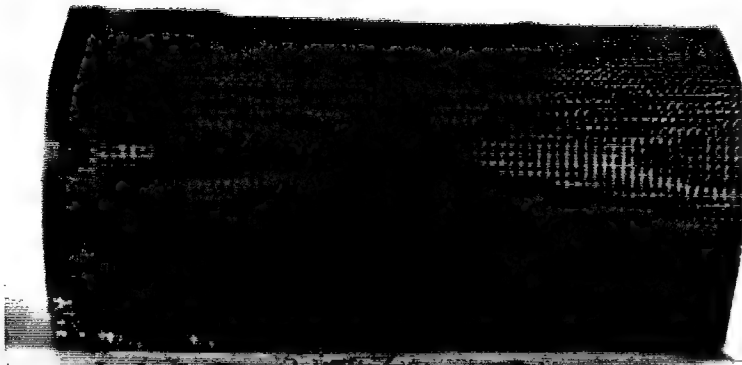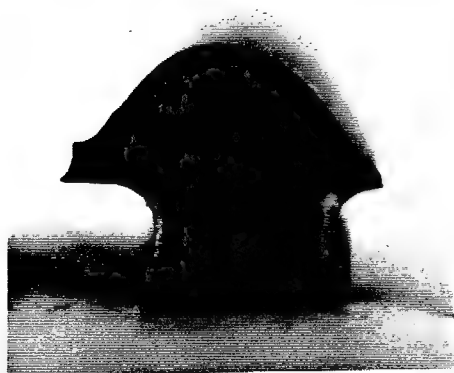
Fore

Aft

Run 09,
223

a) Front View

Fore

Aft
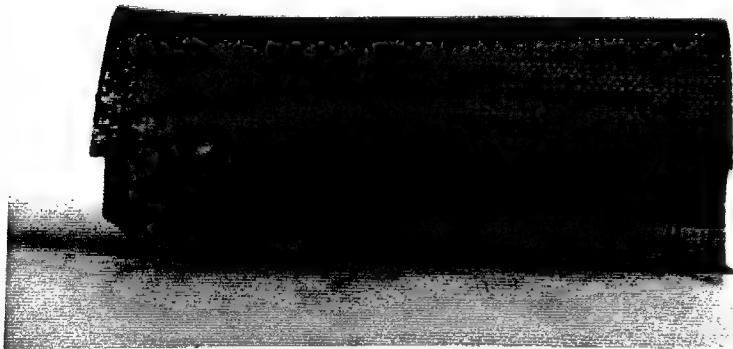
Run 09,
223

b) Planform View
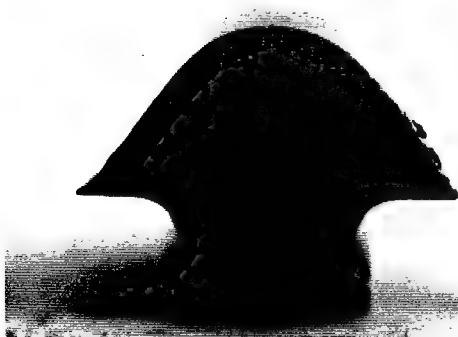
Run 09,
223

c) Profile, Fore

Run 09,
223

d) Profile, Aft

Figure 28 cont'd. Run 59-009 Post Test Ablation Contours
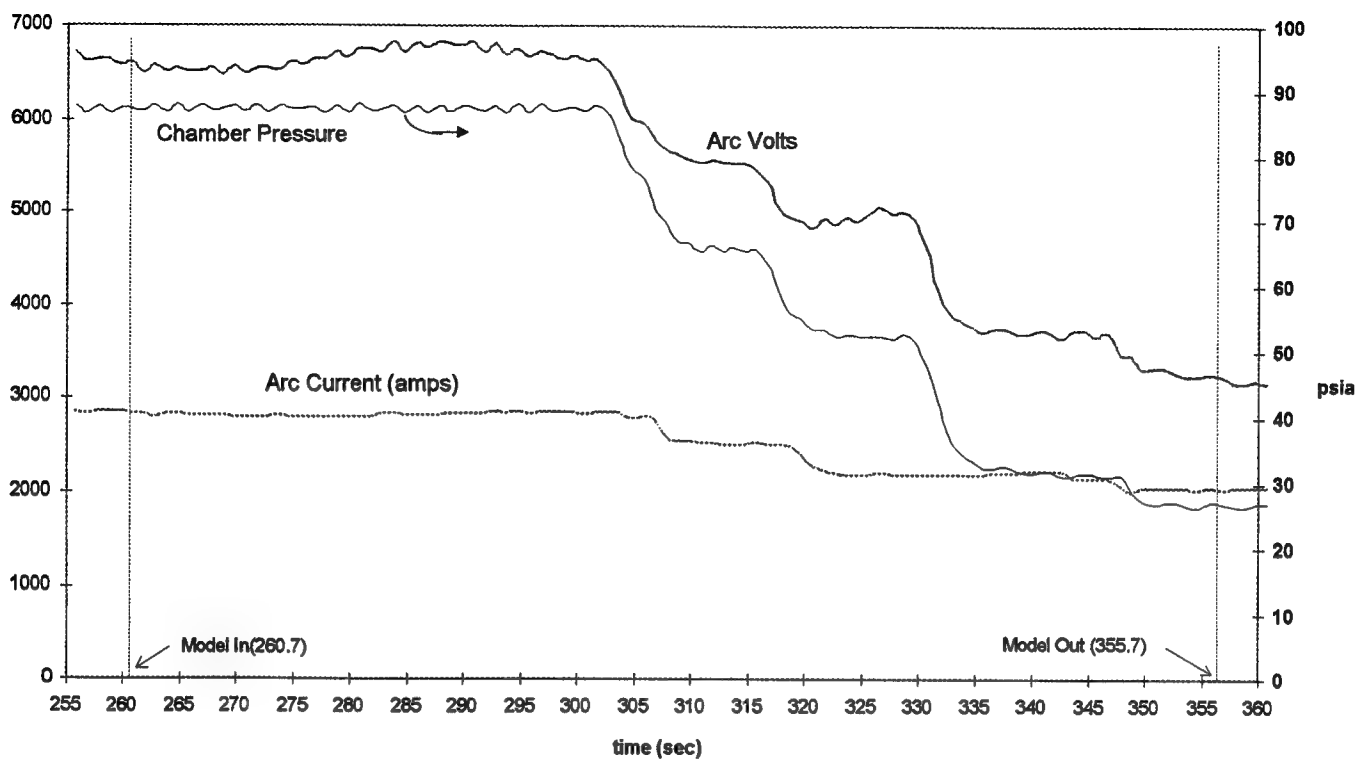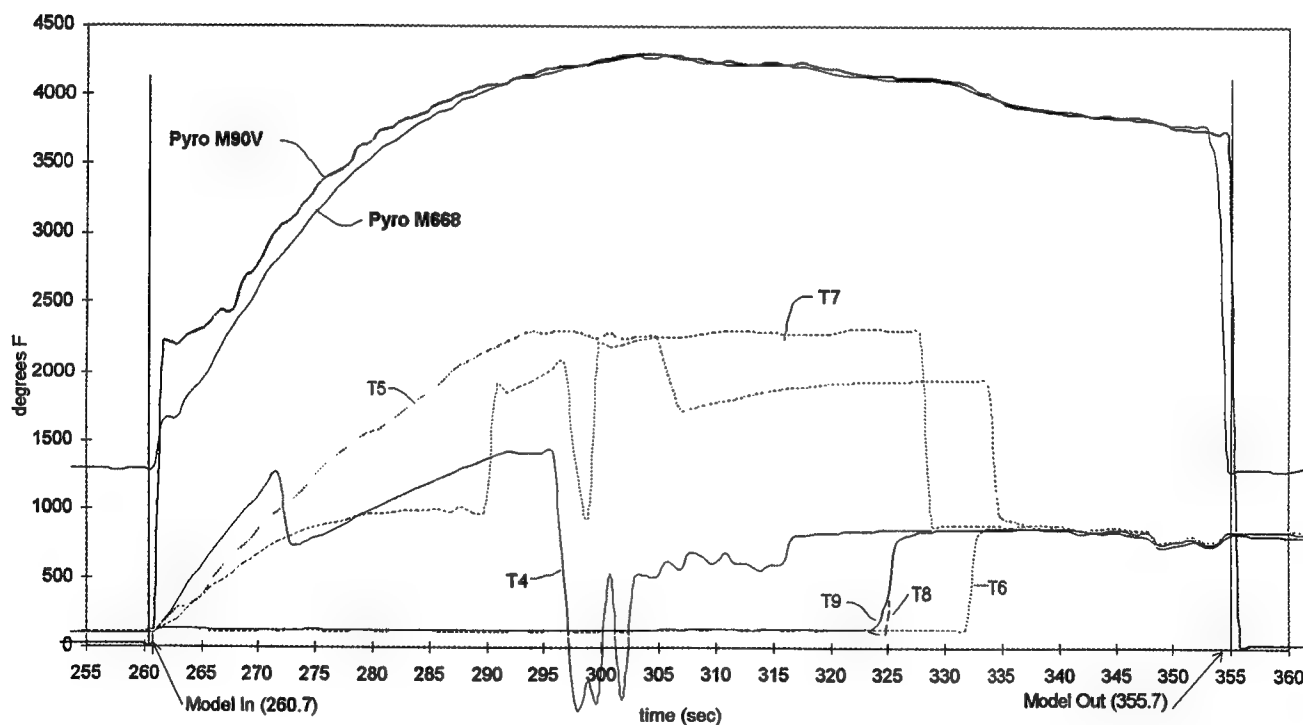
Figure 29. Run 59-013 Facility and Model Data

65

RUN 59-013, PULLOUT, FWPF (WEST) AND 223 (EAST) AT 0° AoA

b) SIDE VIEW OF FWPF (WEST)
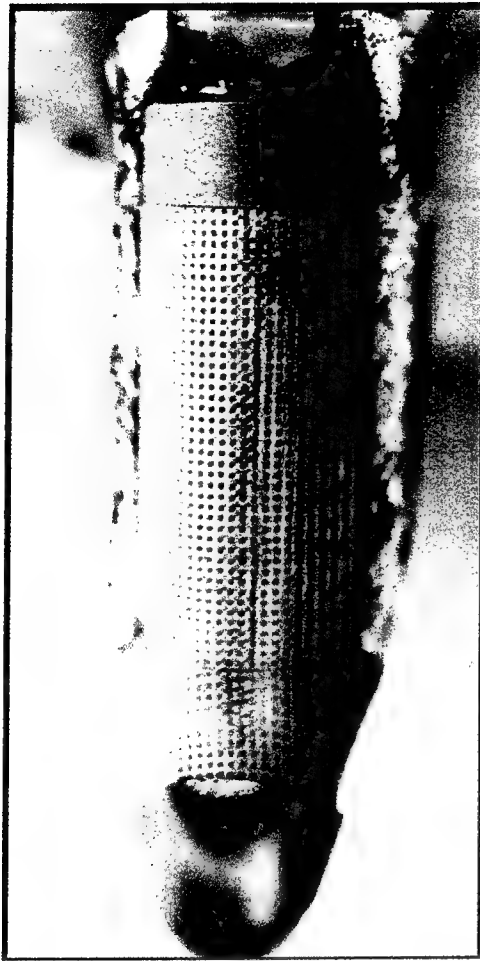
c) SIDE VIEW OF 223 (EAST)

a) PLAN VIEW

FWPF

223

Figure 29 cont'd. Model Photographs

66

RUN 59-013, PULLOUT. VIEW OF POST-TEST NOSETIP AND C-C TRANSITION
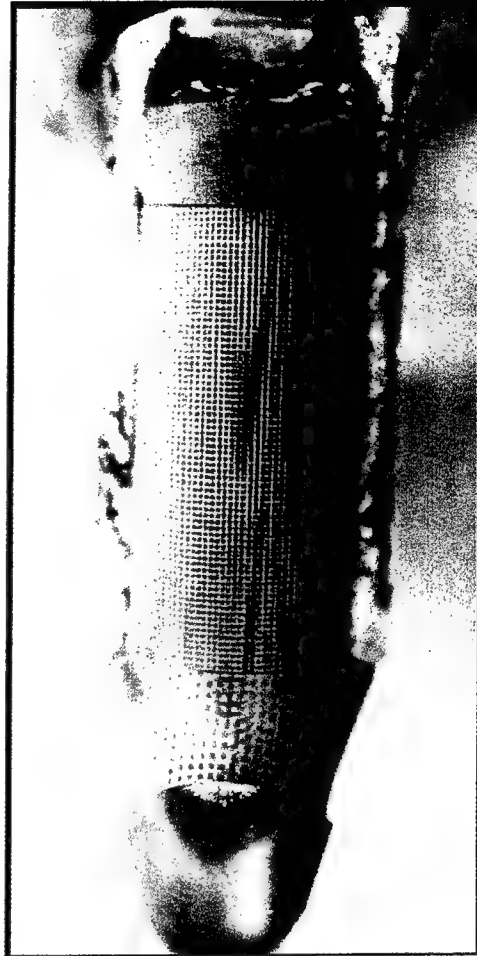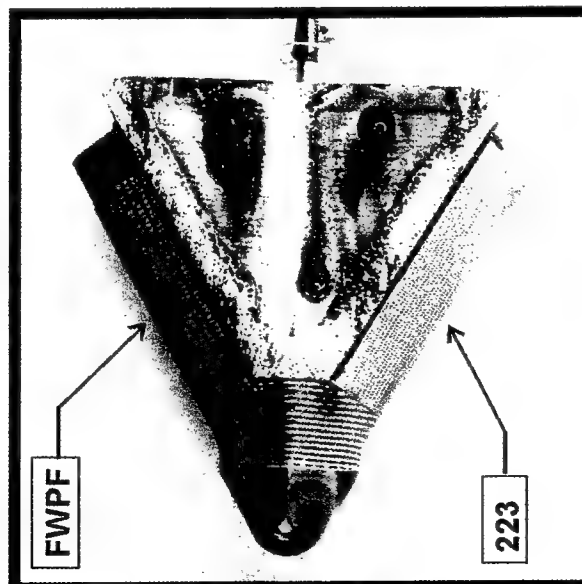
b) PROFILE VIEW (EAST SIDE)
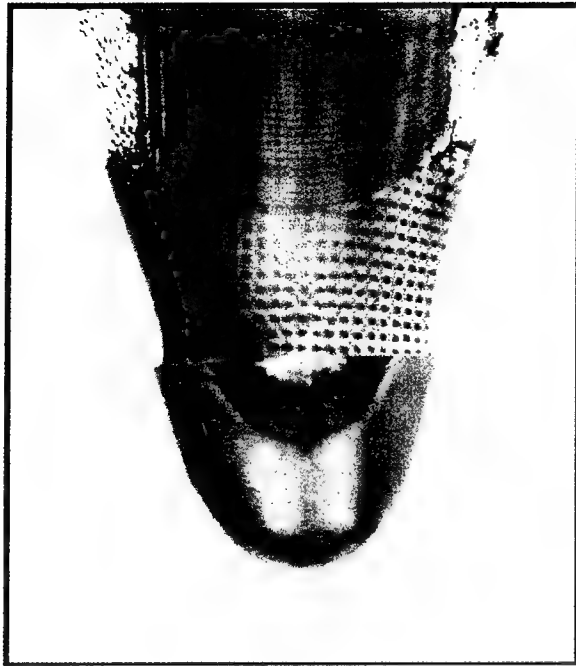
c) PLAN VIEW (EAST SIDE ON TOP)
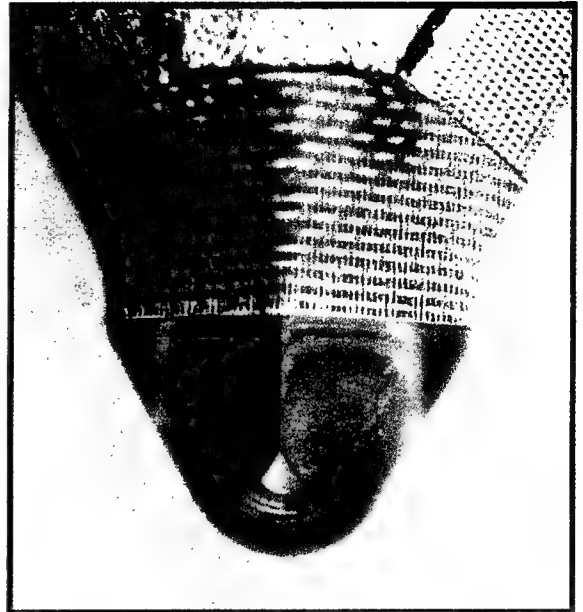
a) NOSE ON VIEW

Note Groove Caused by
Possible Particle Impact
(In Runs -009 through -020,
Possible Particle Impact only Occured
during Run -013)

Figure 29 cont'd.   Model Photographs

67

a) Front View

b) Planform View

c) Profile, Fore

d) Profile, Aft

Figure 29 cont'd. Run 59-013 Post Test Ablation Contours
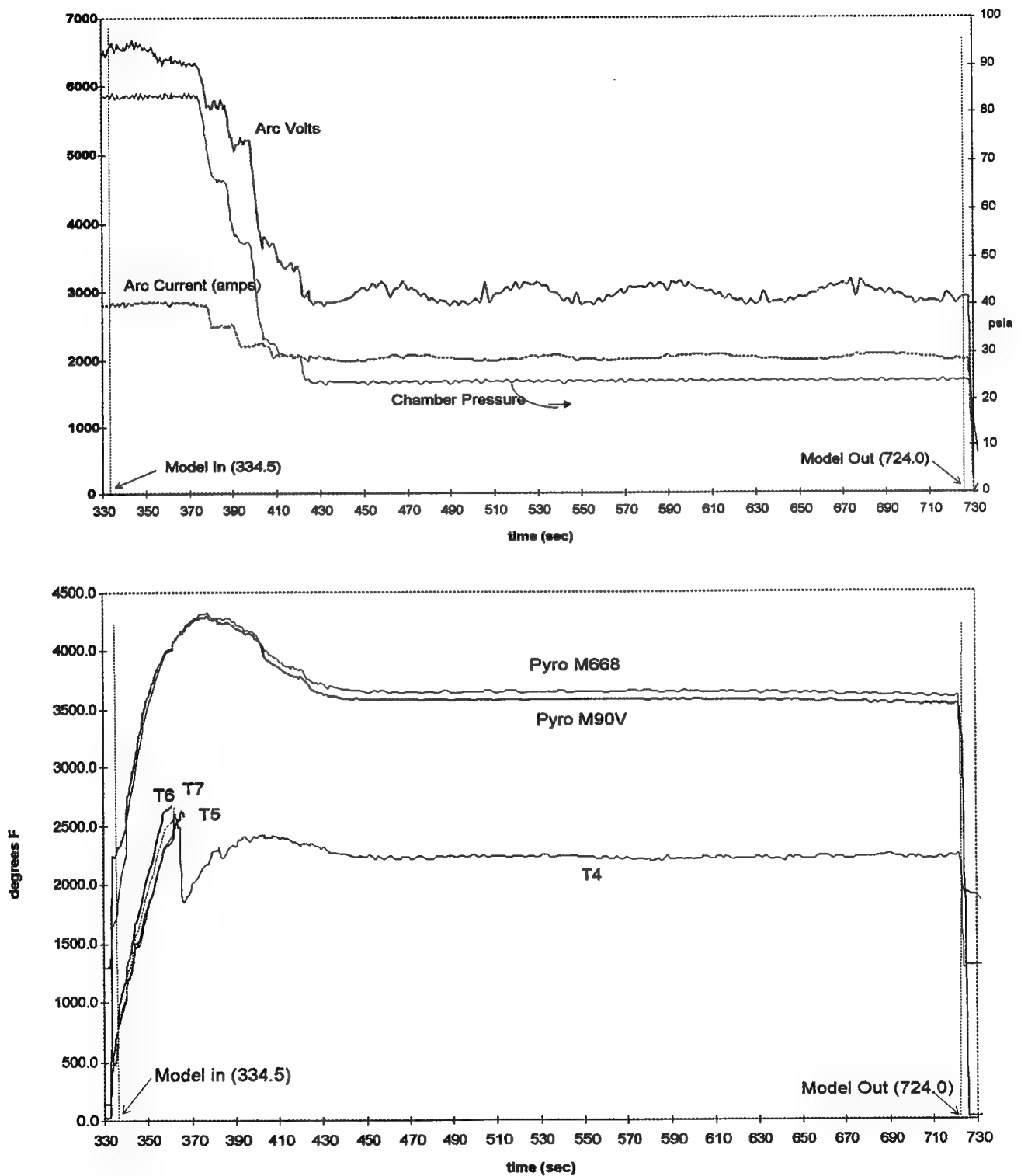
Figure 30. Run59-014, Facility and Model Data

RUN 59-014, PULLOUT-GLIDE, FWPF (WEST) AND 223 (EAST) AT 0° AoA

a) PLAN VIEW OF MODEL UPPER SURFACE
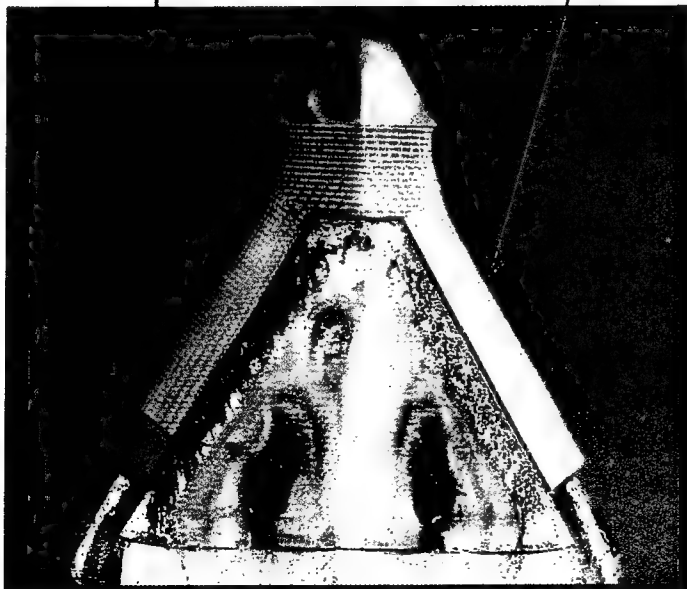
b) PLAN VIEW OF MODEL LOWER SURFACE

FWPF

223

c) PROFILE VIEW OF 223 SIDE (EAST)
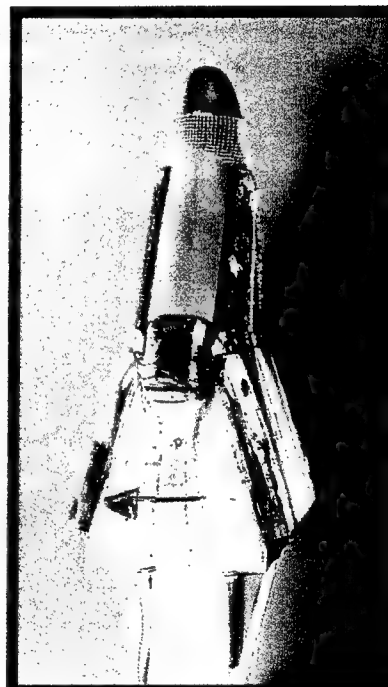
Figure 30 cont'd. Model Photographs
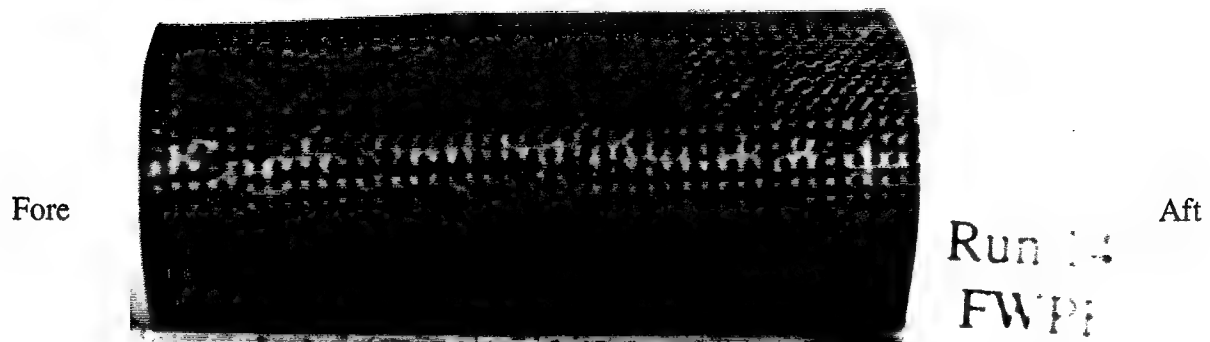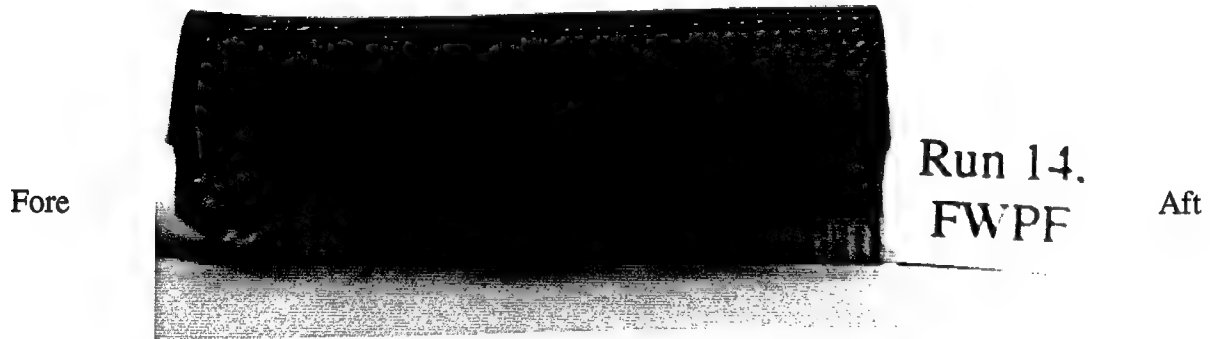
70

a) Front View

b) Planform View

c) Profile, Fore

d) Profile, Aft

Figure 30 cont'd. Run 59-014 Post Test Ablation Contours

Run 59-014, 223 Leading Edge

Fore   Aft
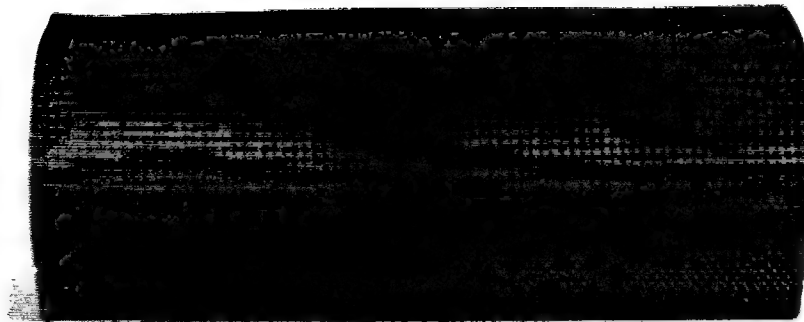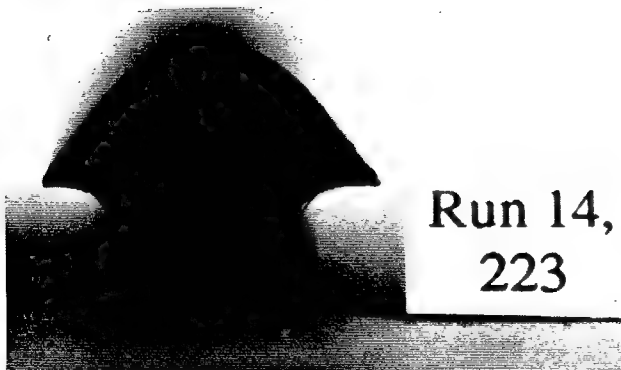
a) Front View

Fore   Aft

b) Planform View

c) Profile, Fore   d) Profile, Aft

Figure 30 cont'd. Run 59-014 Post Test Ablation Contours
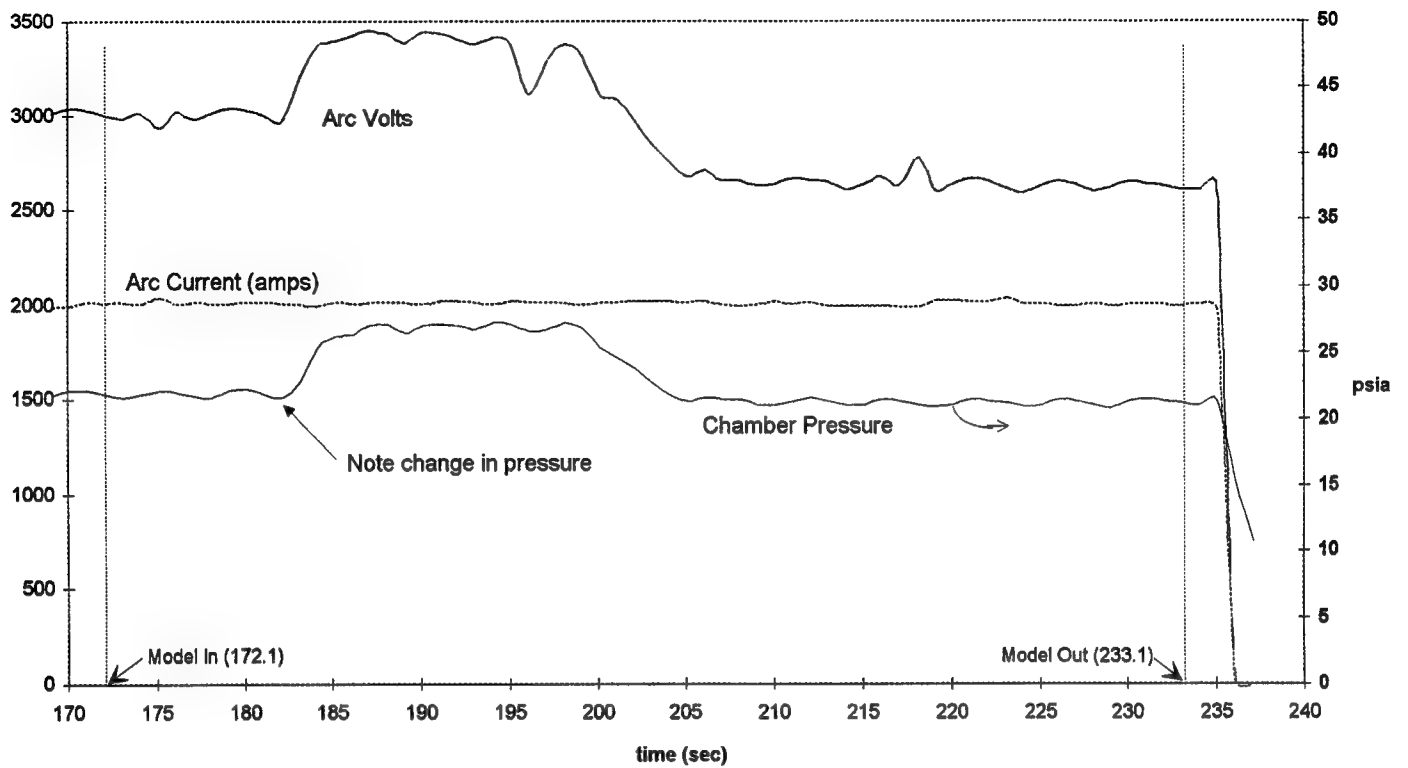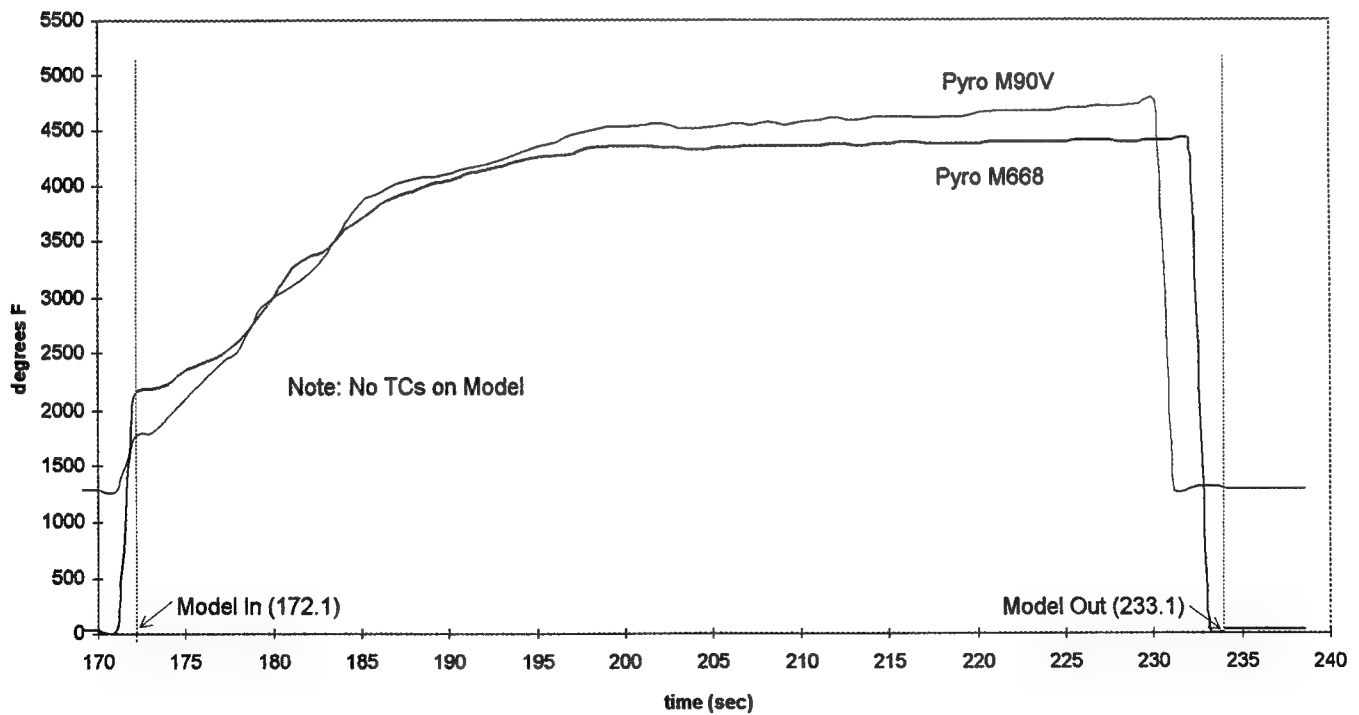
Figure 31. Run 59-015 Facility and Model Data

RUN 59-015, SAIC NOSETIP TEST AT CONSTANT Qcw
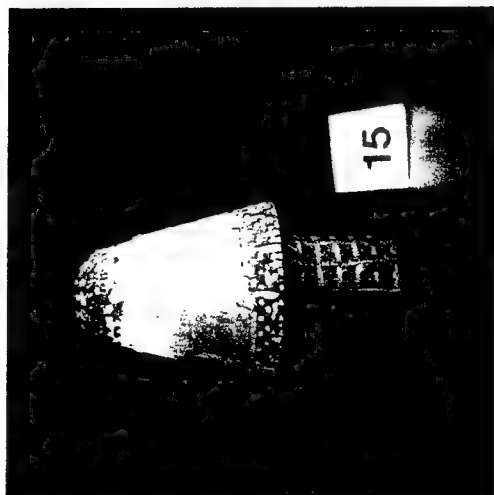
a) PROFILE VIEW

b) NOSE ON VIEW

c) PROFILE VIEW

Figure 31 cont'd. Model Photographs

74

m8
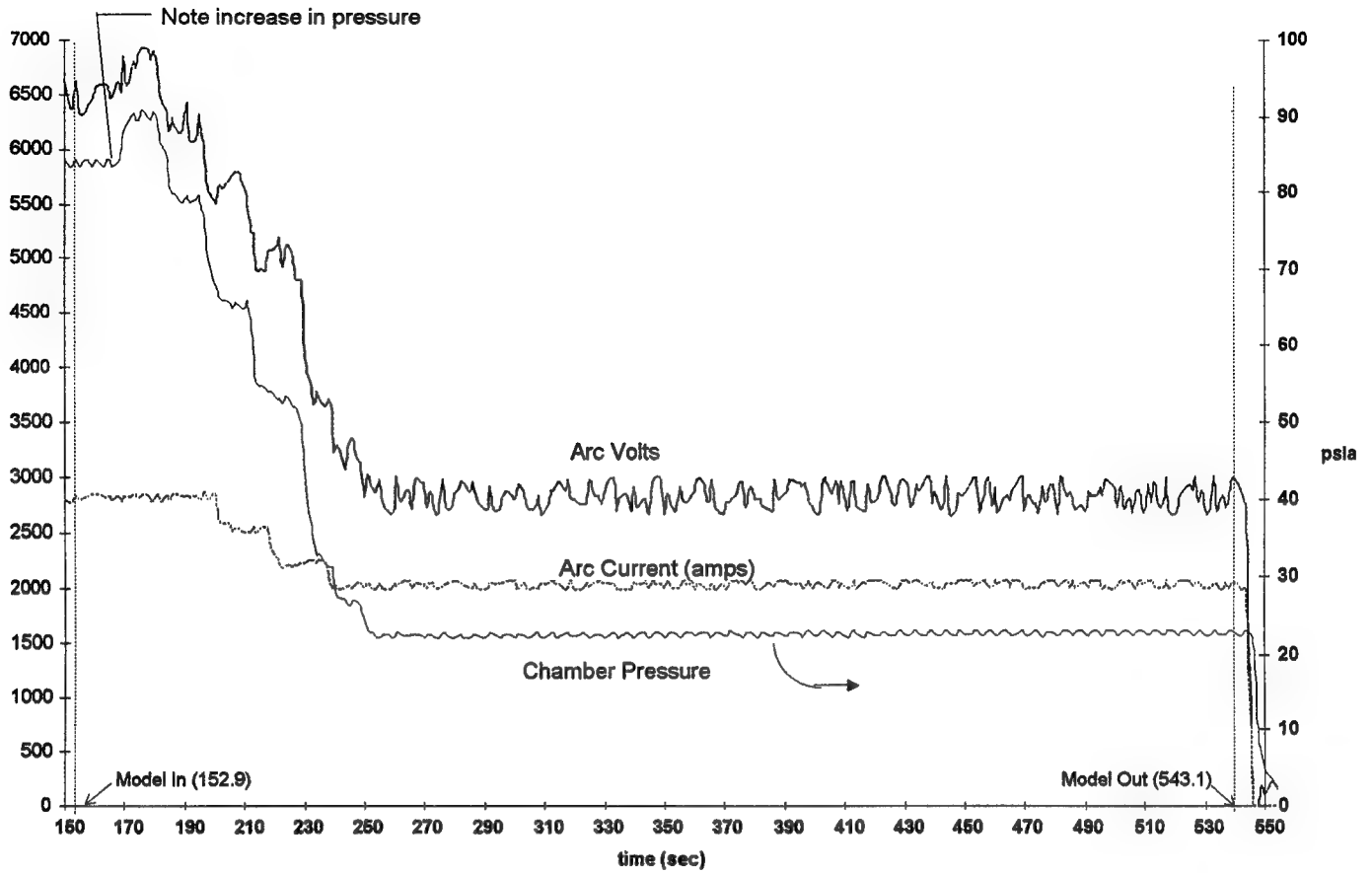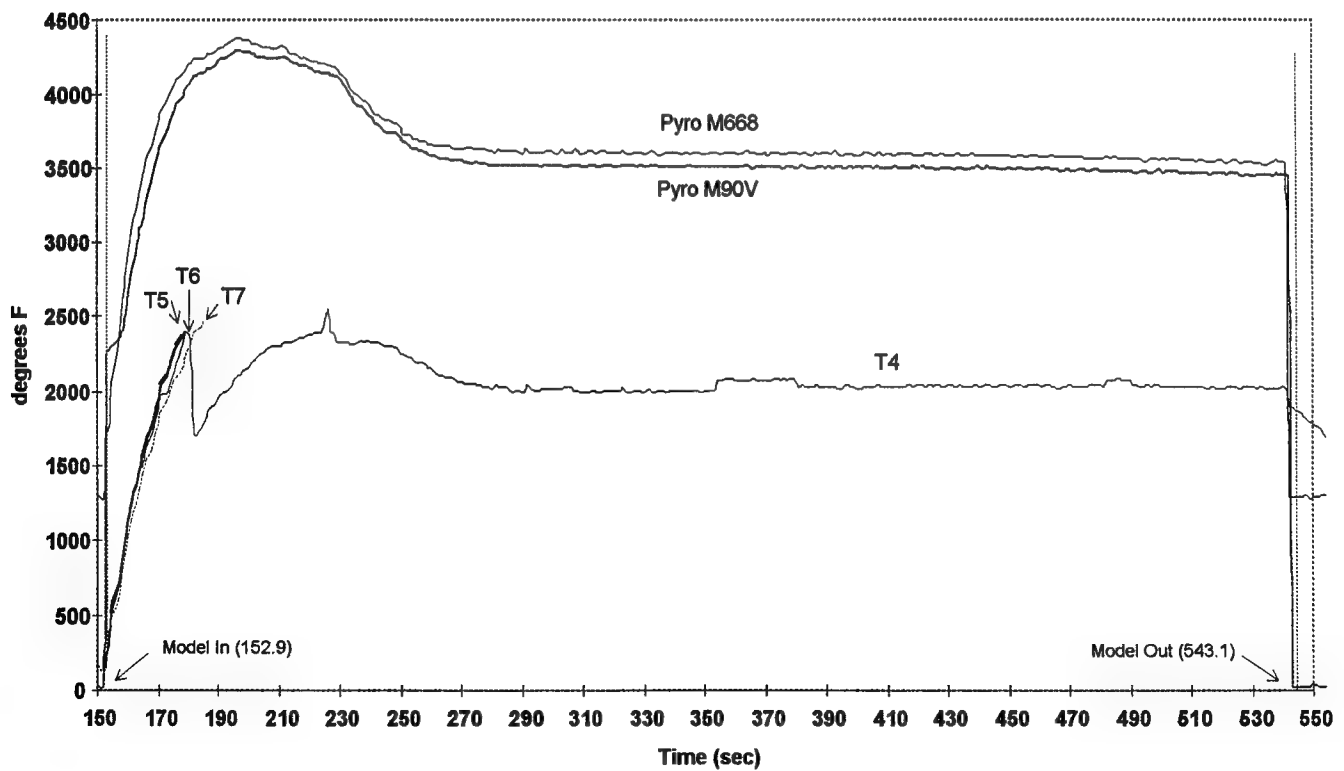
Figure 32. Run 59-016 Facility and Model Data

RUN 59-016, PULLOUT-GLIDE, 4DO (WEST) AND 223 WITH Z // TO SWEEP (EAST)
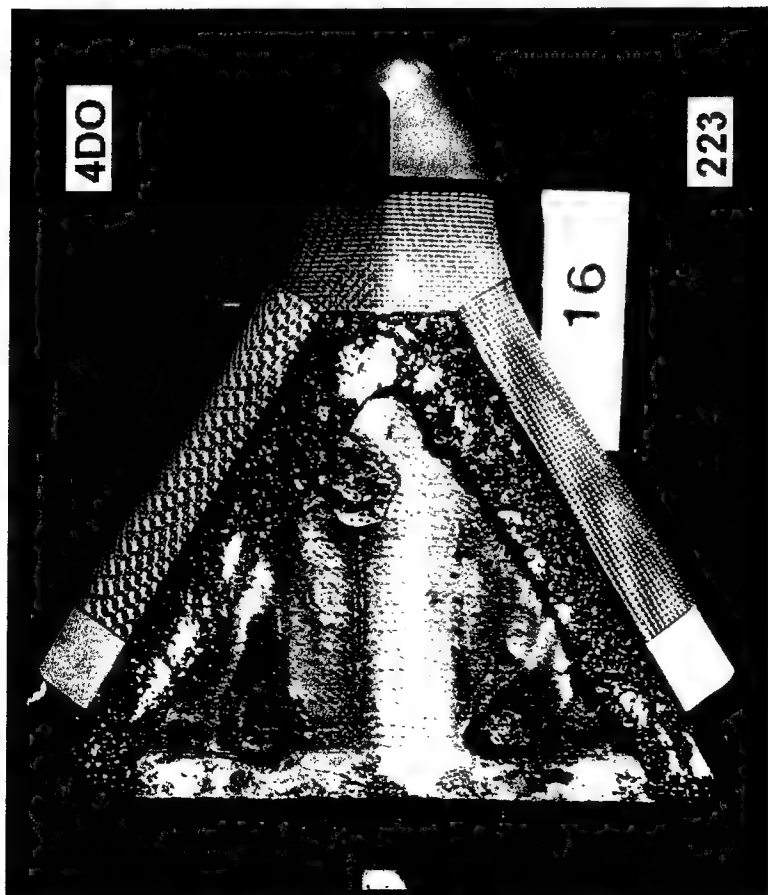
B) SIDE VIEW 223 (EAST)

a) PLAN VIEW
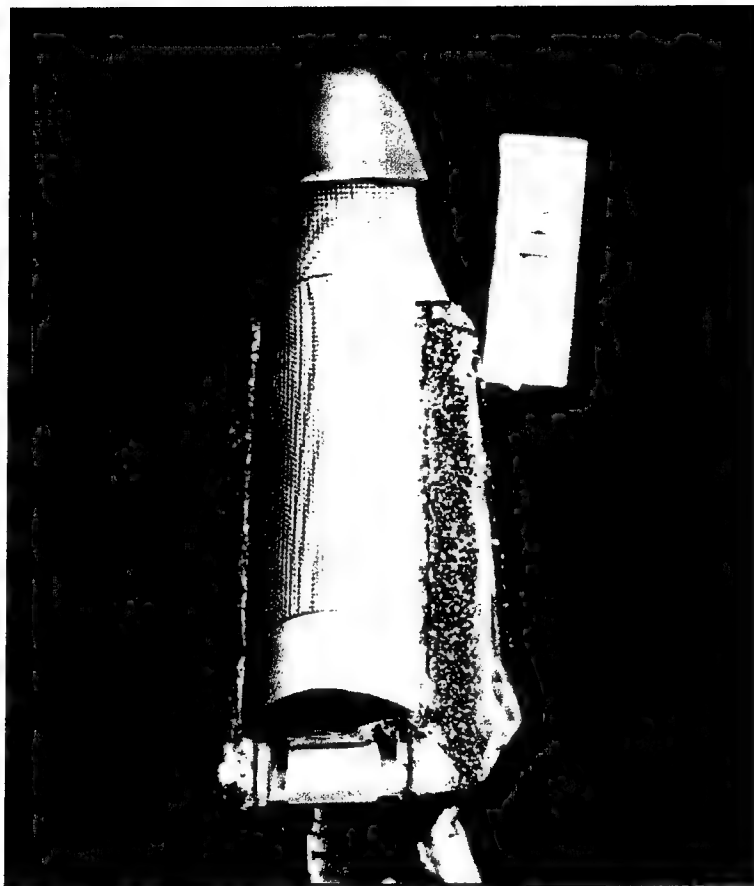
Figure 32 cont'd. Model Photographs

76

Run 59-016, 223 Leading Edge

Fore   Run 16, Aft
                                                    223

a) Front View
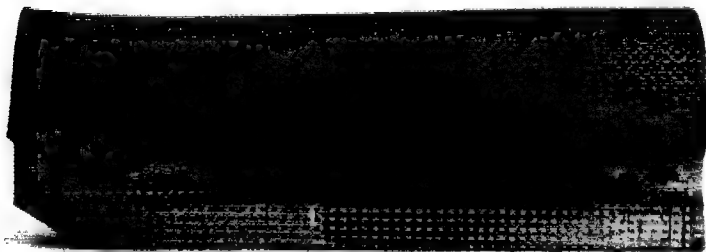
Fore   Run 16. Aft
                                                    223

b) Planform View

Run 16,   Run 16,
223   223
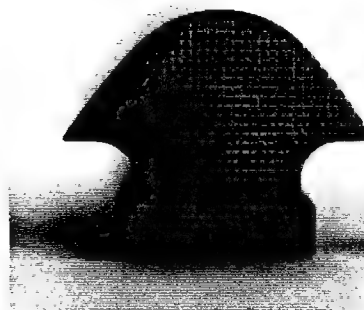
c) Profile, Fore   d) Profile, Aft

Figure 32 cont'd. Run 59-016 Post Test Ablation Contours

77

Run 59-016, 4DO Leading Edge

Fore   Aft
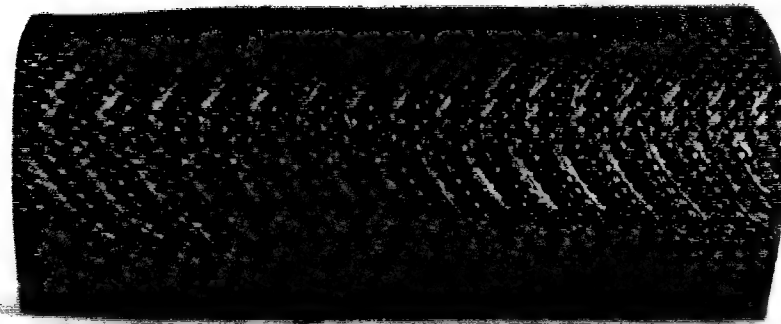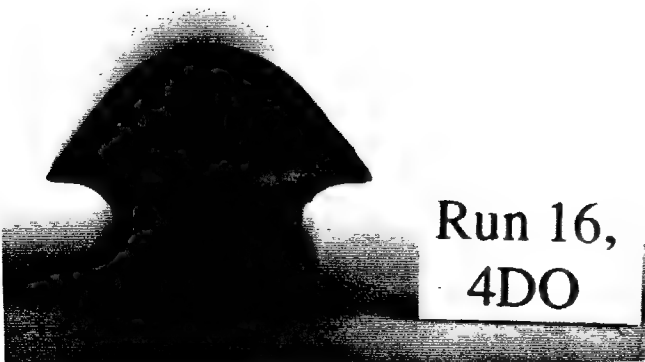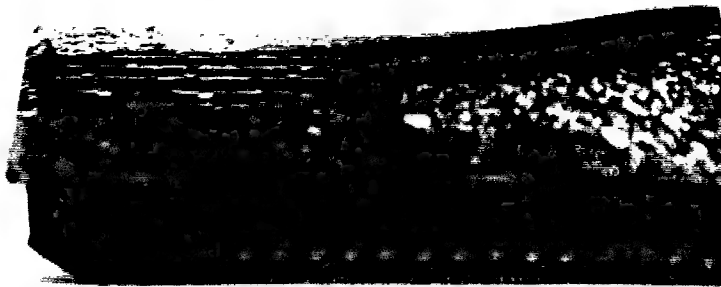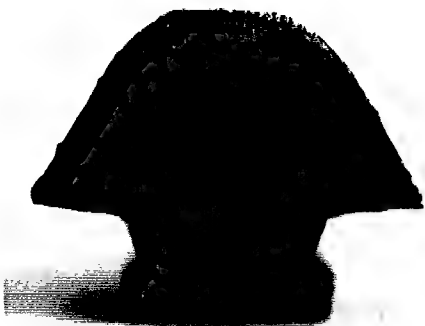
a) Front View

Fore   Run 16,   Aft
                                        4DO

b) Planform View

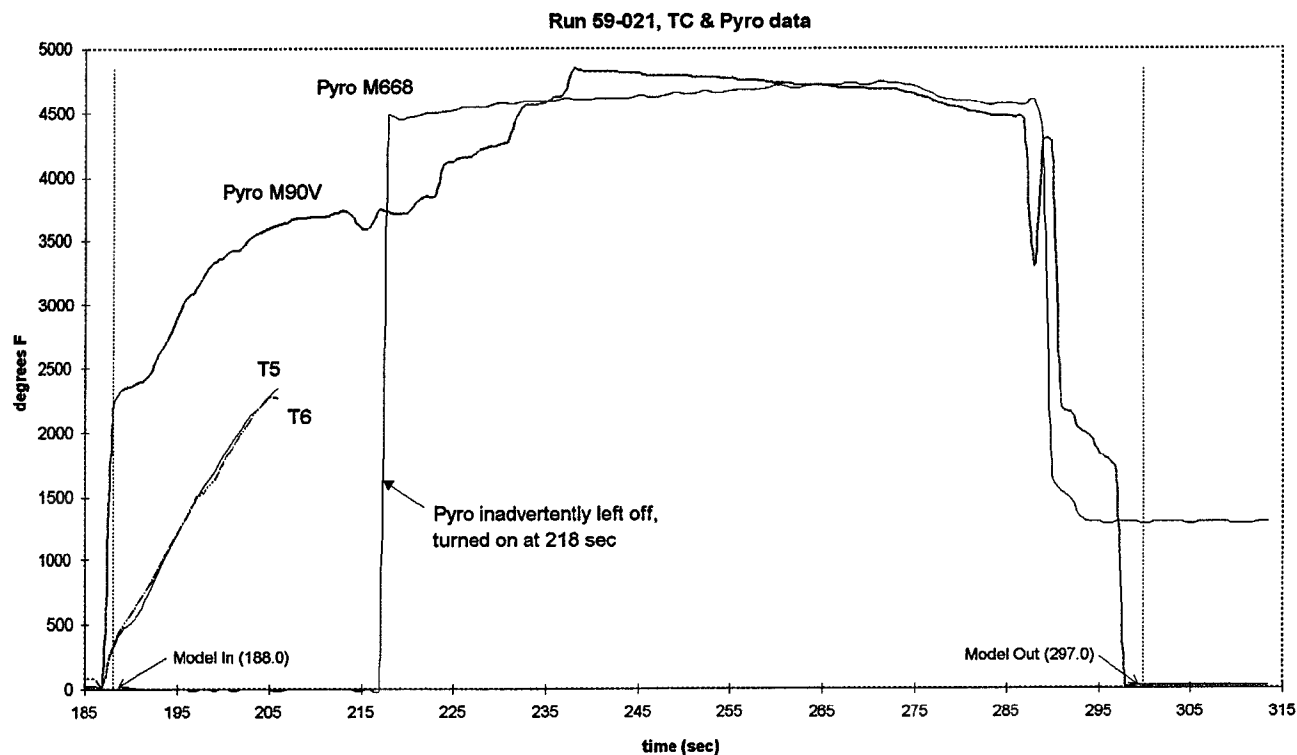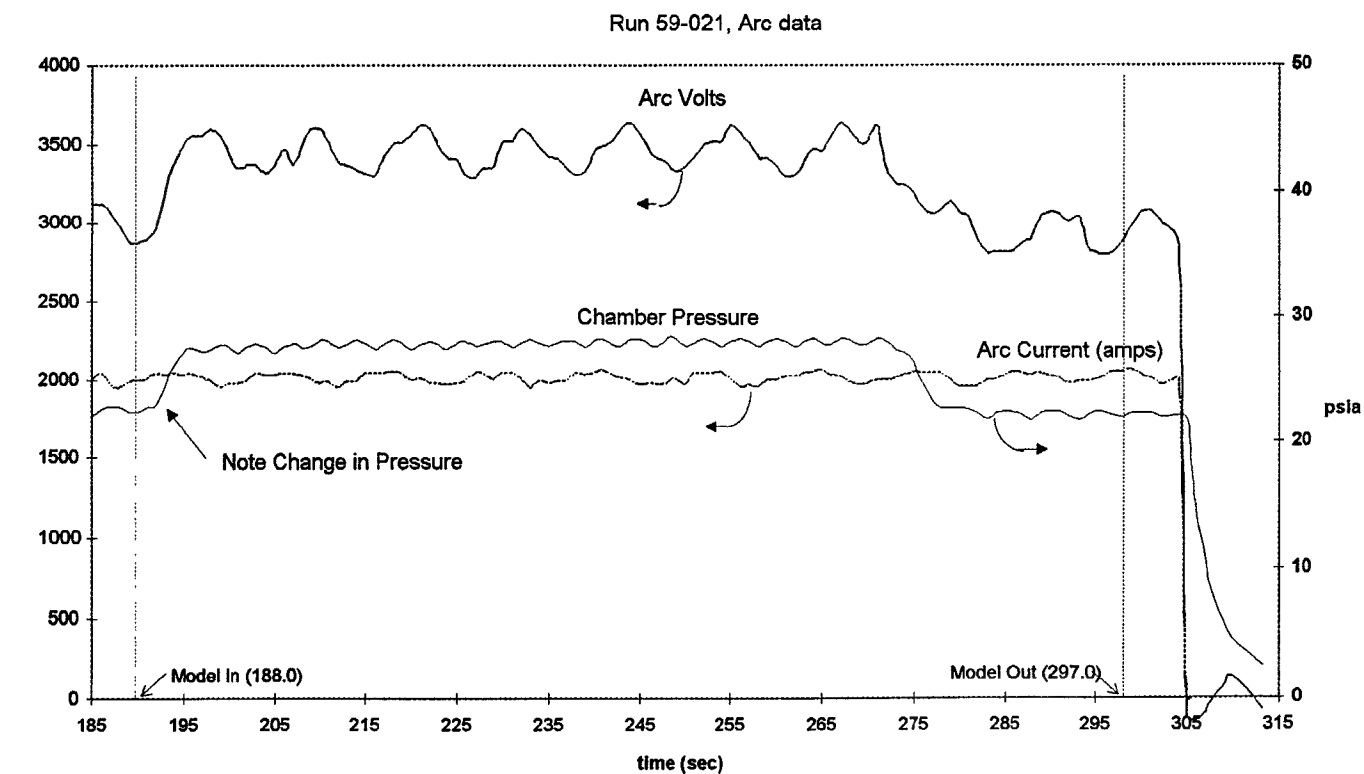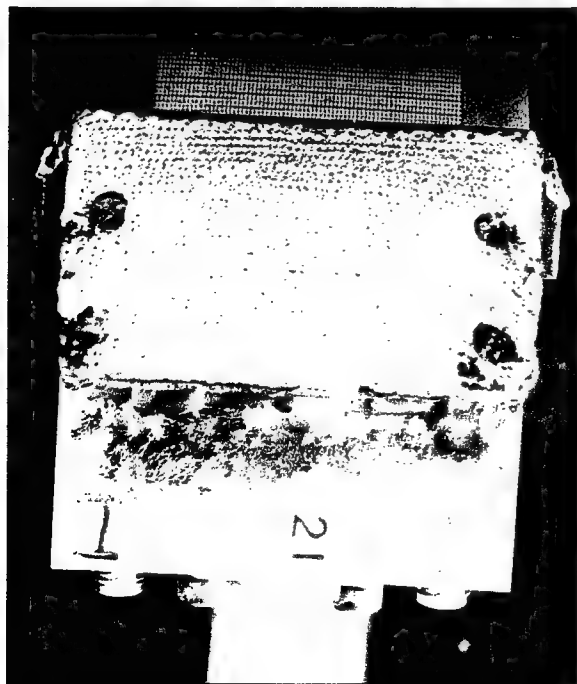

c) Profile, Fore   d) Profile, Aft

Figure 32 cont'd. Run 59-016 Post Test Ablation Contours
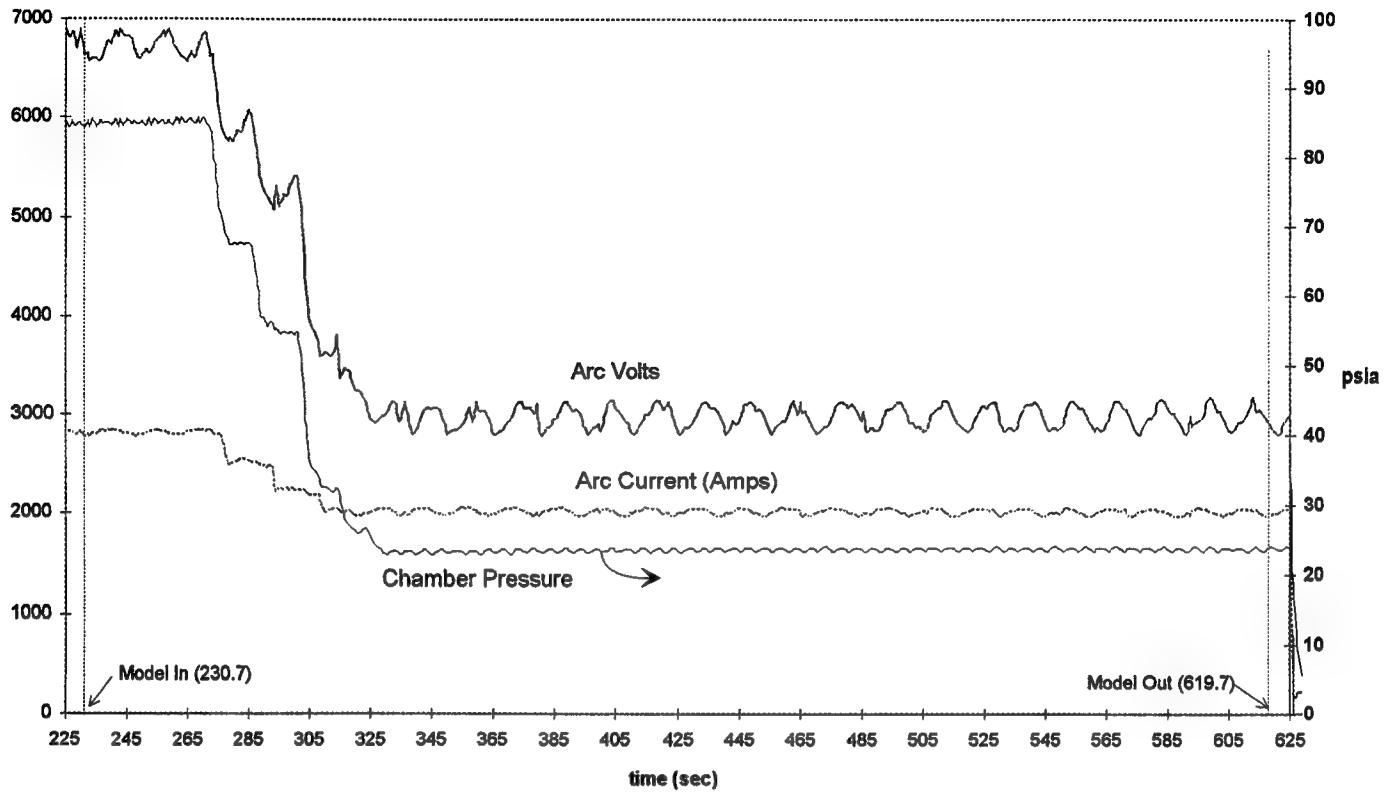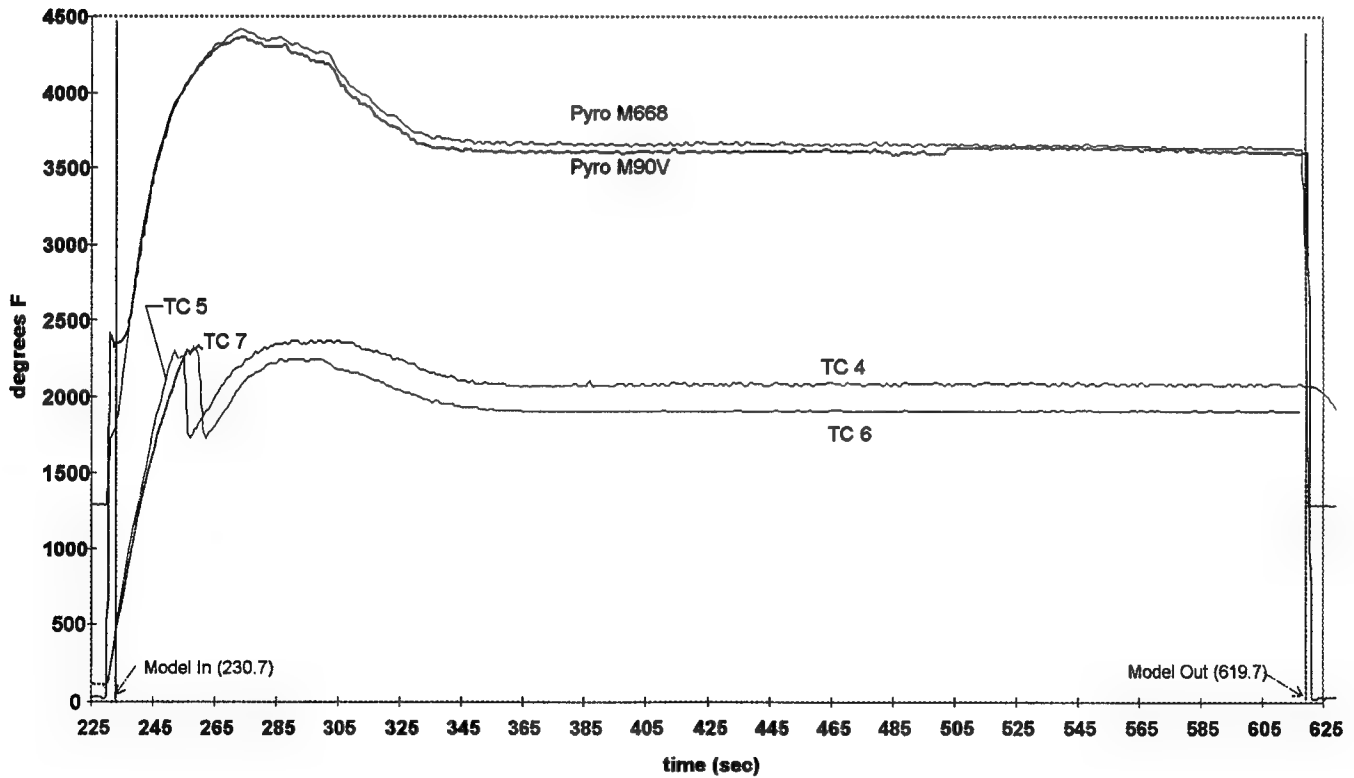
Figure 33. Run 59-017 Facility and Model Data

c) SIDE VIEW OF 4DO (EAST SIDE)

d) SIDE VIEW OF FWPF (WEST SIDE)

a) PLAN VIEW

b) NOSE ON VIEW (WEST ON LEFT)

Figure 33 cont'd. Model Photographs

m13
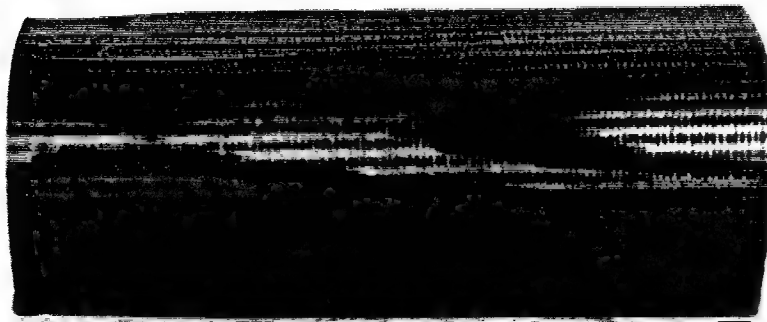
Fore — Run 17, FWPF — Aft
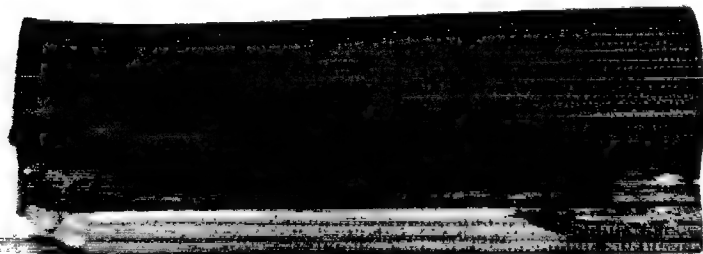
a) Front View

Fore — Run 17, FWPF — Aft

b) Planform View

Run 17, FWPF

c) Profile, Fore

Run 17, FWPF

d) Profile, Aft

Figure 33 cont'd. Run 59-017 Post Test Ablation Contours

a) Front View

b) Planform View

c) Profile, Fore

d) Profile, Aft
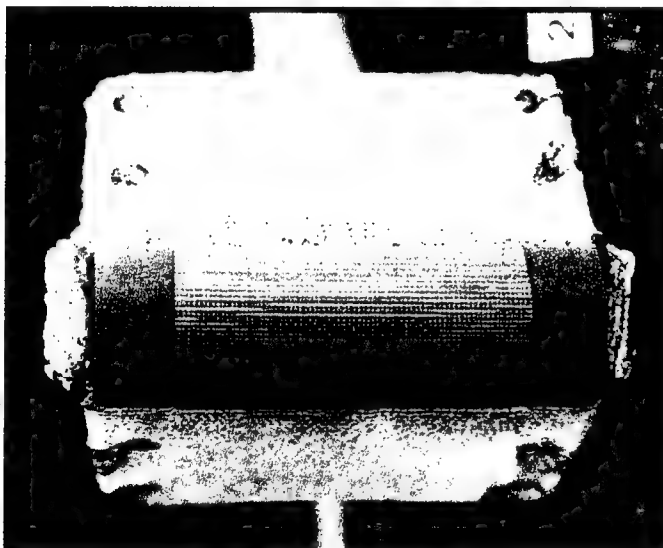
Figure 33 cont'd. Run 59-017 Post Test Ablation Contours
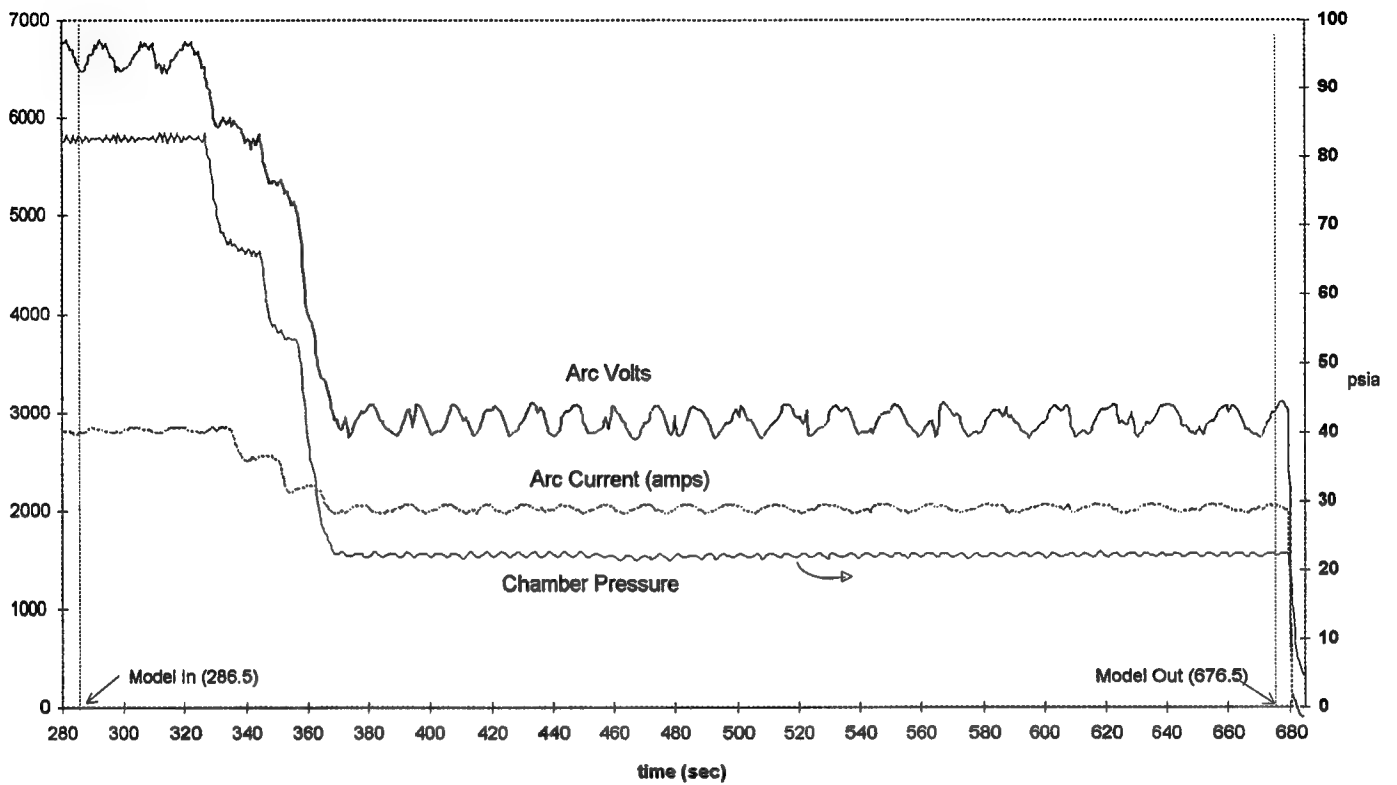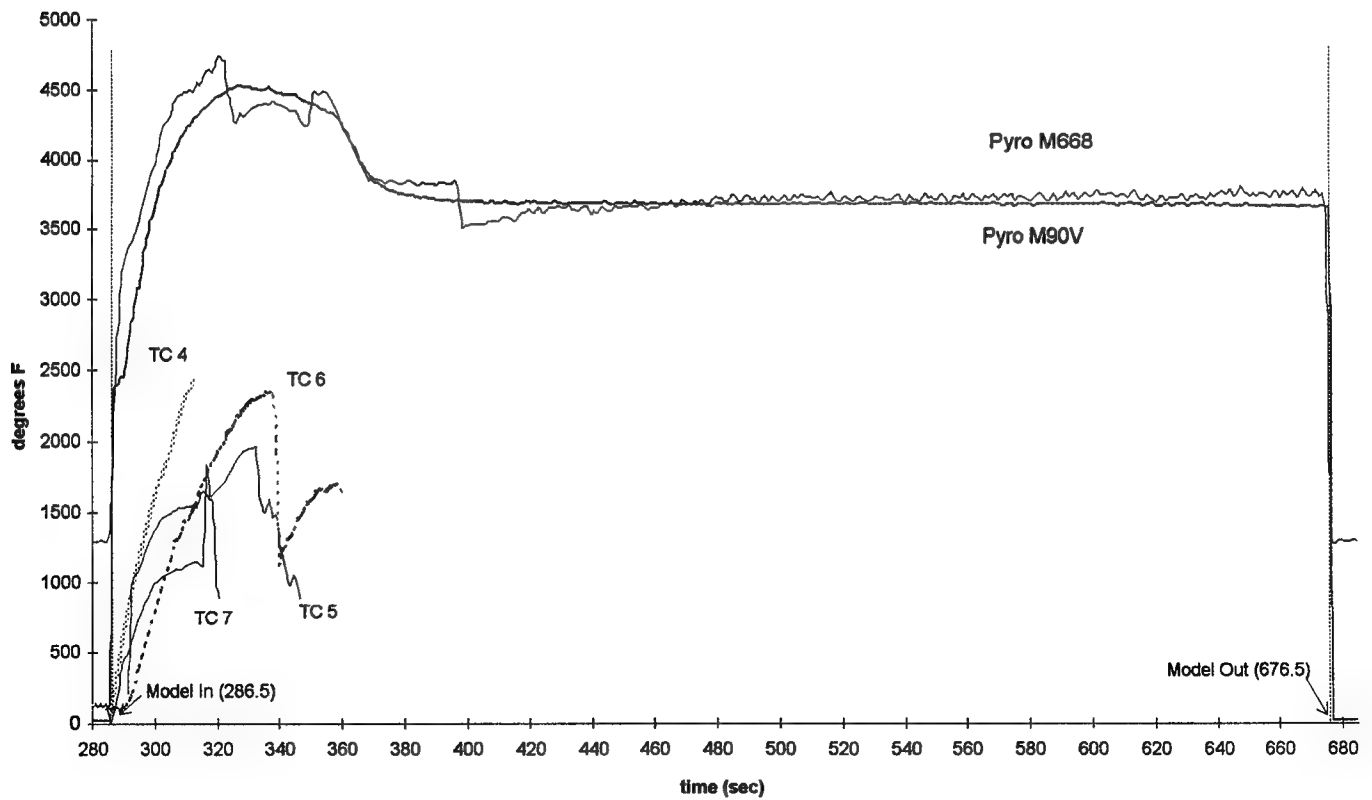
Figure 34. Run 59-018 Facility and Model Data

83

RUN 59-018, PULLOUT-GLIDE. SAIC (EAST) AND FWPF (WEST) AT 0° AoA

c) NOSE ON VIEW (EAST ON LEFT)

d) SIDE VIEW OF SAIC SIDE (EAST)

a) PLAN VIEW
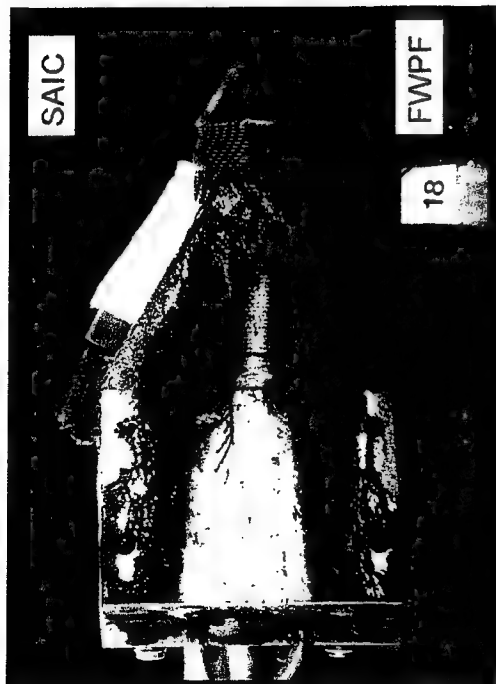
b) PROFILE VIEW OF SAIC SIDE (EAST)

Figure 34 cont'd. Model Photographs

84

Run 59-018, FWPF Leading Edge
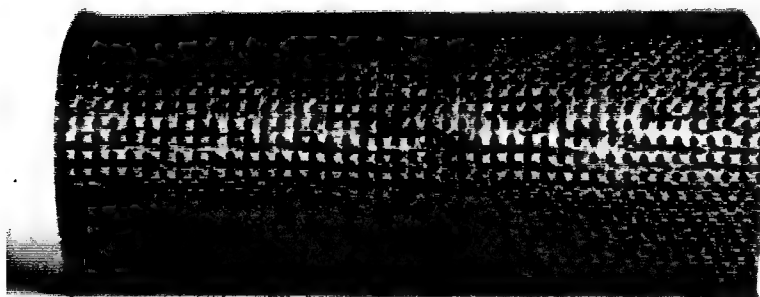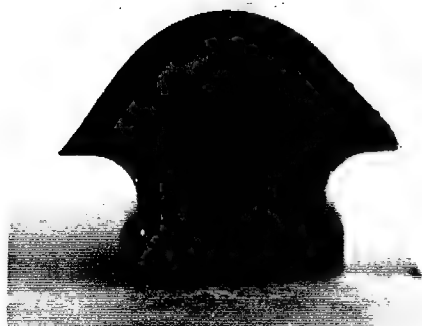
Fore   Aft

a) Front View

Fore   Aft

b) Planform View

c) Profile, Fore   d) Profile, Aft

Figure 34 cont'd. Run 59-018 Post Test Ablation Contours

Fore

Aft

a) Front View

Fore

Aft
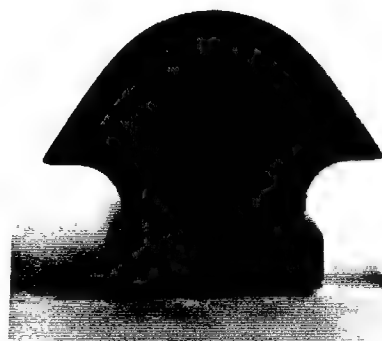
b) Planform View

c) Profile, Fore

d) Profile, Aft

Figure 34 cont'd. Run 59-018 Post Test Ablation Contours

Run 59-019, Arc data

Note increase in Pressure, tried to correct.

Arc Volts

Arc Current (amps)

Chamber Pressure

Model In (1037.8)

Model Out (1428.8)

psia

time (sec)

Run 59-019, TC & Pyro data

Pyro M668

Pyro M90V

TC 6

TC 7

TC 4

TC 5

degrees F

Model In (1037.8)

Model Out (1428.8)

time (sec)
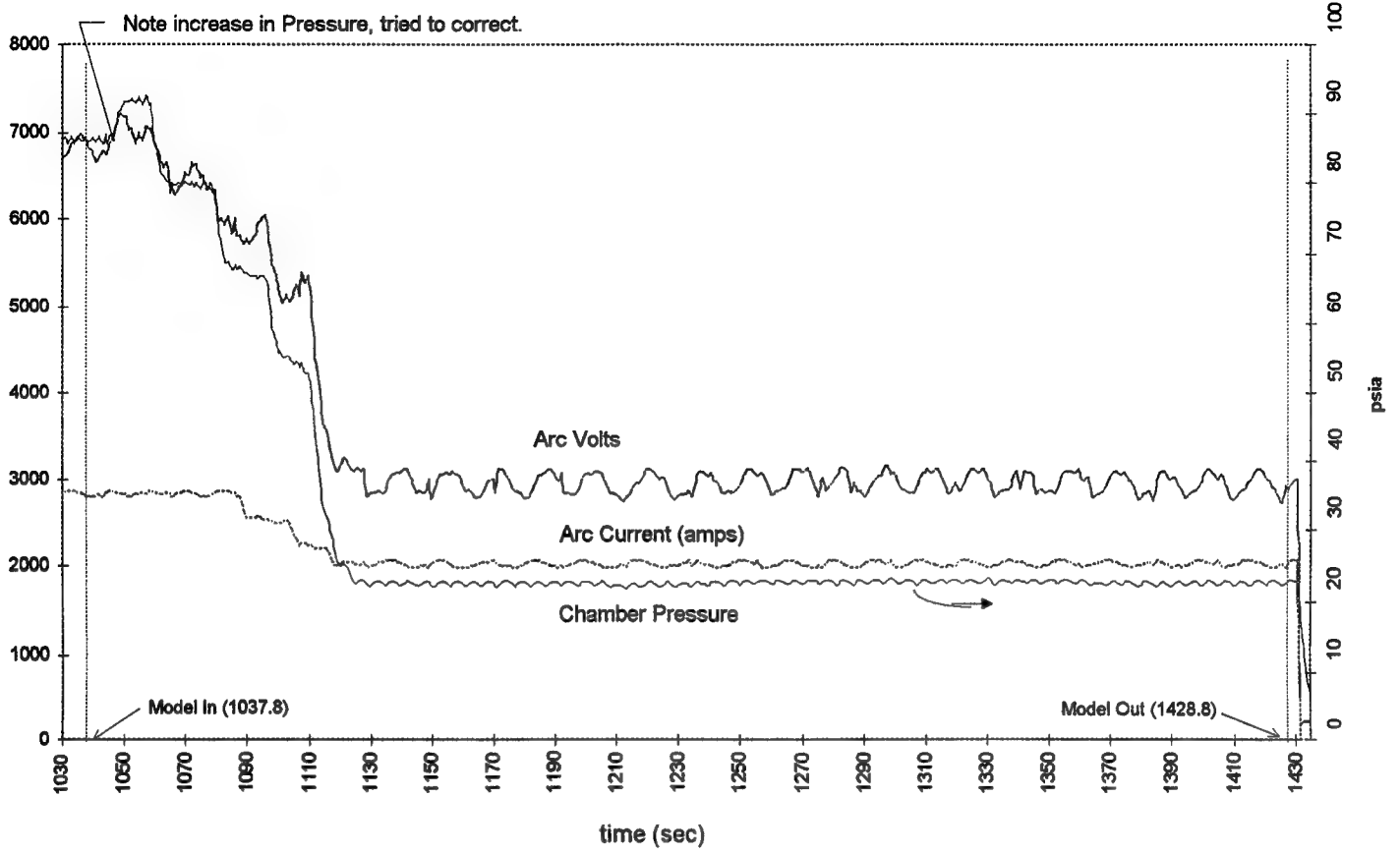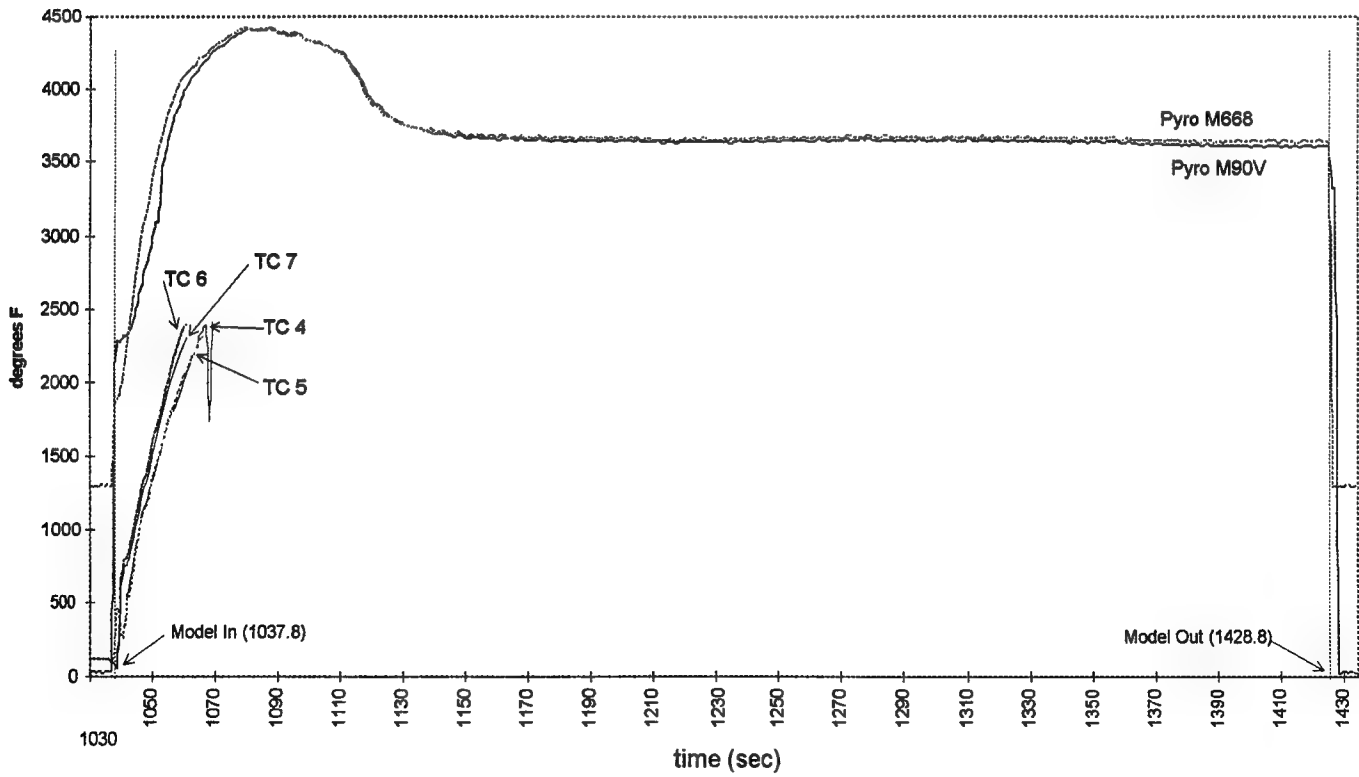
Figure 35. Run 59-019 Facility and Model Data

RUN 59-019, PULLOUT-GLIDE. FWPF (EAST) AND 223 (WEST) AT 10° AoA

c) PLAN VIEW, WINDWARD SIDE

d) PROFILE VIEW OF EAST SIDE (WINDWARD ON TOP)

a) PLAN VIEW, WINDWARD SIDE

b) PLAN VIEW LEEWARD SIDE (WEST ON TOP)

Figure 35 cont'd. Model Photographs

m11

Fore   Run 19,   Aft
              FWPF

a) Front View

Fore   Aft

b) Planform View

Run 19,
FWPF

c) Profile, Fore

Run 19,
FWPF

d) Profile, Aft

Figure 35 cont'd. Run 59-019 Post Test Ablation Contours

Run 59-019, 223 Leading Edge

a) Front View

b) Planform View

c) Profile, Fore

d) Profile, Aft

Figure 35 cont'd. Run 59-019 Post Test Ablation Contours
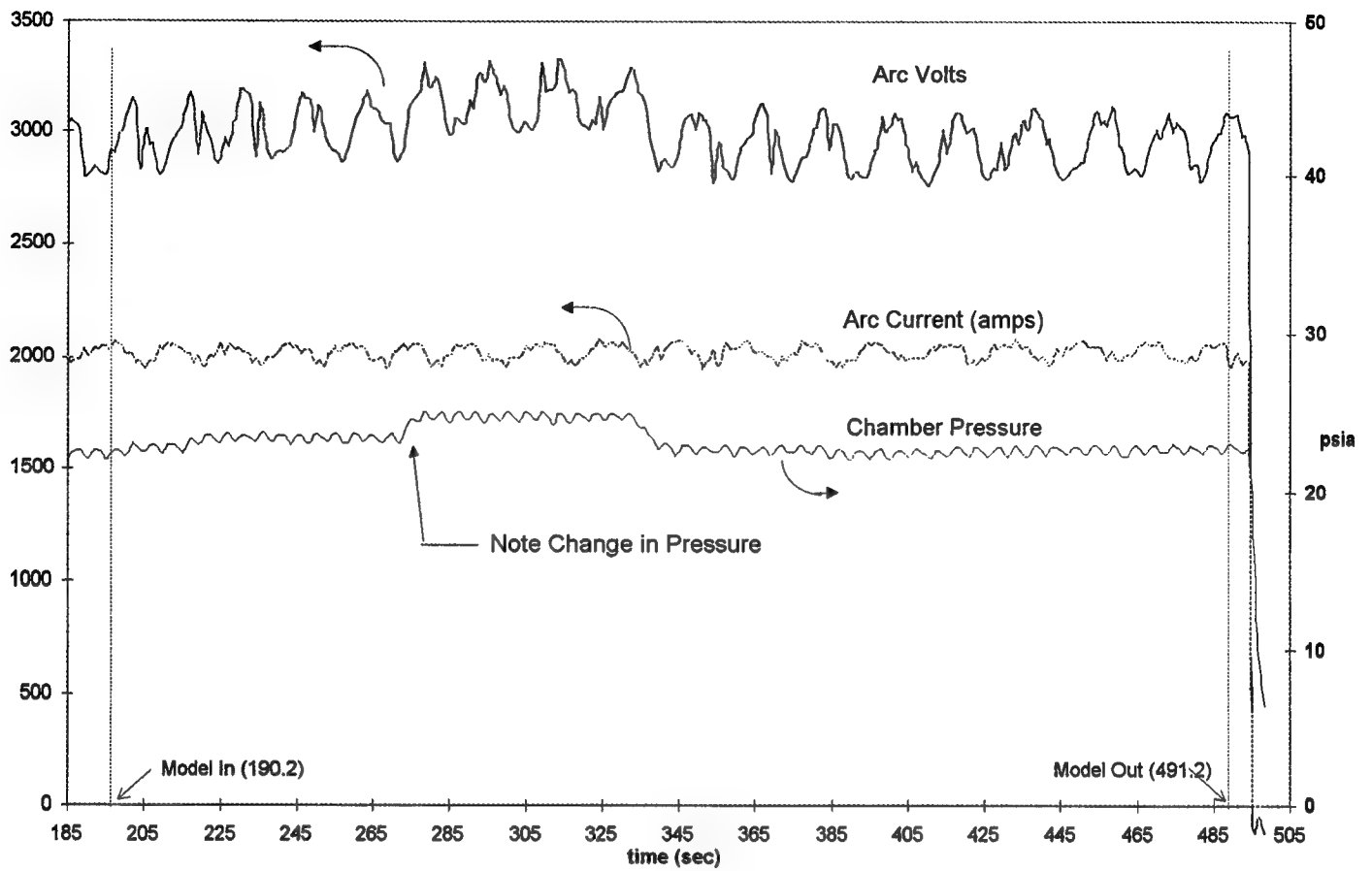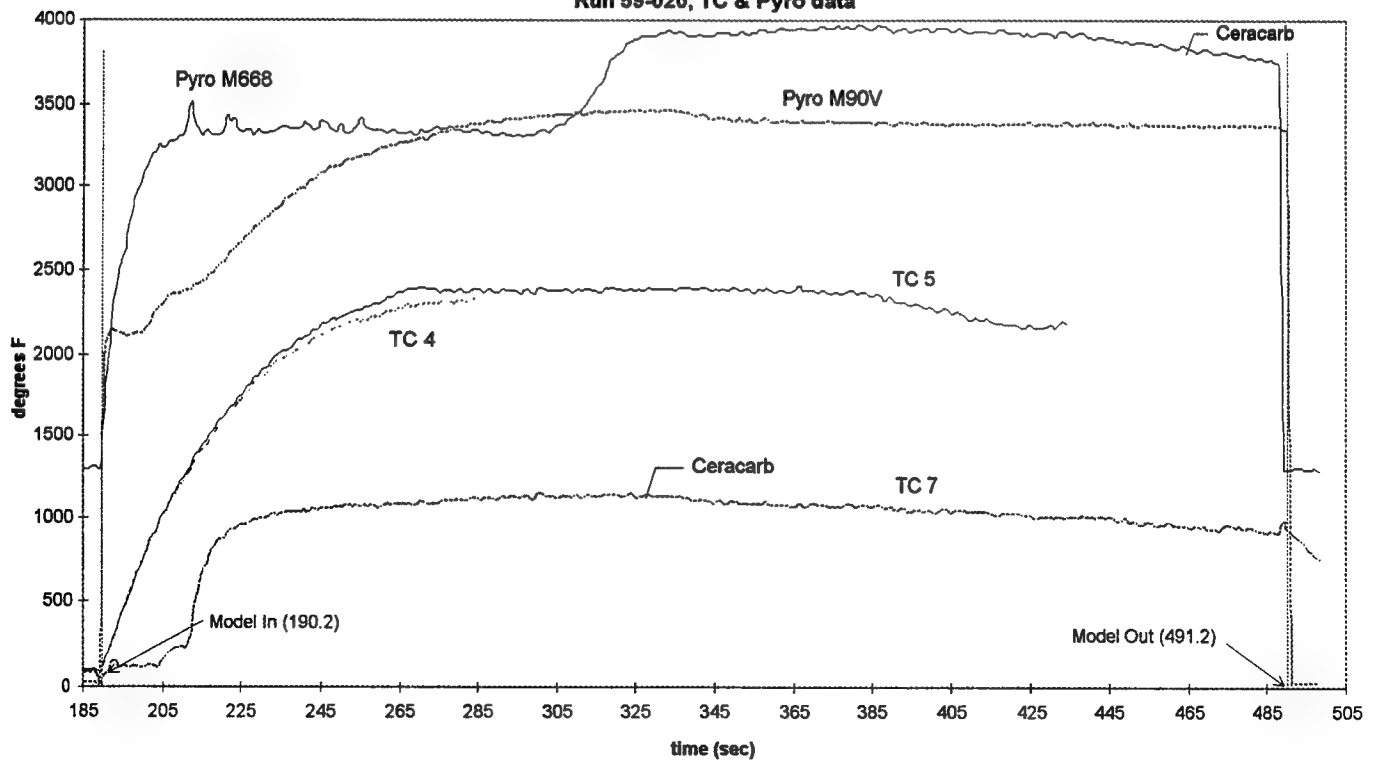
Figure 36. Run 59-020 Facility and Model Data

RUN 59-020, GLIDE ONLY. BP-HITCO (EAST) AND FWPF FROM RUN-013 (WEST)

c) BP-HITCO SIDE OF MODEL (EAST), POST-TEST
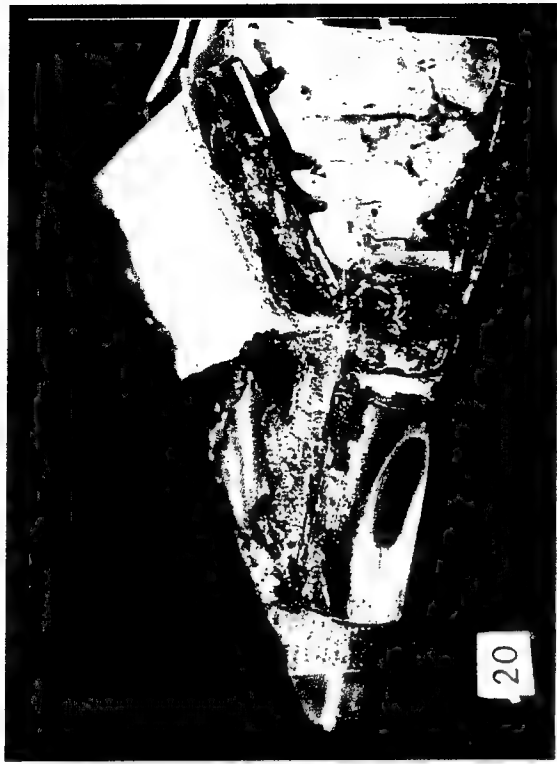
d) FWPF SIDE OF MODEL (WEST), POST -TEST

a) PRE-TEST MODEL (EAST ON TOP)

Note Aft Facing Step on FWPF Side
($\Delta = 0.096''$)

b) POST-TEST PLAN VIEW (EAST ON TOP)

Figure 36 cont'd. Model Photographs

92

m7

f) SIDE VIEW OF BP-HITCO LEADING EDGE

g) VIEW NORMAL TO IMPINGEMENT LINE OF BP-HITCO

e) CLOSEUP OF NOSETIP, C-C TRANSITION SECTION AND FORWARD PART OF BP-HITCO LEADING EDGE
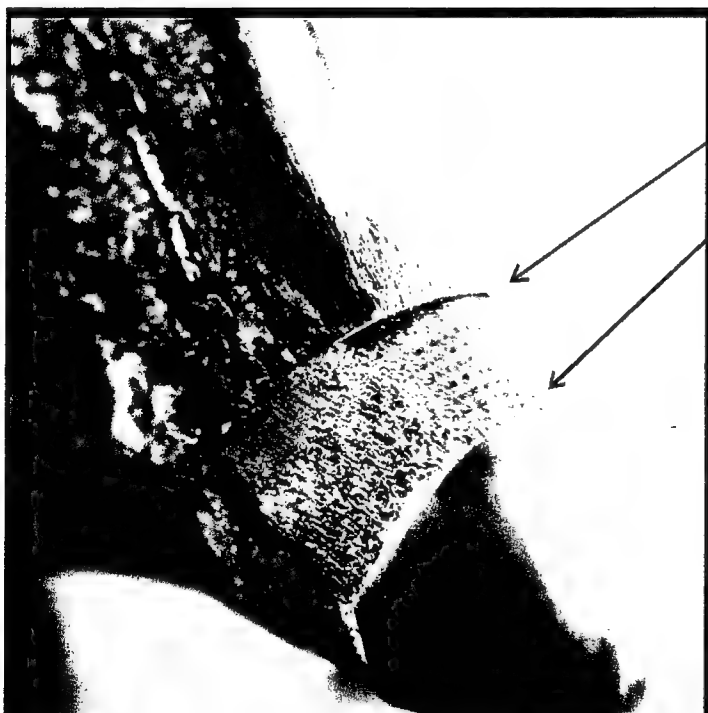
Note Deposits on C-C Section, Aft of Nosetip

Note Foward Facing "Step" Produced by BP Leading Edge

Figure 36 cont'd. Model Photographs

93

m19

Run 59-020, FWPF Leading Edge
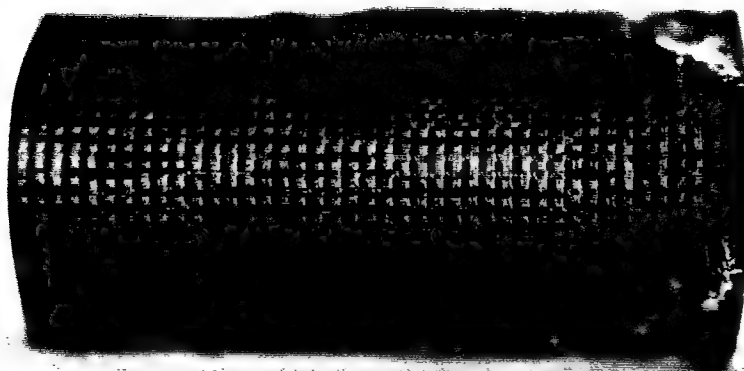
Fore

Aft

Run 20,
FWPF

a) Front View

Fore

Run 20,
FWPF

Aft

b) Planform View

Run 20,
FWPF

Run 20,
FWPF

c) Profile, Fore

d) Profile, Aft

Figure 36 cont'd. Run 59-020 Post Test Ablation Contours

Fore   Aft

Run 20.
Hitco

a) Front View

Fore   Aft

b) Planform View

c) Profile, Fore   d) Profile, Aft

Figure 36 cont'd. Run 59-020 Post Test Ablation Contours

Figure 37. Run 59-021 Facility and Model Data

RUN 59-021, 223 AT 0° SWEEP AND CONSTANT Qcw

a) PLAN VIEW OF UPPER SIDE

b) NOSE ON VIEW

c) PLAN VIEW OF LOWER SIDE
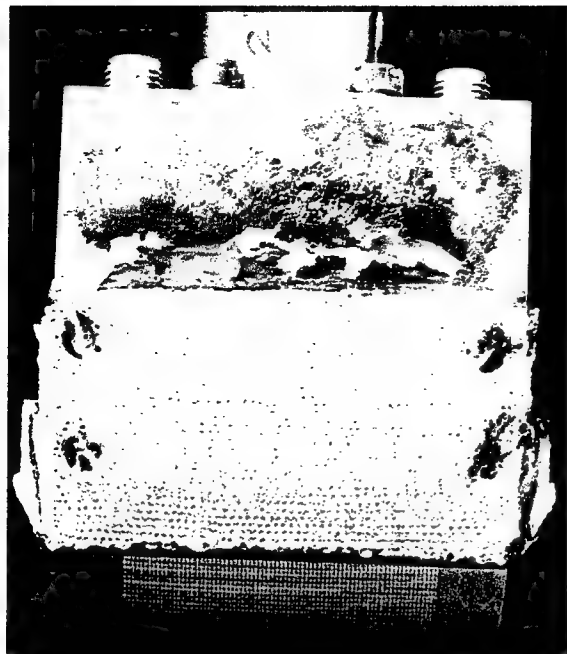
Figure 37 cont'd. Model Photographs

97

Run 59-021, 223 Leading Edge

a) Front View

b) Planform View

c) Profile

Run 21, 223

d) Profile

Run 21 223
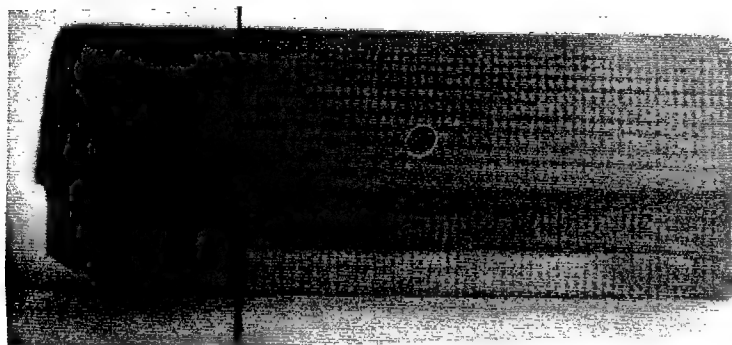
Figure 37 cont'd. Run 59-021 Post Test Ablation Contours
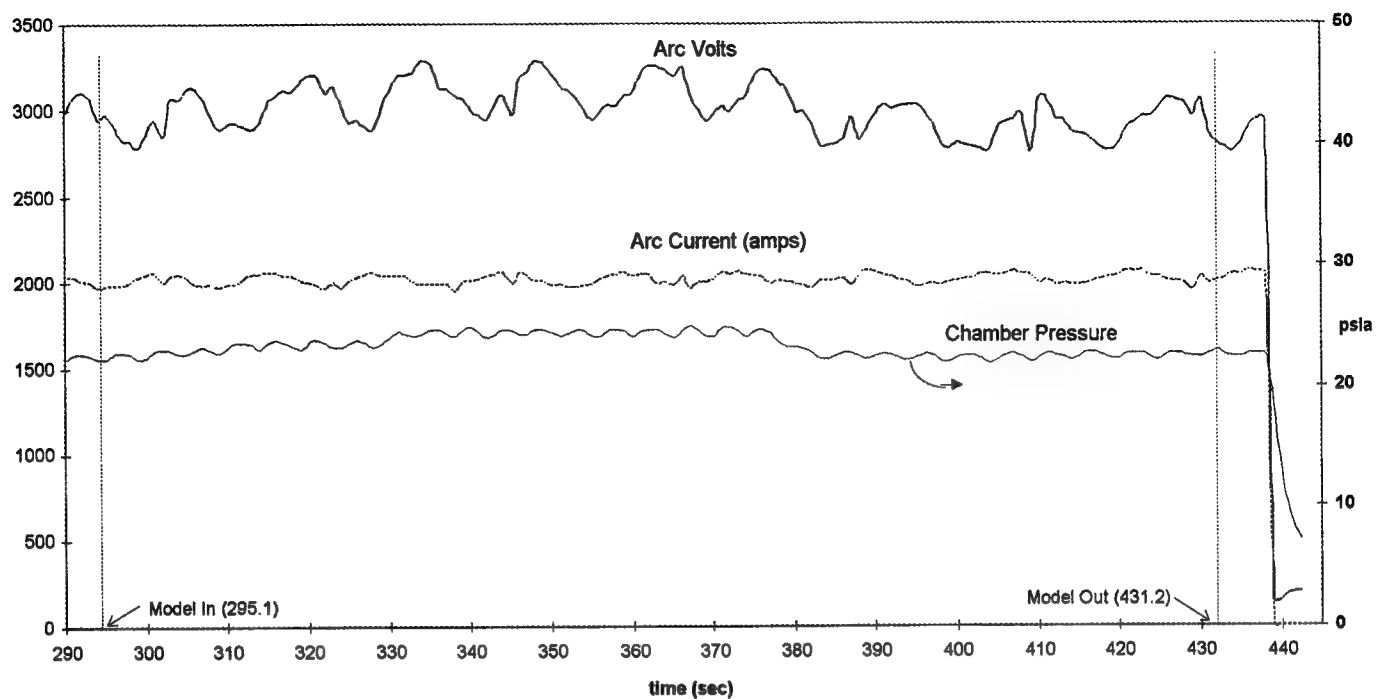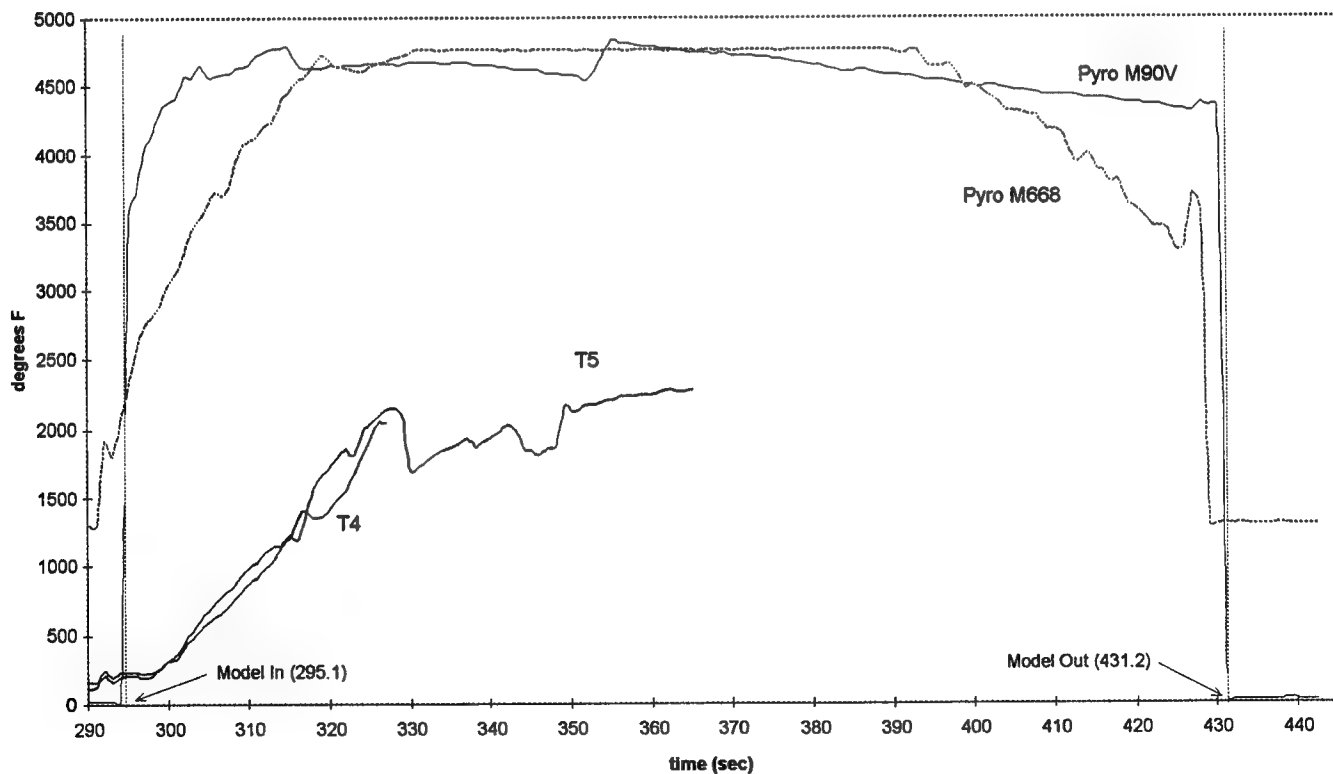
Figure 38. Run 59-022 Facility and Model Data

99

RUN 59-022, SAIC AT 0° SWEEP AND CONSTANT Qcw

a) PRE-TEST NOSE ON VIEW
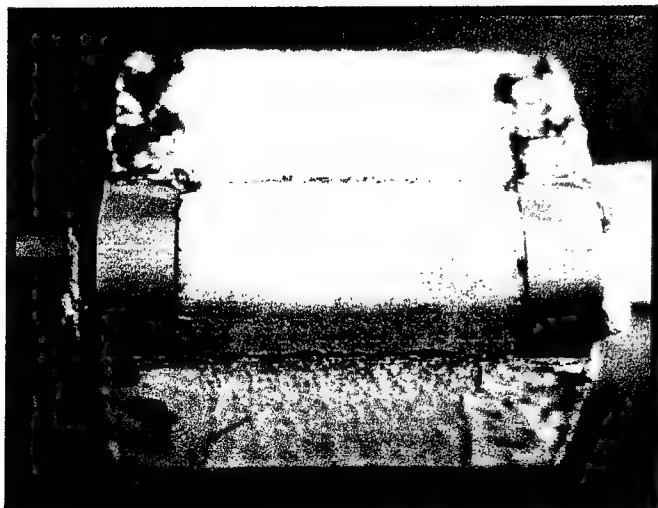
b) PRE-TEST PLAN VIEW OF UPPER SIDE

c) POST TEST

d) Post Test Plan View of Upper Side
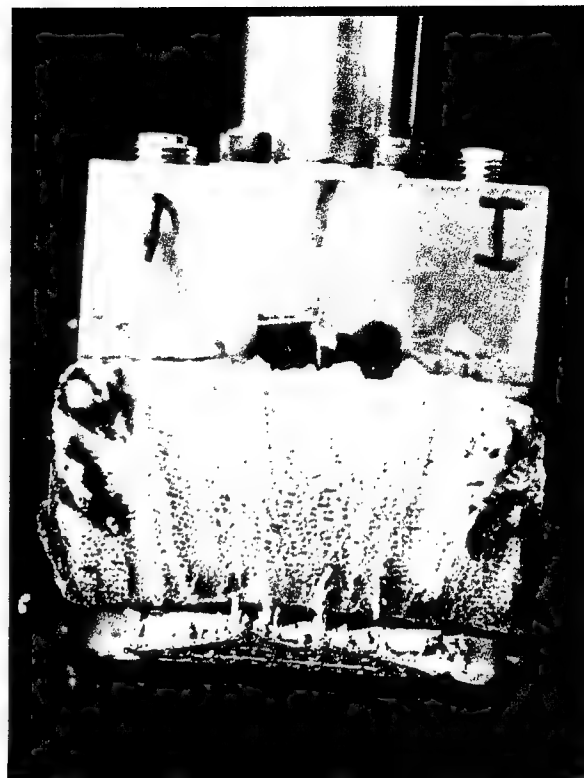
Gouge on West Side
Between Leading Edge and End Cap

Figure 38 cont'd. Model Photographs

100

RUN 59-022, SAIC AT 0° SWEEP AND CONSTANT Qcw, Cont'd

a) PLAN VIEW OF UPPER SIDE

b) NOSE ON VIEW

c) PLAN VIEW OF LOWER SIDE

Figure 38 cont'd. Model Photographs

101
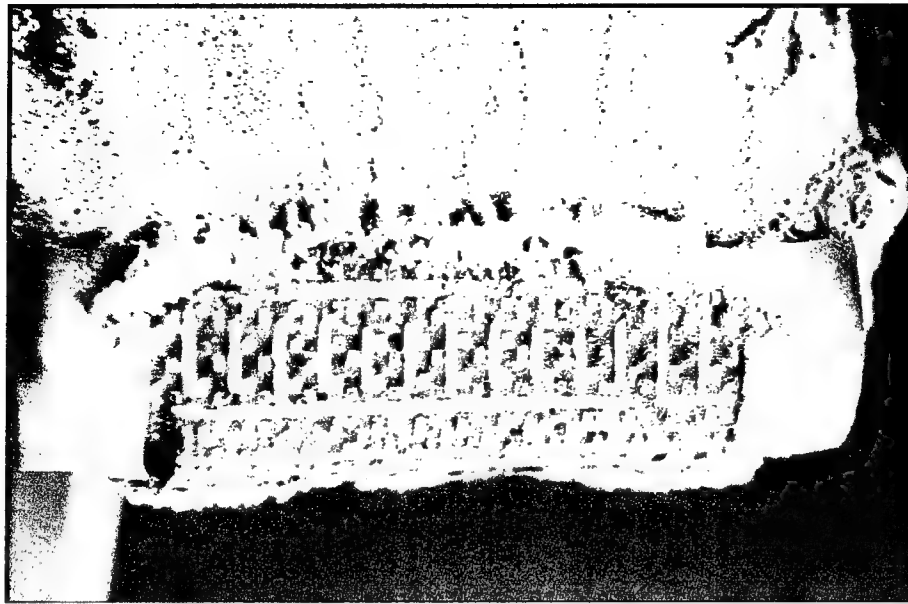
Run 59-022, SAIC Leading Edge
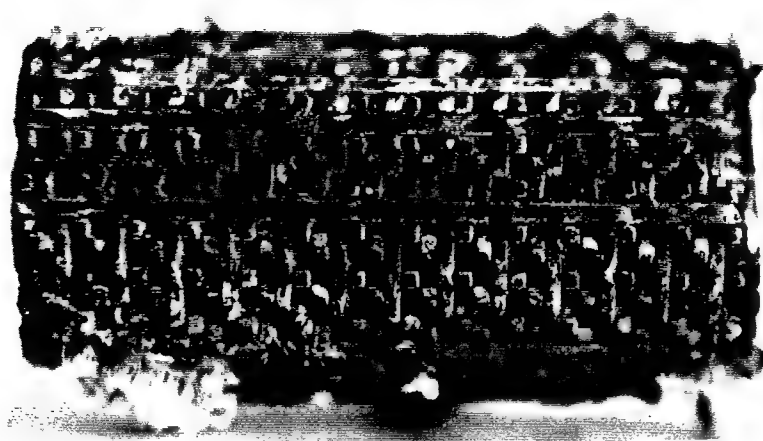
a) Front View

b) Planform View

c) Profile

d) Profile

Figure 38 cont'd. Run 59-022 Post Test Ablation Contours
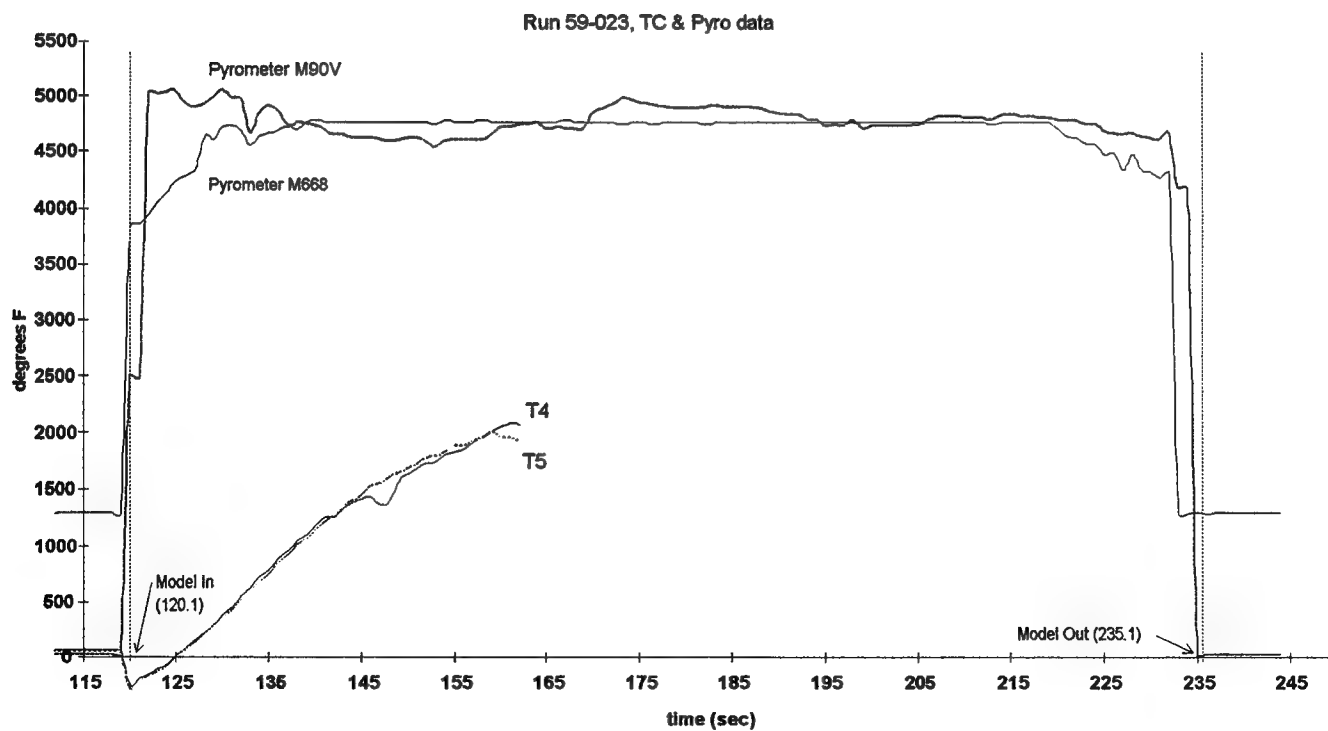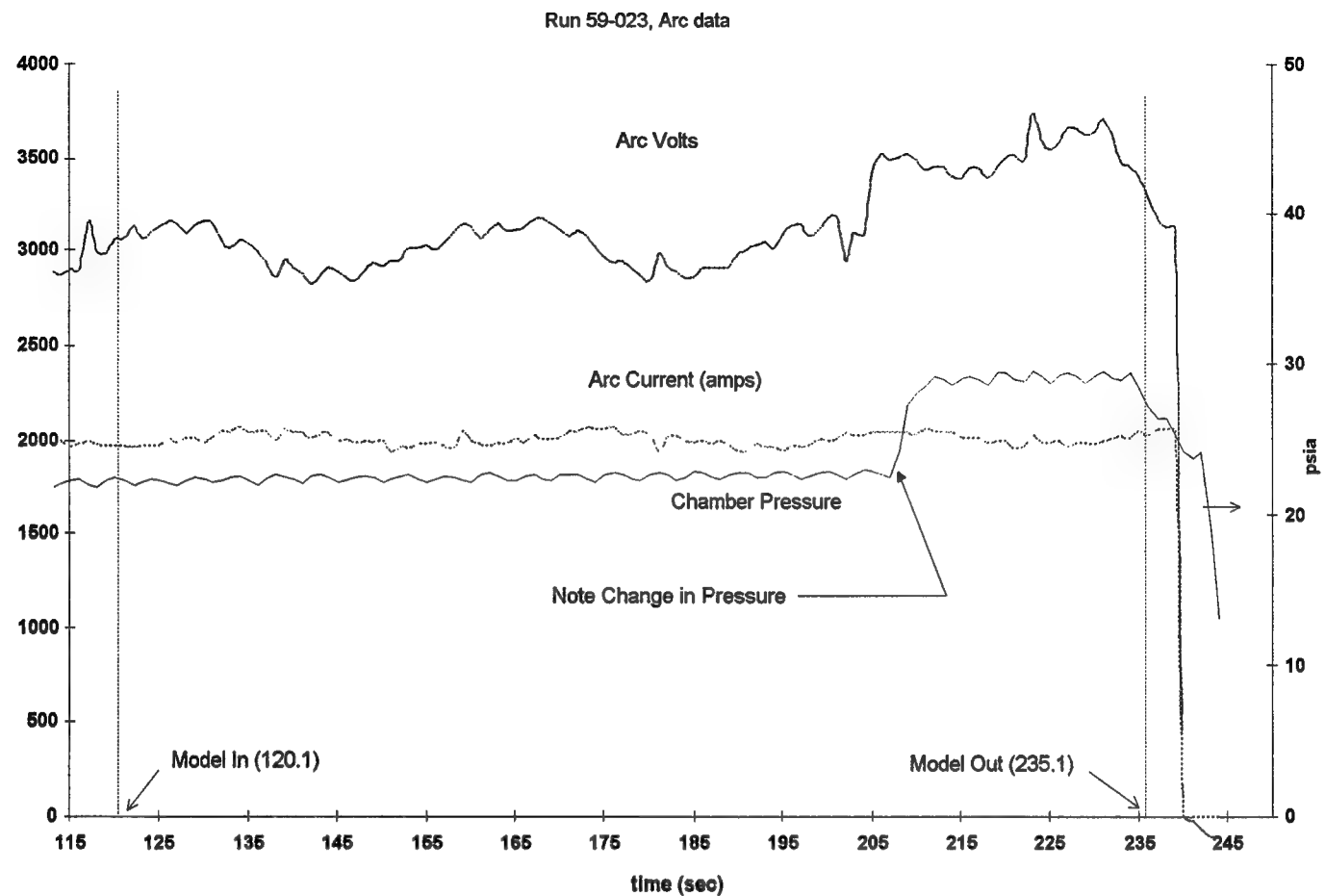
Figure 39. Run 59-023 Facility and Model Data

RUN 59-023, MSNW AT 0° SWEEP AND CONSTANT Qcw

a) PLAN VIEW OF UPPER SIDE
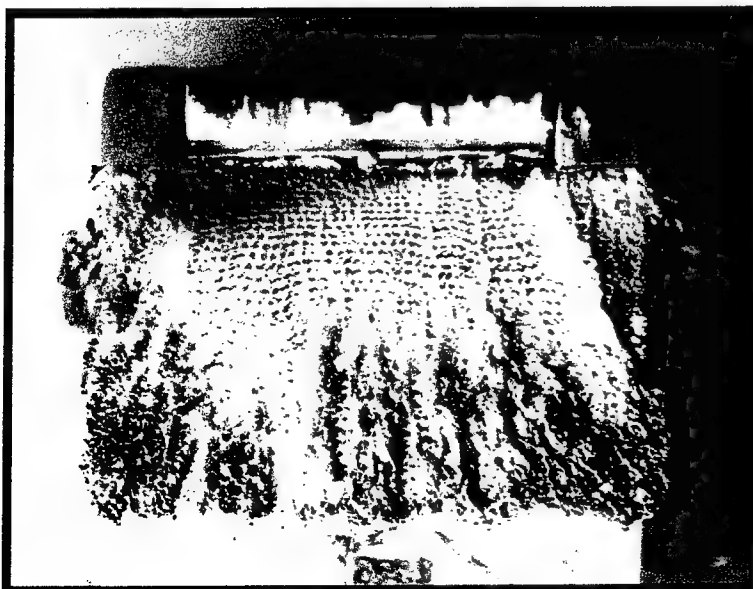
b) NOSE ON VIEW
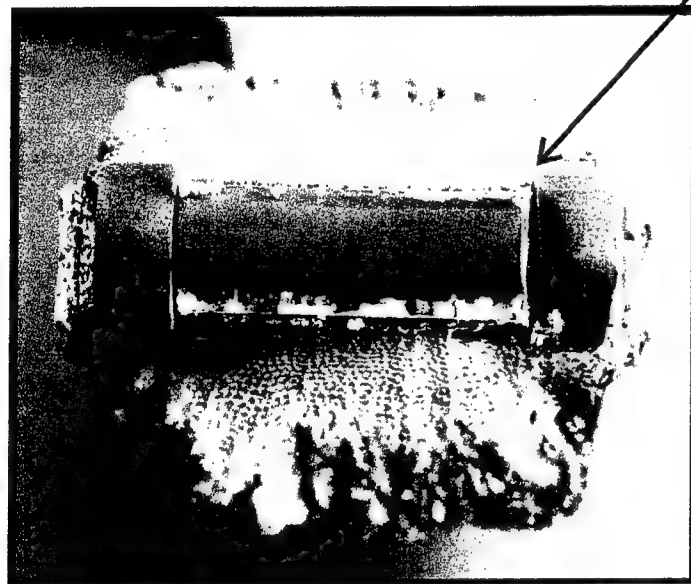
c) PLAN VIEW OF LOWER SIDE
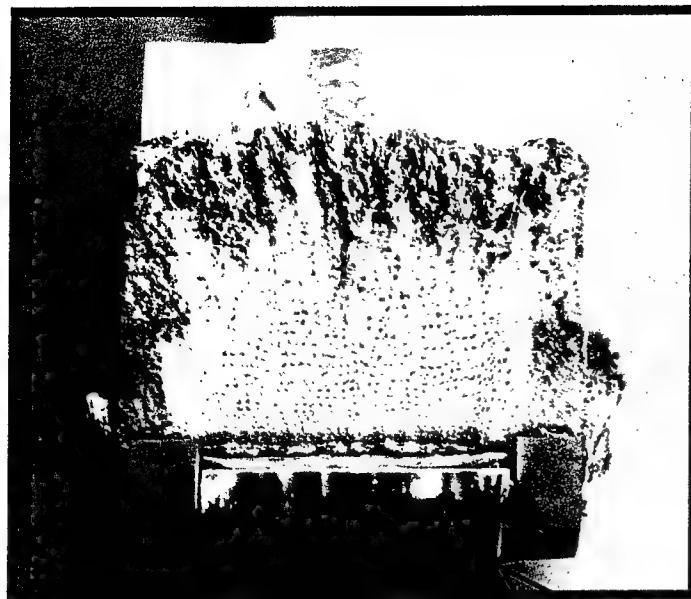
Note Gouge Between
Leading Edge and
End Cap

Figure 39 cont'd. Model Photographs

104

a) Front View

b) Planform View
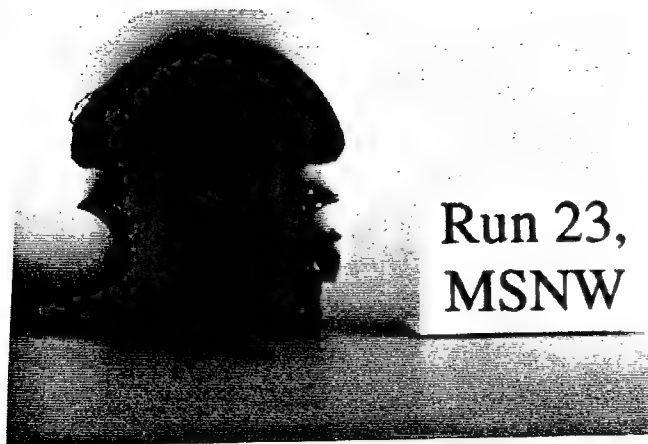
c) Profile

d) Profile

Figure 39 cont'd. Run 59-023 Post Test Ablation Contours

Table 1. Leading Edge Model Design Tradeoff for Conducting Extended Range Testing

Design Parameter	Aft-Facing Four Strut Design	Boomerang Design	Four Sector with Nosetip
Flow Quality Over Test Articles	Excellent defined flow over leading edges if in test rhombus	Excellent defined flow over leading edges if nosetip blunting not significant	Complex, ill-defined flow: shock-B.L. interactions and nosetip shaping
Pullout and Glide Heating Simulation	Model cannot be ramped up into nozzle	Model can be ramped up into nozzle to increase heating	Model can be ramped up into nozzle to increase heating
Test Article Size	Size limited by sweep angle and central separation of struts to prevent normal shock implications	limited by sizes of nosetip and transition to leading edge	limited by sizes of nosetip and transition to leading edge
Upstream Component Effects	No nosetip, leading edge transition piece used to minimize shaping effects caused by test rhombus edge	Influenced by nosetip shaping	Influenced by nosetip shaping
Number of Test Articles	Four (4)	Two (2)	Four (4)
Facility Interface	Large structure external to test rhombus, new interface concept. Complex test cabin flow.	Central strut, standard interface	Central strut, standard interface
Test Other Components	Can test only leading edges	Heatshield screening (probably not correct insulation)	Can test only leading edges
Uncertainties	Central separation of struts required to prevent normal shock. Need cold wind tunnel test.	Effects of nosetip blunting on leading edge conditions. Use cooled nosetip.	Possibly complex and ill-defined flow

* SINGLE SWEPT LEADING EDGE NOT INCLUDED, SIMILAR TO 4-AFT FACING STRUTS BUT TESTS ONE MODEL AND WON'T HAVE SHOCK IMPLICATION.
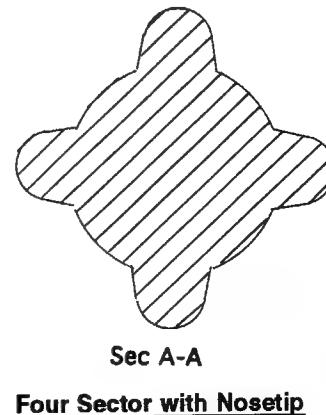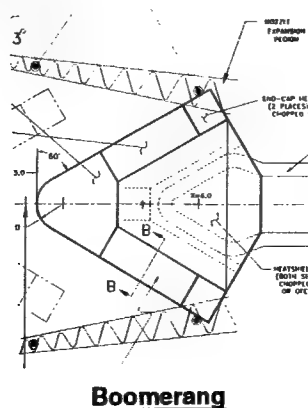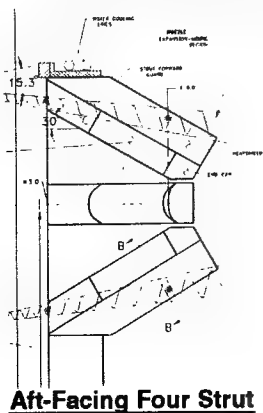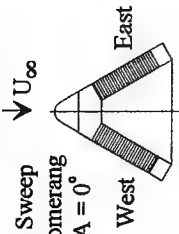

Aft-Facing Four Strut

Boomerang
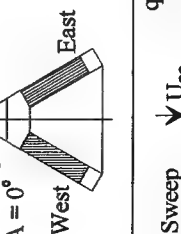

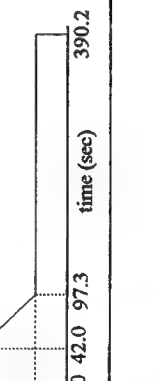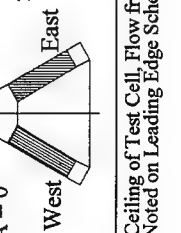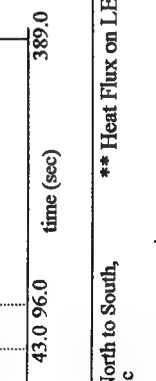Sec A-A

Four Sector with Nosetip
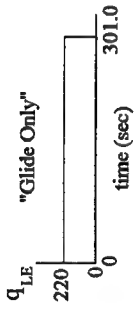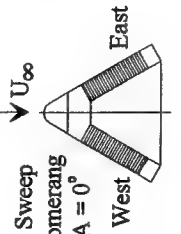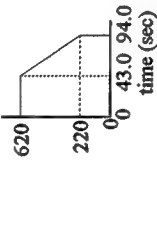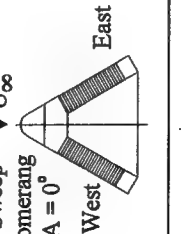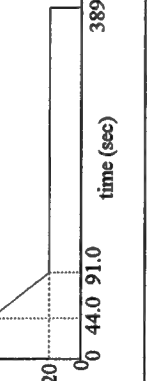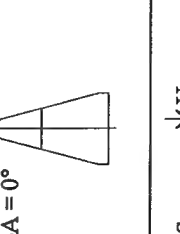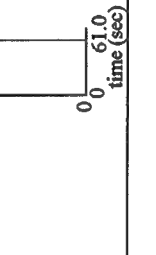
Table 2. Leading Edge Calibration Test Data

o UNITS: Cal Data = Btu/ft2-sec, Pressure Data = atm
o See Appendix A for Calorimeter and Pressure Responses

NASA Run No	Condition, & AoA	Arc Amps	Arc Volts	Arc Pressure (psia)	Cold Air Inject	Cal Data				Pressure Data		
						NT-Q4	East LE Fore-Q5	East LE Aft-Q7	West LE Fore-Q6	NT-P1	East LE-P3	West LE-P2
59-01a	Glide, 0°	2040	2740	21.6	No	920	210	190	200	0.23	0.04	0.06
-01b		2040	2800	42.0	Yes	Noise	Noise	Noise	Noise	0.41	0.09	0.12
-01c		2040	2850	55.0	Yes	Noise	Noise	Noise	Noise	0.57	0.13	0.12
59-02a	Glide, 0°	2040	2700	20.7	No	830	215	160	160	0.21	0.04	0.05
-02b		2020	2870	30.7	Yes	Noise	Noise	Noise	Noise	0.25	Noise	Noise
-02c		1500	2700	20.0	No	Noise	Noise	Noise	Noise	0.20	0.04	0.05
59-03a	Glide, 0°	2000	2700	20.5	No	Noise	Noise	Noise	Noise	0.21	0.04	0.05
-03b		2020	2820	31.3	Yes	Noise	Noise	Noise	Noise	Noise	Noise	Noise
59-04	.7xPullout, 0°	2030	4700	46.0	No	Noise	Noise	Noise	Noise	0.46	0.10	0.10
59-05	.7xPullout, 0°	2020	4500	42.0	No	Noise	400	315	345	0.41	0.09	0.09
59-06	Pullout, 0°	2820	6700	88.6	No	gt 2050	620	550	560	0.87	0.18	0.18
59-07a	Glide, 0°	2020	2800	21.7	No	--	220	175	195	0.22	0.04	0.06
-07b		2020	3000	30.8	Yes	--	Noise	Noise	Noise			
59-08	Pullout, 10°	2820	6700	87.0	No	--	630	480	610	0.92	0.18	0.19
59-10	Glide, 0°	2040	2740	21.2	No	900	220	170	220	0.24	--	--
59-11	Glide, 0°	2080	2750	21.8	No	950	225	170	220	0.23	--	--
59-12	.7xPullout, 0°	2040	4620	45.2	No	gt 1400	430	320	400	0.44	--	--

NOTE: West Aft LE Cal (Nullpt) lost on assembly. NT Cal replaced after Run 59-08 requiring P2 & P3 to be disconnected.

Table 3. Summary of Leading Edge Material Testing

NASA Run No.	Model Configuration*	Heat Flux** History	Material****	wt. loss (gm)	Impingement Line Ablation (Inches) Fore	Aft	Impingement Line Temperature (°F)***	Comments
59-009	60° Sweep Boomerang AoA = 0° West / East, ↓U∞	"Glide Only" q_{LE} 220, 301.0, time (sec)	West: FWPF (#1) Z⊥ Sweep	8.93	0.149	0.106	3540 (m90v)	Glide Only. Test of 223 and FWPF
			East: 223 (#7) Z⊥ Sweep	9.23	0.151	0.120	3560 (m668)	
59-013	60° Sweep Boomerang AoA = 0° West / East, ↓U∞	q_{LE} 620, 220, 43.0 94.0 time (sec)	West: FWPF (#4) Z⊥ Sweep	6.21	0.096	0.074	4290 @ 43 sec	Pullout and Transition to Glide, but NO Glide. Test of 223 and FWPF
			East: 223 (#8) Z⊥ Sweep	6.39	0.104	0.086	4290 @ 43 sec	
59-014	60° Sweep Boomerang AoA = 0° West / East, ↓U∞	q_{LE} 620, 220, 44.0 91.0, 389.4 time (sec)	West: FWPF (#3) Z⊥ Sweep	16.50	0.255	0.194	4290 @ 44 sec 3530 @ 389 sec	Pullout, Transition to Glide and Glide. Test of 223 and FWPF. This is a reference test for the test series.
			East: 223 (#11) Z⊥ Sweep	16.91	0.265	0.219	4320 @ 44 sec 3600 @ 389 sec	
59-015	Nosetip, AoA = 0° ↓U∞	q_{NT} 900, 61.0 time (sec)	SAIC/Ultramet Nosetip	TBD	0.137	----	West: 4390 (ε = 1.0) East: 4760 (ε = 1.0)	Test of Coated SAIC Nosetip from LCAT. Tested at Lowest Calibrated Heat Flux in NASA's 6" Nozzle
59-016	60° Sweep Boomerang AoA = 0° West / East, ↓U∞	q_{LE} 620, 220, 42.0 97.3, 390.2 time (sec)	West: 4DO (#14) Z⊥ Model Base	16.82	0.264	0.205	4300 @ 44 sec 3460 @ 390 sec	Pullout, Transition to Glide and Glide. Test of 4DO and 223 with Z∥ to Sweep.
			East: 223 (#12) Z∥ Sweep	16.69	0.261	0.211	4380 @ 44 sec 3540 @ 390 sec	
59-017	60° Sweep Boomerang AoA = 0° West / East, ↓U∞	q_{LE} 620, 220, 43.0 96.0, 389.0 time (sec)	West: FWPF (#6) Z∥ Sweep	17.17	0.262	0.203	4360 @ 43 sec 3600 @ 389 sec	Pullout, Transition to Glide and Glide. Test of 4DO on Side Opposite of Run 16 and FWPF with Z∥ to Sweep.
			East: 4DO (#13) Z⊥ Model Base	16.61	0.256	0.208	4420 @ 43 sec 3620 @ 389 sec	

* Video View from Ceiling of Test Cell, Flow from North to South, Z Fiber Dirction Noted on Leading Edge Schematic

** Heat Flux on LE Impingement line or NT Stag Pt, Btu/ft²-sec

*** Unless Noted, Emissivity Assumed to be 0.85 in Pyrometer Temp Conversions.

**** The Number in ( ) Corresponds to FMI Designated Number Used to ID Test Articles

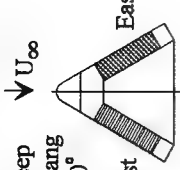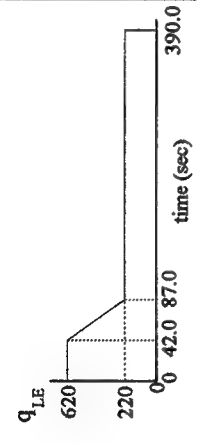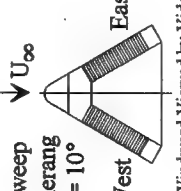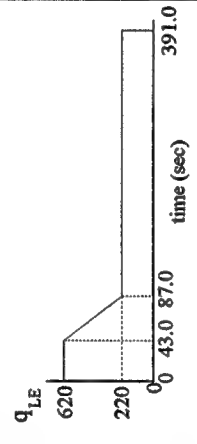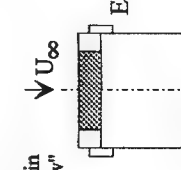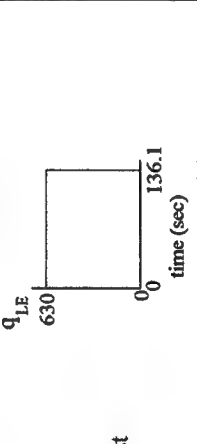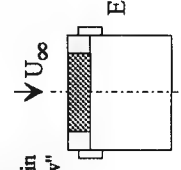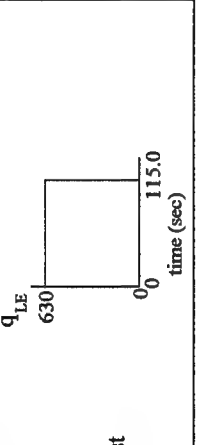Table 3, contd. Summary of Leading Edge Material Testing
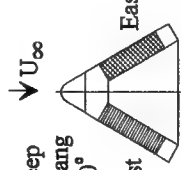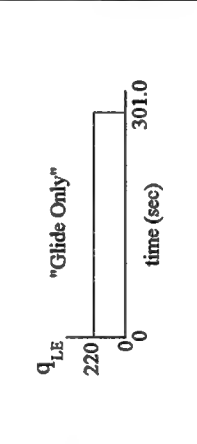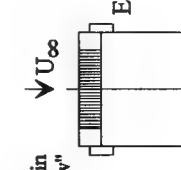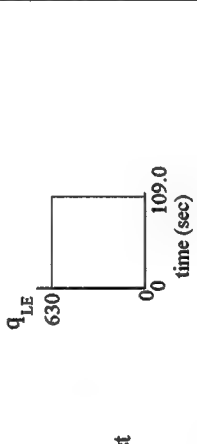
NASA Run No.	Model Configuration	Heat Flux History	Material	wt. loss (gm)	Impingement Line Ablation (Inches) Fore	Impingement Line Ablation (Inches) Aft	Impingement Line Temperature (°F)	Comments
59-018	60° Sweep Boomerang AoA = 0°; West / East; Windward Viewed by Video	q_{LE} 620, 220, 0; 42.0 87.0; 390.0; time (sec)	West: FWPF (#2) Z⊥ Sweep; East: SAIC (#1-1)	16.72; ~5.0	0.250; 0.133	0.195; 0.0	4530 @ 42 sec, 3660 @ 390 sec; 4700 @ 36 sec and oscillating, 3750 @ 390 sec	Pullout, Transition to Glide and Glide. Test of SAIC Material and FWPF. FWPF for Repeatability.
59-019	60° Sweep Boomerang AoA = 10°; West / East	q_{LE} 620, 220, 0; 43.0 87.0; 391.0; time (sec)	West: 223 (#9) Z⊥ Sweep; East: FWPF (#5) Z⊥ Sweep	16.70; 16.36	0.255; 0.236	0.194; 0.189	4400 @ 43 sec, 3600 @ 390 sec; 4410 @ 43 sec, 3650 @ 390 sec	Pullout, Transition to Glide and Glide. 10° AoA. Axial LE Center Placed on Nozzle's Center Plane. Windward Viewed by Video.
59-020	60° Sweep Boomerang AoA = 0°; West / East	q_{LE} 220; "Glide Only"; 0; 301.0; time (sec)	West: FWPF (#4) From Run 13; East: BP-Hitco Ceracarb (#A)	8.05; 3.48	0.161; 0.053	0.095; 0.003	3370 @ 300 sec; peak = 3960 @ 190 sec; 3760 @ 300 sec	Glide Only. Test of BP-Hitco and Test of FWPF that saw Pullout and Transition to Glide (from Run 13). Used New C-C Transition.
59-021	0° Sweep, "Cylinder in Cross Flow"; East	q_{LE} 630, 0; 109.0; time (sec)	223 (#10), Z in Direction of Flow	9.94	East 0.146 Mid 0.151	West 0.145	4820 Max on stag line (West pyro), 4720 Max on sonic line (East pyro)	Constant Heating @ Pullout Level so ∫qdt = above Pullout-Transition-Glide. Model Ejected Early because of Facility Positioner Malfunction,160 Planned vs 109 sec Actual
59-022	0° Sweep, "Cylinder in Cross Flow"; East	q_{LE} 630, 0; 136.1; time (sec)	SAIC/Ultramet (# 1-2)	21.5	0.220 0.223	0.213	4800 Max on stag line (West pyro), 4780 Max on sonic line (East pyro)	Same as Run 021 Except Run Terminated because of "gouge" between end cap and test article
59-023	0° Sweep, "Cylinder in Cross Flow"; East	q_{LE} 630, 0; 115.0; time (sec)	MSNW	no pre-test weight	0.253 0.245	0.231	Varied between 5000 & 4600 during run, stag line (West pyro); 4700 Max on sonic line (East pyro)	Same as Run 021 Except Run Terminated because of "gouge" between end cap and test article

Table 4. Summary of Video Data

Run	Video Model Times In Out	Pyro Model Times In Out	Video Quality	Test Rhombus Indications	Streamline Indications	Transition Section	Ablation West LE	Phenomena East LE	End Caps	Comments
-009	45:19 50:18 Dwell = 299	406. 708. Dwell = 302	Poor, NT clear but LEs are fuzzy & too bright	Early in run aft part of end caps are dark	Nothing shows flow	Cooler than LEs. Separation aft of NT: at end of run, separation covers ¼ of Tran	LE forward cooler than mid (conducting into Tran), even ablation over length	same as west	Early in run, aft part of 994 is cooler than fore part	Glide only
-013	28:21 29:55 Dwell = 94	261. 355. Dwell = 94	NT not in FoV, LE fuzzy & too bright	"	"	Separation aft of NT: at end of run, separation covers ¼ of Tran Section	similar to -009	similar to -009	"	Pullout and ramp to glide, but no glide
-014	33:01 39:30 Dwell = 389	334. 725. Dwell = 391	Quality has improved but too bright early, OK later in run	"	"	Separation aft of NT: covers 25% of Tran @ 34:00, 50% @ 37:40, 75% @ 39:30	Well behaved ablation, similar to -009	same as west	"	Pullout, ramp to glide and glide
-015	36:29 37:29 Dwell = 60	172. 233. Dwell = 61	Good Quality	-	Not applicable	Sparks visible off NT @ 36:38 and continues for test	-	-	-	Nosetip test at glide only
-016	50:29 56:59 Dwell = 390	152. 543. Dwell = 390	Quality OK	994 cooler than LEs during entire run	Nothing shows flow	Forward face step on east side @ 53:00 but may be illusion. Separation aft of NT: covers 25% of Tran @ 52:00, 66% @ 55:00, 75% @ 56:59	similar to -014	similar to -014	"	Pullout, ramp to glide and glide
-017	43:32 50:02 Dwell = 390	230. 619. Dwell = 390	Quality good, clear view of LEs but NT & Tran are too dark during most of run	-	East side RTV flow shows streamlines	Video too dark to show separation	similar to -014, gap between HS/LE	similar to -014	"	Pullout, ramp to glide and glide
-018	49:34 56:03 Dwell = 389	286. 676. Dwell = 390	Quality good, clear view of LEs but NT & Tran are too dark	-	HS melt flow shows streamlines over HS	"	similar to -014	some sparks @ 49:38, lots @ 49:58; melt flow in fore & mid areas. LE causing forward face step @ Tran	994 really ablating on east side by 50:40	Pullout, ramp to glide and glide
-019	15:59 22:28 Dwell = 389	1037. 1428. Dwell = 391	Quality good, LE & NT are clear	East end cap a little cooler than LE	Streamlines evident by HS melt flow	@ 17:14 separation covers 30% of Tran, @ 21:00 50%, @ 22:28 75%	similar to -014	similar to -014		Pullout, ramp to glide and glide

110

Table 4 cont'd. Summary of Video Data

Run	Video Model Times In / Out	Pyro Model Times In / Out	Video Quality	Test Rhombus Indications	Streamline Indications	Transition Section	Ablation West LE	Phenomena East LE	End Caps	Comments
-020	16:32 21:31 Dwell = 299	190. 491. Dwell = 301	Quality good, LE & NT are clear	-	Nothing shows flow	New Tran but west has LE from -009. Deposits on Tran aft of NT evident @ 17:00, continues to build up and stays there for run	LE forms aft face step with Tran, LE fore region cooled until Tran ablates even with LE	Fore edge remains cool during run, mid is hot, ablation starts @ 18:00 and continues. During run, I saw melt flow along stag line	-	Glide only
-021	33:28 35:10 Dwell = 101	188. 295. Dwell = 107	Quality good, but debris appears to cover part of east side	-	melt uniform across width except east side where bolt appears to influence	-	uniform LE ablation and temp	-	east corner of 994 looks dark after 33:40, model removal indicates debris covering FoV	0° sweep @ constant Qcw. Model ejected premature because of NASA cable burn thru
-022	05:44 08:00 Dwell = 136	295. 431. Dwell = 136	Good quality	-	-	-	LE started ablating on entry, gouge forms on west side	-		0° sweep @ constant Qcw. I ejected model because of gouge
-023	32:59 34:53 Dwell = 114	120. 235. Dwell = 114	quality OK	-	-	-	LE started ablating early = 33:05, something comes off @ 34:25, gouge forms on east	-	-	0° sweep @ constant Qcw. I ejected model because of gouge

Table 5. Summary of Leading Edge Ablation Data

60° SWEEP, BOOMERANG

MATERIAL	Z FIBERS ORIENTATION	AoA (°)	WEIGHT LOSS (gms)	RECESSION (inches)			TOTAL TIME (sec)	CASE	LOCATION	RUN
				FORE	AFT	AVG				
FWPF	⊥	0	6.21	0.096	0.074	0.085	94	P+T	W	-013
		0	8.93	0.149	0.106	0.128	301.1	G	W	-009
		0	16.50	0.255	0.194	0.255	389.4	P+T+G	W	-014
		0	16.72	0.250	0.195	0.223	390	P+T+G	W	-018
	⊥	10	16.36	0.236	0.189	0.212	391	P+T+G	E	-019
	‖	0	17.17	0.262	0.203	0.233	389	P+T+G	E	-017
223 PAN	⊥	0	6.39	0.104	0.086	0.095	94	P+T	E	-013
		0	9.23	0.151	0.120	0.136	301	G	E	-009
		0	16.91	0.265	0.219	0.242	389.4	P+T+G	E	-014
	⊥	10	16.70	0.255	0.194	0.225	391	P+T+G	W	-019
	‖	0	16.69	0.261	0.211	0.236	390.2	P+T+G	E	-016
4DO	⊥	0	16.82	0.264	0.205	0.235	390.2	P+T+G	W	-016
		0	16.61	0.256	0.208	0.232	389	P+T+G	E	-017
SAIC	‖	0	~5.0	0.133	0.0	0.066	390.0	P+T+G	E	-018
BP, CERACARB	----	0	3.48	0.053	0.003	0.028	301.0	G	E	-020

0° SWEEP, CYLINDER IN CROSS FLOW

MATERIAL	Z FIBERS ORIENTATION	AoA (°)	WEIGHT LOSS (grams)	RECESSION (inches)			TOTAL TIME (sec)	RUN
				EAST/WEST	MID	AVG		
223 PAN	‖	0	9.94	0.146/0.145	0.151	0.147	109	-021
SAIC	‖	0	21.5	0.220/0.213	0.223	0.232	136.1	-022
MSNW	----	0	no pre-test weight	0.253/0.231	0.245	0.243	115	-023

Notes:
1. See Table 1 for material descriptions.
2. Z-fiber bundle orientation either ⊥ or ‖ to the sweep angle, except: ⊥ to base for 4DO and ‖ to flow for cylinder.
3. AoA in degrees, weight loss in grams, recession in inches, time in seconds.
4. P = pullout, T = transition, G = glide, W = west, E = east

112

Appendix A

Calibration Test Data

Appendix A presents most of the data that was acquired from the calibration runs using the Boomerang calorimeter model. The calibration runs are summarized in Table 2. The data presented in this appendix are the facility instrumentation and calorimeter transient response measurements. The calorimeter measurement identifications are presented in Figure 20.

113
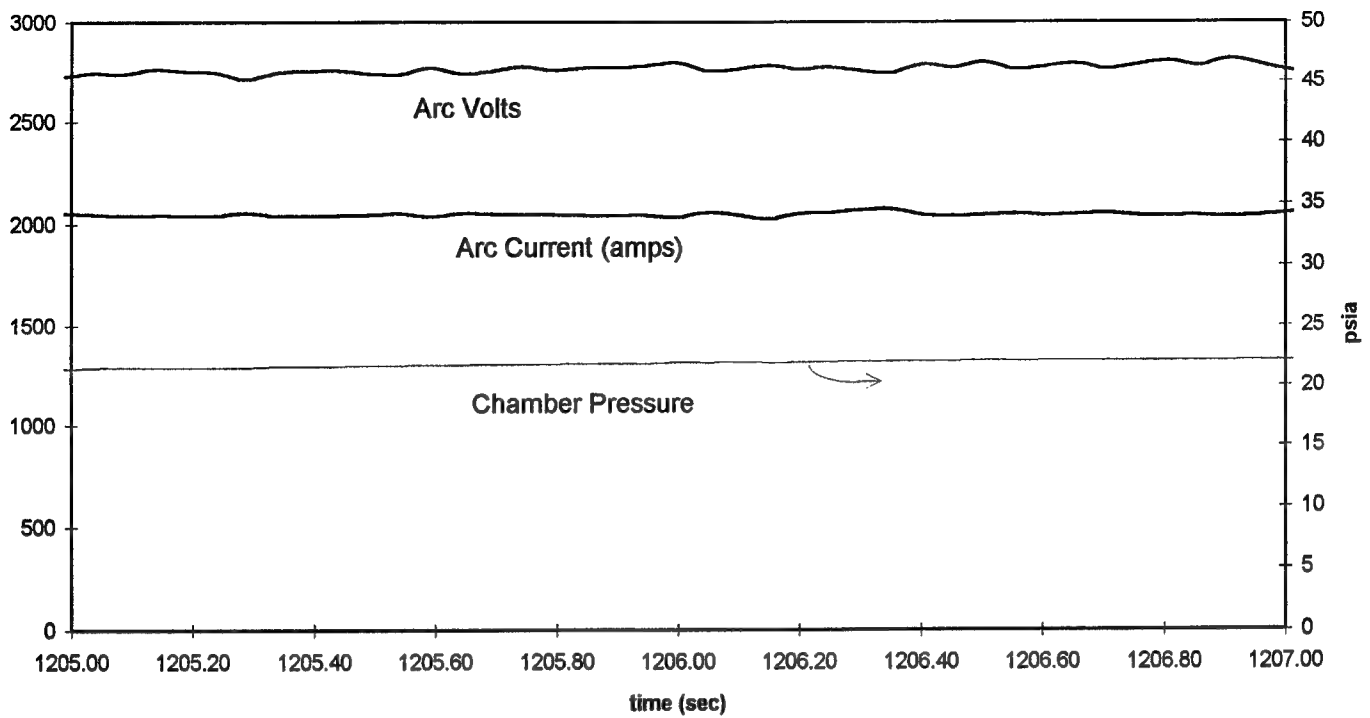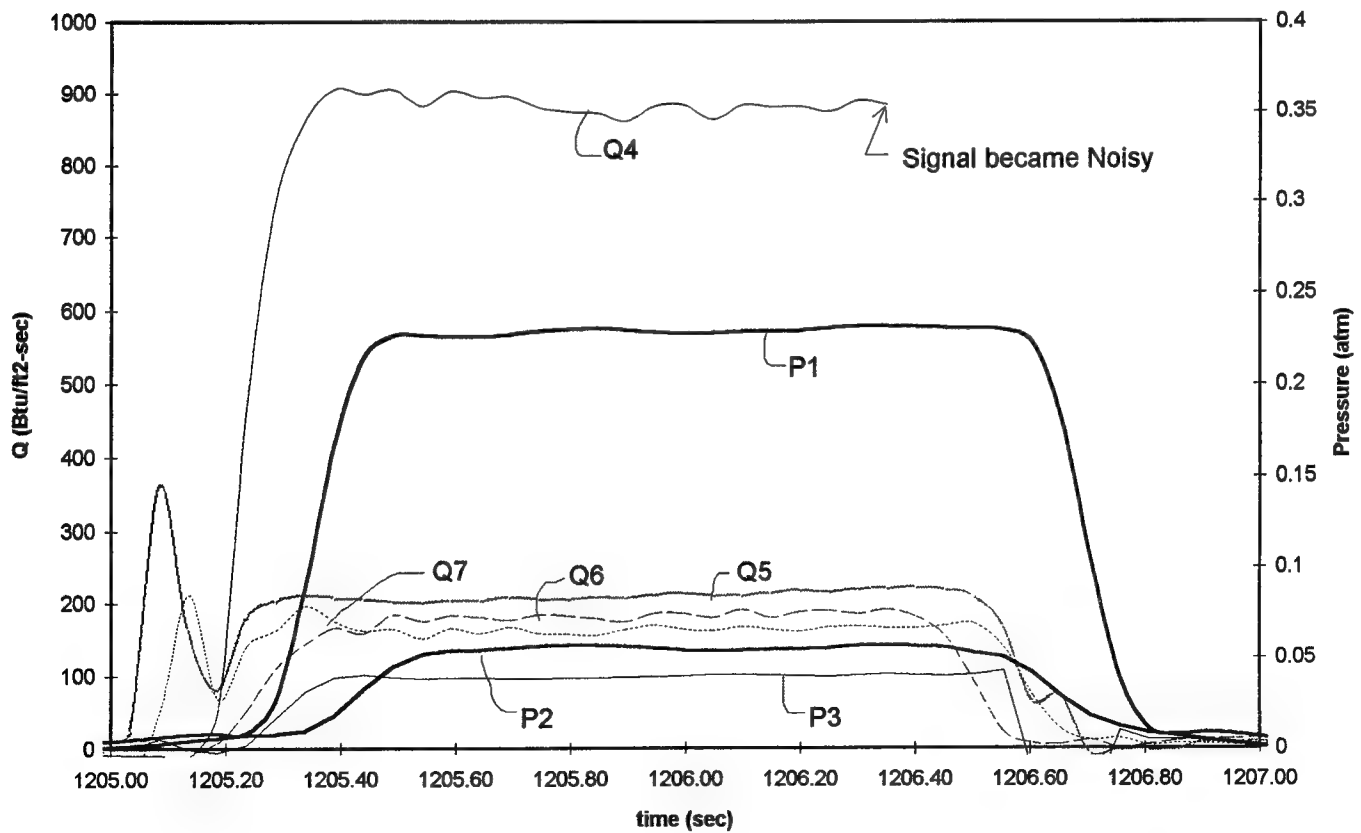
Figure A-1. Run 59-001a Facility and Cal Model Data

114

Run 59-002a, Arc data
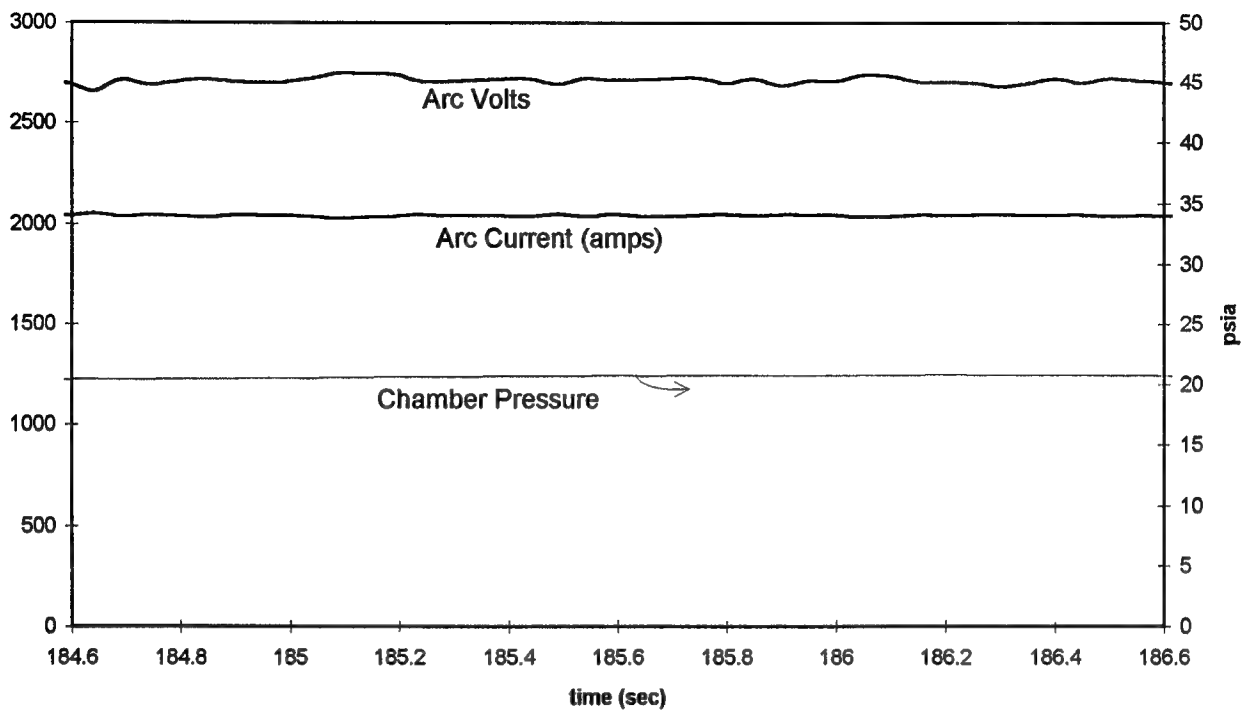
Run 59-002a, Cal & Pressure data
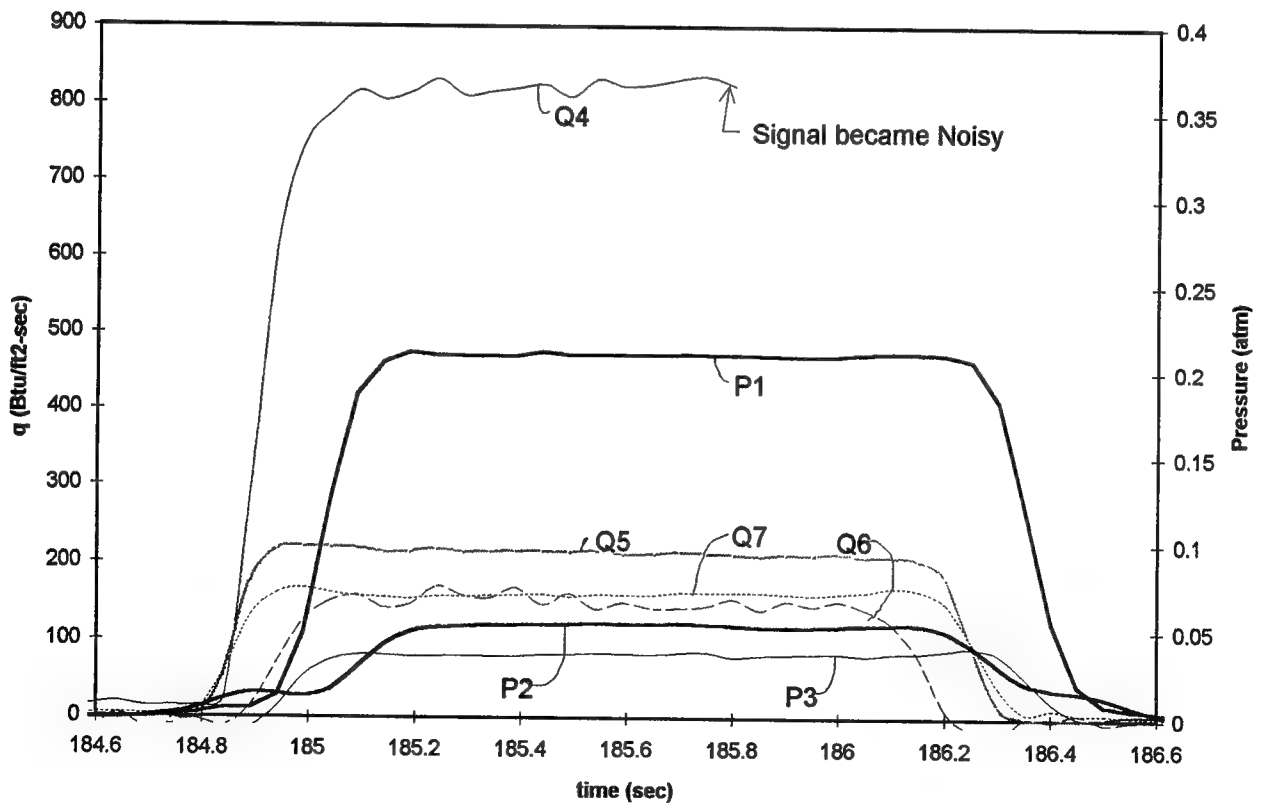
Figure A-2. Run 59-002a Facility and Cal Model Data

115

Figure A-3. Run 59-005 Facility and Cal Model Data

Run 59-006, Arc data
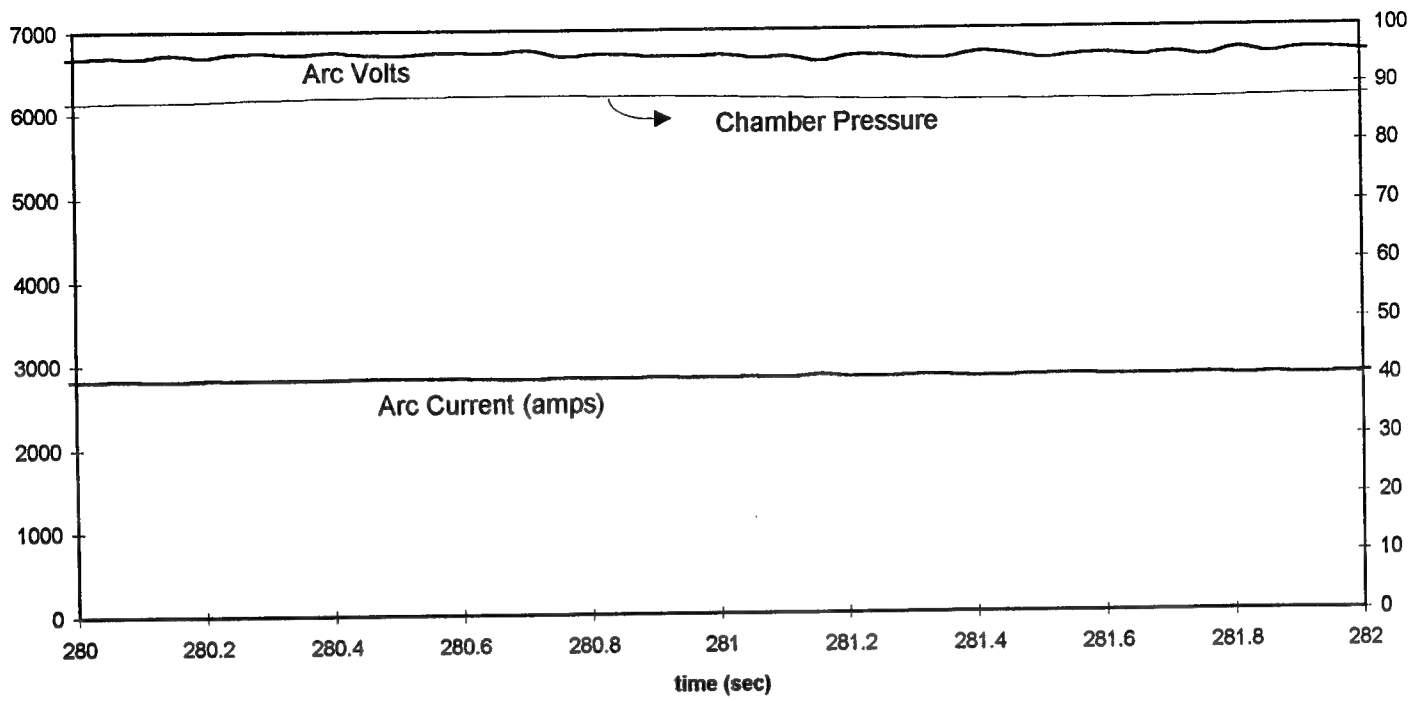
Run 59-006, Cal & Pressure data
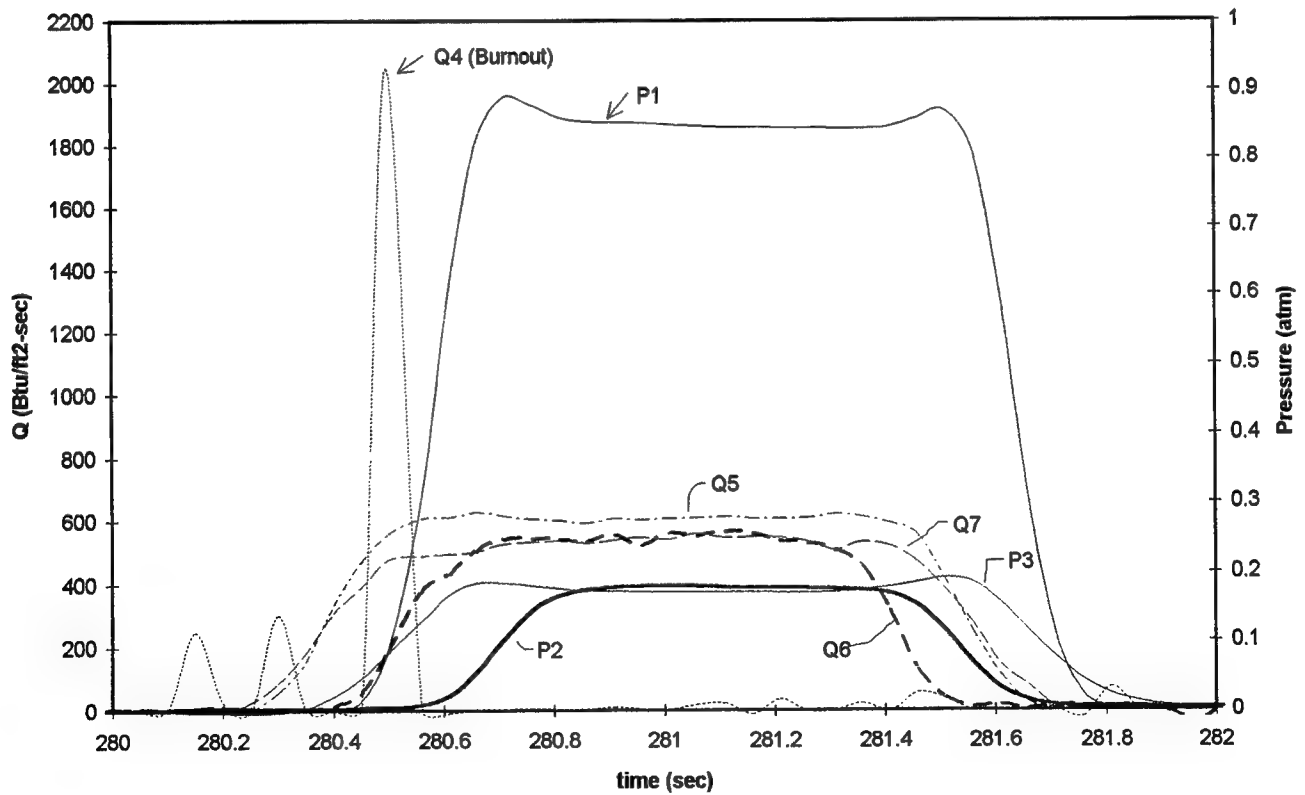
Figure A-4. Run 59-006 Facility and Cal Model Data

117
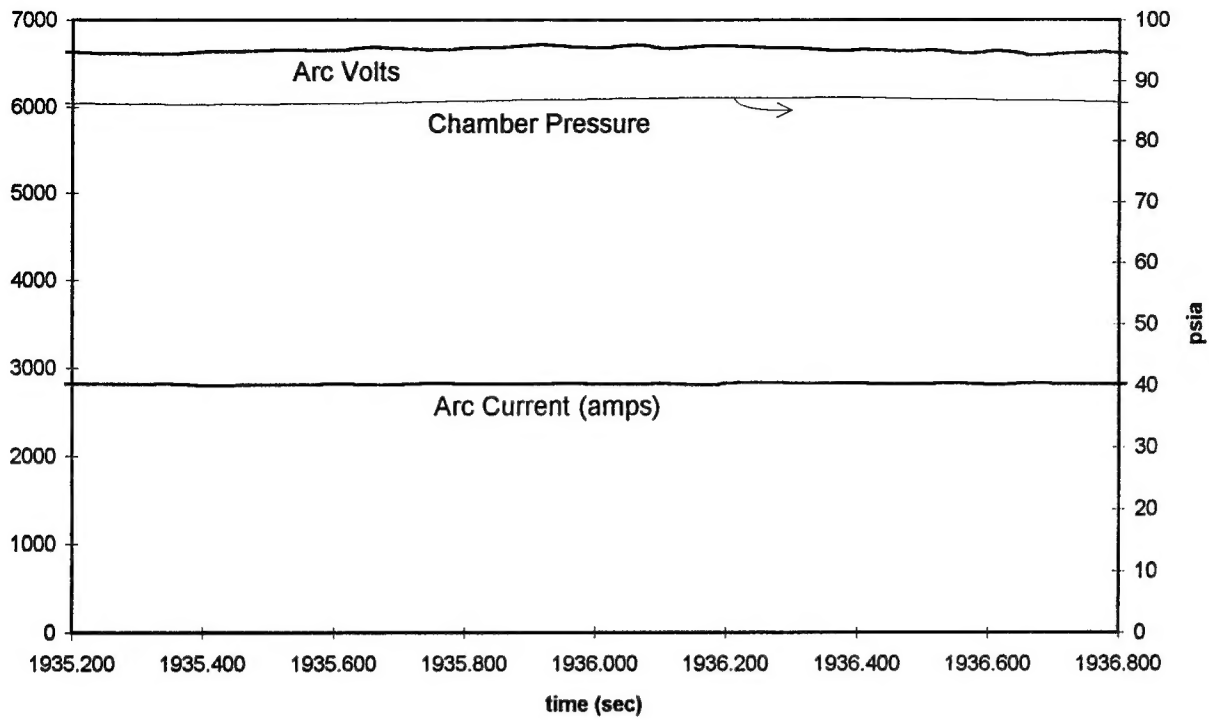
Run 59-008, Arc data
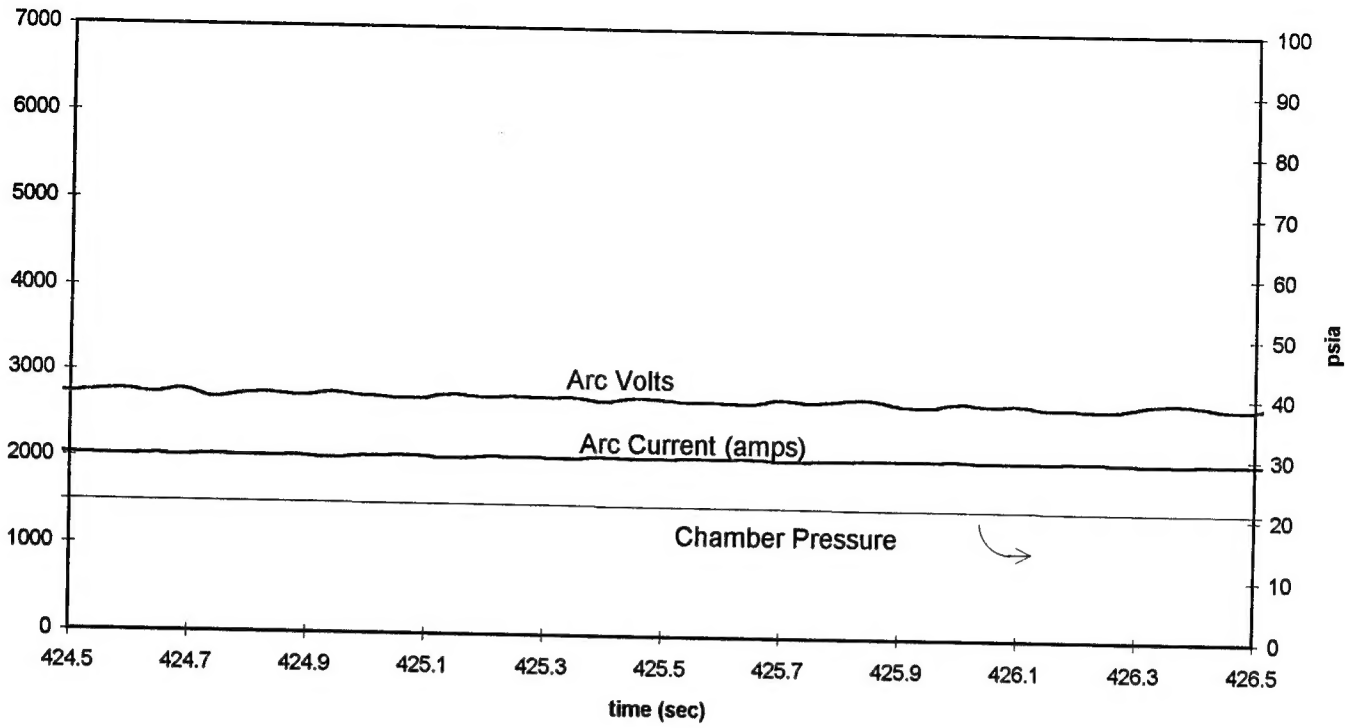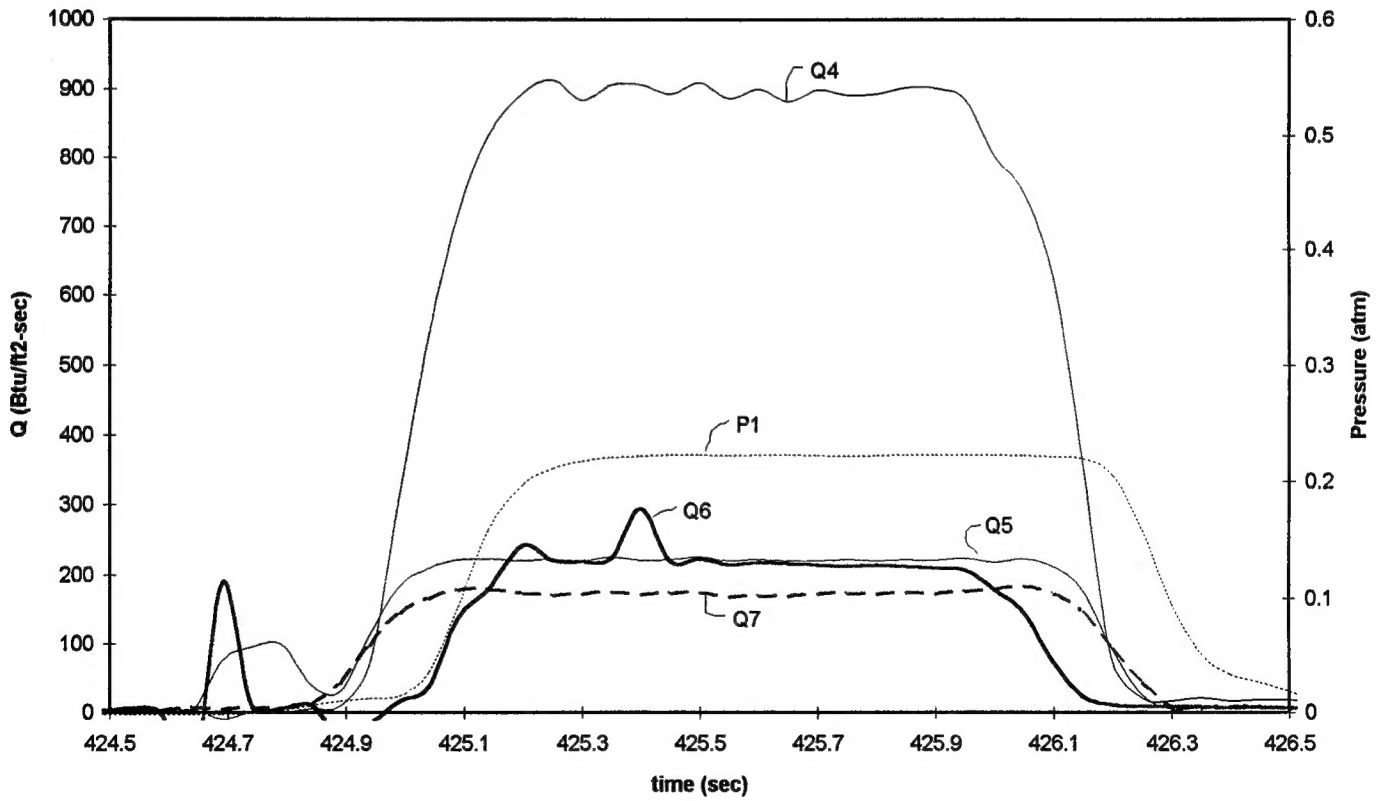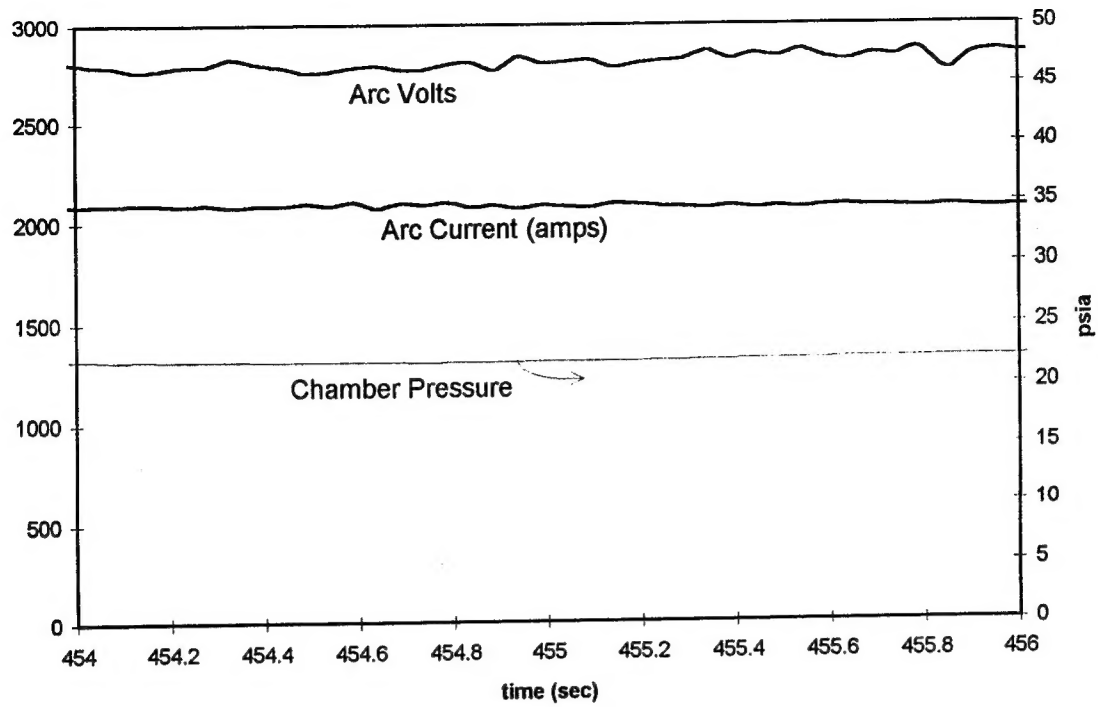

Run 59-008, Cal & Pressure data
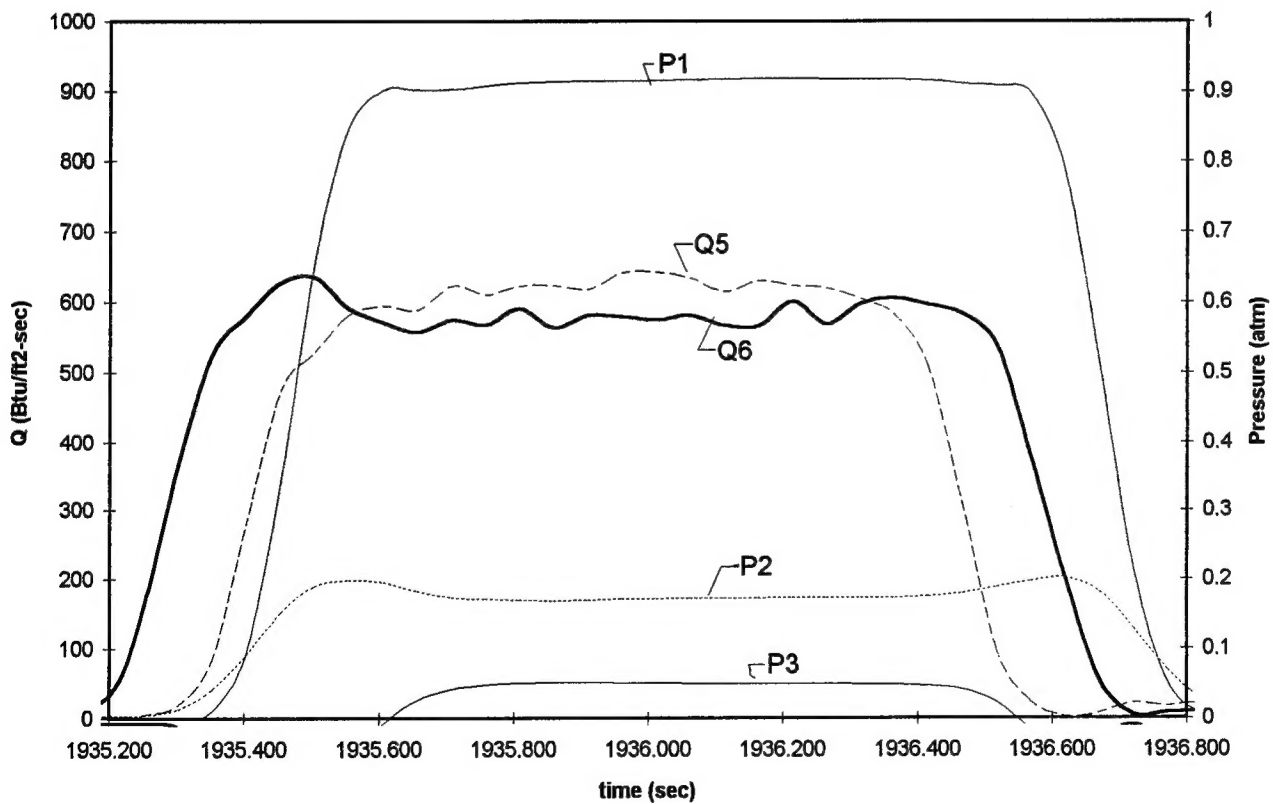
Figure A-5. Run 59-008 Facility and Cal Model Data

118

Run 59-010, Arc data

Run 59-010, Cal & Pressure data

Figure A-6. Run 59-010 Facility and Cal Model Data

119

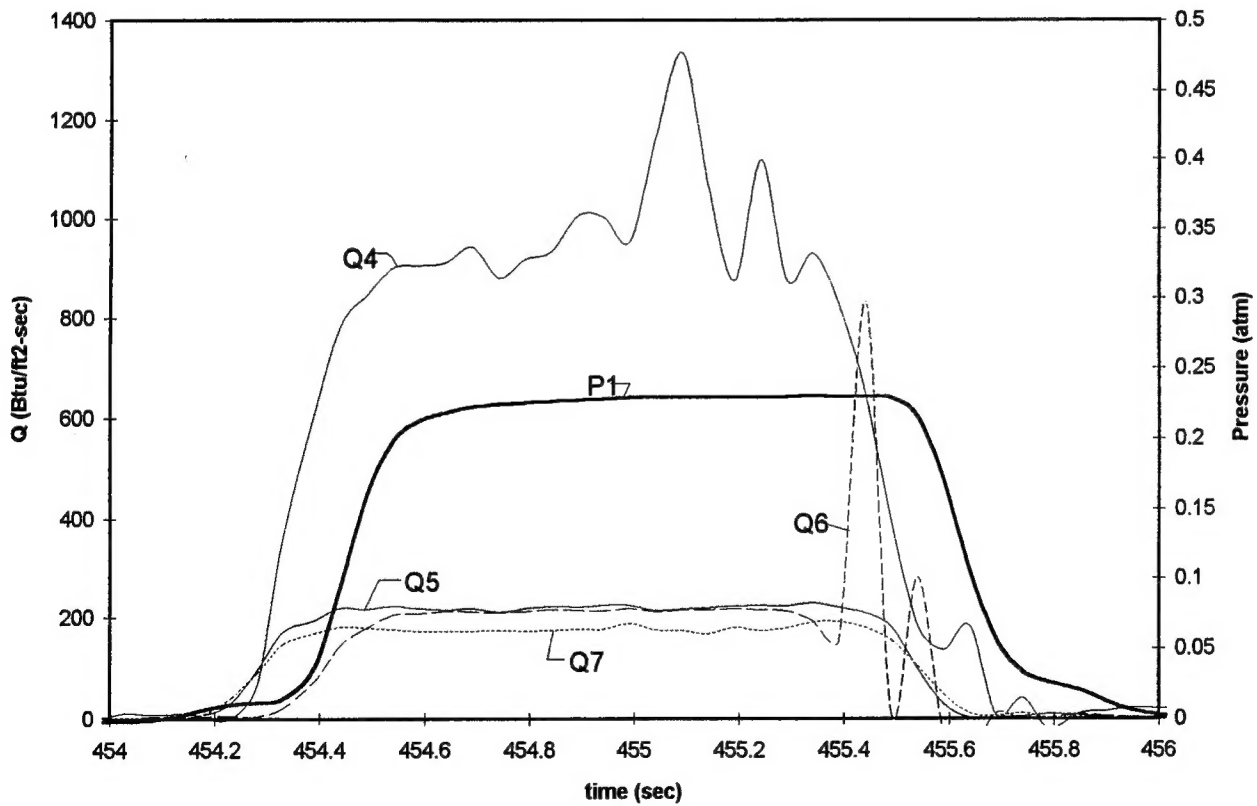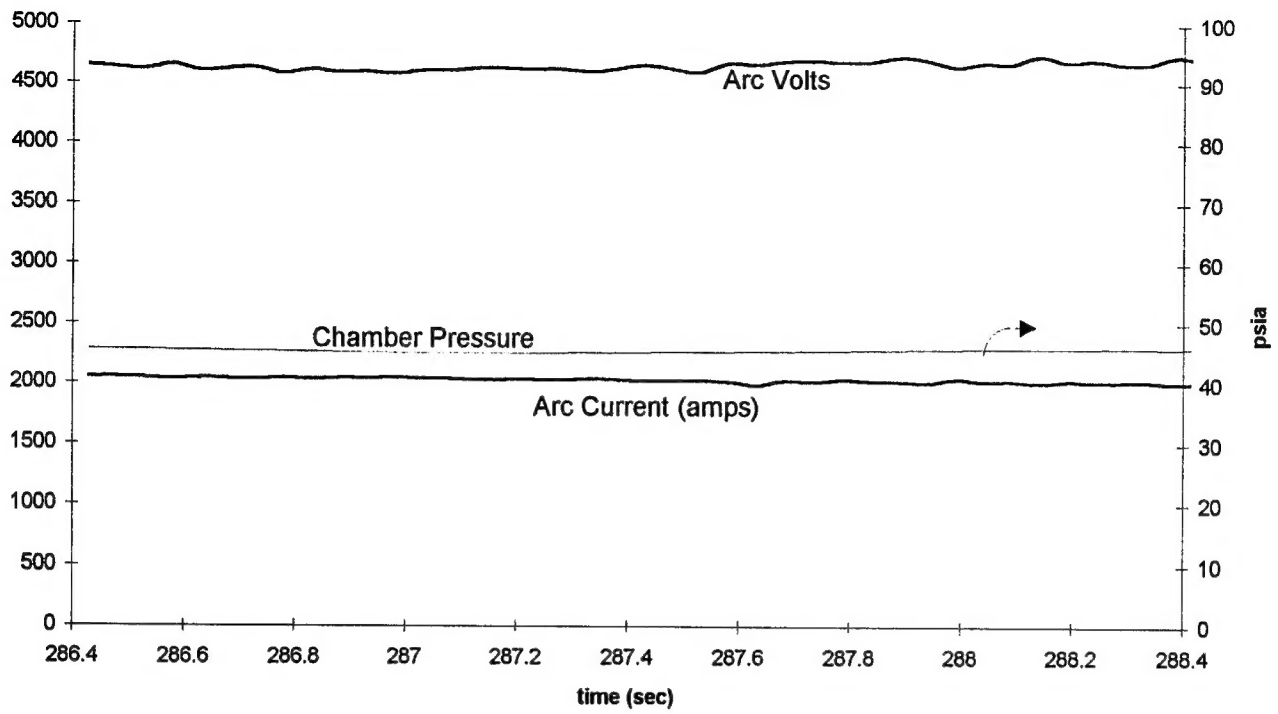**Run 59-011, Arc data**

Run 59-011, Cal & Pressure data

Figure A-7. Run 59-011 Facility and Cal Model Data
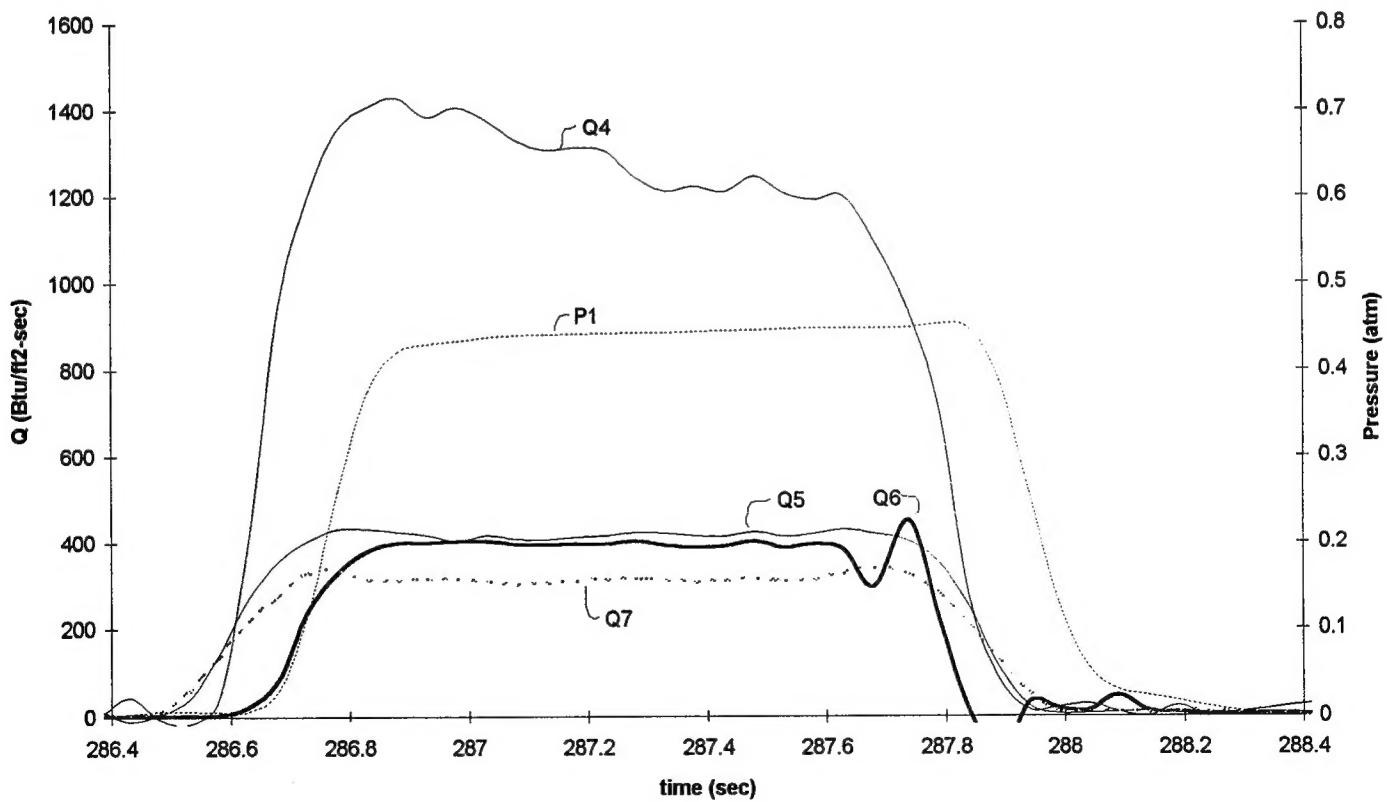
120

Run 59-012, Arc data

Run 59-012, Cal & Pressure data

Figure A-8. Run 59-012 Facility and Cal Model Data

121